A modelling investigation into the impacts of the convective parameterization on the tropical circulation

by

Shawn Corvec

A thesis
presented to the University of Waterloo
in fulfillment of the
thesis requirement for the degree of
Master of Mathematics
in
Applied Mathematics

Waterloo, Ontario, Canada, 2017

I hereby declare that I am the sole author of this thesis. This is a true copy of the thesis, including any required final revisions, as accepted by my examiners.

I understand that my thesis may be made electronically available to the public.

Abstract

Many studies have shown that the tropical circulations (Walker and Hadley circulations) will weaken in a warmer world. This is sometimes attributed to changes in the tropical mean water cycling rate (driven by convective mass flux), which does not increase as fast as boundary layer water vapour in the tropics. However, this theory is only valid for the large scale upward convective mass flux in the tropics, not necessarily to the local circulations, which are not as energetically constrained. Here, we show that there is also a potential regime in which this argument does not hold by simply changing the convective scheme in a climate model. This regime is one in which the tropical mean convective mass flux can actually increase with warming, provided the precipitation efficiency decreases significantly. Our work supports the theory that the uniform tropical mean static stability increase is the physical driver of the weakening of the tropical circulations with climate change, which is mainly driven by the tropical mean SST increase, regardless of the change in strength of convective mass flux. The local changes in tropospheric diabatic heating from heating are shown to influence the magnitude of the weakening of the Walker circulation.

We find that the precipitation efficiency decreases in an increased sea surface temperature AMIP-type experiment using the CAM4 AGCM with an alternate convective scheme using a unique mass flux closure, leading to a plausible scenario where tropical mean convective mass flux may increase, while the large-scale tropical circulations still weaken. While large-scale upward motion and convective mass flux are closely correlated spatially, the nature of this relationship can change in a warmer world if the precipitation efficiency changes. A decrease in precipitation efficiency can allow for increased upward convective mass flux, but the same tropospheric heating rate response, as the increased rate of condensational heating is offset by increased evaporational cooling. A decrease in precipitation efficiency leads to a lower heating rate per unit of upward mass flux due to a compensating increase in evaporation. The large tropical mean evaporation response seen with this scheme allows for stronger tropical mean convective updrafts, especially of the shallow variety, to balance where the evaporational cooling response is maximized.

Acknowledgements

I would like to thank Chad Thackeray for helping me setup and configure CESM on SciNet, Ian Folkins for guidance on compiling CAM4 with the IF scheme and for scientific guidance as well. I would also like to thank Christopher Fletcher whose encouragement and mentorship has gone a long way to helping me get this far.

Dedication

This thesis is dedicated to my parents, Carol and John, who encouraged me from a young age to follow my passion for meteorology.

Table of Contents

List of Tables

List of Figures

Chapter 1

Introduction

1.1 Tropical Convection and Clouds

1.1.1 Background

The tropics play an integral role in the Earth's climate system; circulations here transport atmospheric momentum, mass, moisture and heat poleward towards the mid-latitudes (Holton, 2004, p.370) and drive patterns of rainfall that are vital to billions of people worldwide. These circulations drive and are driven in part by deep moist convection - tropical thunderstorms and downpours - caused by towering plumes of positively buoyant air which derive their buoyancy primarily from the latent heat of condensation. This convection tends to occur over regions where the ocean surface is the warmest (such as in the tropical western Pacific), or over certain land regions during certain times of the year (monsoon season). Moist convection is what drives a majority of the rainfall in the tropics (Holton, 2004, p.370-371) and patterns of convection are thus vital to the freshwater supply of those living in tropical regions.

As atmospheric concentrations of greenhouse gases increase due to human activities, these patterns of rainfall are projected to change with some areas likely to get wetter and some to get drier. However, there is larger uncertainty in projections of precipitation under climate change than projections of temperature. Even worse, tropical rainfall, which is the majority of the global precipitation, has large uncertainties in highly populated regions such as south Asia (Turner & Annamalai, 2012). Part of the uncertainty in projections of tropical rainfall and climate sensitivity under climate change in climate models is related to the fact that moist convection can not be explicitly resolved in today's climate models

and needs to be parameterized (Arakawa, 2004; Randall et al., 2003; Rybka & Tost, 2014). This is because convection occurs at very small scales (on the order of 1-10 km). Thus, improving convection schemes in climate models is (or should be) a top priority. This thesis examines a new type of convective scheme under development for use in a version of the NCAR atmospheric climate model (CAM4) (Neale et al., 2010).

1.1.2 Hydrological cycle

Rainfall in the tropics is quite different from what we are used to in the mid-latitudes where it is usually associated with large scale storm systems. While rainfall in the tropics is mainly generated by many localized convective cells that are $\mathcal{O}(1$ km) in size, these cells become organized. There are many different ways the rainfall in the tropics organizes on many different spatial and temporal scales including mesoscale convective systems, Kelvin waves, equatorial Rossby Waves, tropical cyclones, monsoons, the MJO (Madden-Julian Oscillation) and more (Holton, 2004). However, it is best to start in the broadest sense with the basic equations for water conservation in the tropical atmosphere. In any given atmospheric column, the vertically integrated flux convergence of water vapor, plus surface evaporation, into the column must be equal to the rainfall rate, assuming a steady-state tropospheric water vapour content (Holton, 2004, p. 393):

$$P = -\int_0^z \nabla \cdot (\rho q \mathbf{V}) dz + E. \tag{1.1}$$

P is the precipitation rate (kg m^{-2}), ρ is the density of air (kg m^{-3}), q is the water vapour mixing ratio (kg of vapour per kg of dry air) and E is the surface evaporation rate (kg m^{-2}). The top integration limit, z, could be the entire troposphere, however this is not necessary as most of the moisture in the tropics is in the boundary layer. This is because of the exponential relationship between the amount of water vapour the atmosphere can hold and temperature and also the fact that most of the tropics are ocean and this is where the evaporated ocean water is mixes into (q in the boundary layer is roughly constant with height). So z can be taken to be approximately 2 km (Holton, 2004, p.393-394). It is also important to relate time mean evaporation over the ocean (which is a turbulent process) to known time mean variables; this is known as the bulk aerodynamic formula for latent heat flux (units of W m^{-2}) (Katsaros, 2001):

$$\overline{F}_{LH} = \bar{\rho} L_v C_E \|\bar{\mathbf{v}}\| (\overline{q_s} - \overline{q_a}), \tag{1.2}$$

where $\bar{\rho}$ is the time mean air density of the air at the ocean-atmosphere interface, L_v is the latent heat of vaporization, $\|\bar{\mathbf{v}}\|$ is the 10-meter wind speed, $\overline{q_s}$ is the water vapour mixing ratio at the ocean surface which is taken to be the saturation water vapour mixing ratio determined by the sea surface temperature (SST), and $\overline{q_a}$ is the water vapour mixing ratio of the atmosphere just above the ocean surface. C_E is an empirically determined non-dimensional constant (sometimes called the drag constant) determined to be $\approx$ 1.1-1.2 $\cdot$ 10^{-3} for weak surface winds (which are typical in the tropics) (Katsaros, 2001). We have added the overbar ($\bar{*}$) to stress that these are time mean quantities (this notation is consistent throughout the thesis). From this equation it is easy to see that the drier and windier the air above the ocean the greater the evaporation rate (latent heat flux). Also, the warmer the SST, the greater the evaporation rate (since q_s solely depends on SST). Since SSTs are mainly warmed via incoming shortwave solar radiation in the tropics, any change in incoming solar radiation (clouds, for example) can change the evaporation rate via SST.

On sufficiently long time scales (certainly those used to study climate) global mean evaporation must balance with precipitation:

$$\langle \overline{P} \rangle - \langle \overline{E} \rangle = -\left\langle \int_0^z \nabla \cdot (\bar{\rho}\bar{q}\overline{\mathbf{V}}) dz \right\rangle = 0. \tag{1.3}$$

Here, $\langle * \rangle$ denotes a global mean (will be used for the tropical mean in the remained of this thesis). In other words, global time mean precipitation must balance global time mean evaporation and the global mean, time mean moisture flux convergence must also be zero. This is actually a very important constraint for studying climate change as any changes in global mean evaporation will thus change the global mean precipitation rate. In a warming climate, SSTs will warm and thus q_s will increase by the Clausius-Clapeyron (C-C) relation:

$$\frac{d \ln e_s}{dT} = \frac{L_v}{RT^2}, \tag{1.4}$$

R is the gas constant and e_s is the saturation vapour pressure, which is directly proportional to the saturation water vapour mixing ration, q_s. From this relation, it is clear that there is a nearly exponential relationship between saturation vapour pressure (and thus saturation water vapour mixing ratio) and temperature. The rate of increase in q_s as a function of temperature for temperature values seen in the tropics is $\approx$ 7% K^{-1} based on this relation and is indeed validated by modeling studies (Held & Soden, 2006; Vecchi et al., 2006).

1.1.3 Moist convection

Moist convection manifests itself in the tropics and elsewhere as towering and bubbling plumes of cloud called cumulus clouds that can eventually reach the tropopause and spread out into what is referred to as an "anvil" (composed of ice crystals). Once the cloud begins to form an anvil it is referred to as a cumulonimbus cloud, which can produce lightning. In the tropics, cumulonimbus clouds can easily reach heights of 55000 feet ($\approx$ 17 km) or more (Hollars et al., 2004). Tropical cyclones (tropical storms and hurricanes) are driven by organized clusters of moist convection that sometimes occur in the tropics and subtropics. See figure 1.1 for examples of different tropical cumuli clouds in various stages of development.

Figure 1.1: Tropical cumuli in different stages of development. From Evans & Laing (2011).

To better understand the physics of moist convection, a simple model called "parcel theory" is used in meteorology. This theory makes the simplification that a bubble or parcel of buoyant air (air with a lower density than the environment), is lifted upwards until it condenses and then reaches a level where it is positively buoyant (the LFC or level of free convection). The buoyancy of a parcel is simply (Holton, 2004, p.295):

$$b^{'}(z) = g\frac{T_p - T_e}{T_e}, \tag{1.5}$$

where g is the gravitational acceleration, T_p is the temperature of the parcel, and T_e is the temperature of the environment.

The vertical integral of this parcel buoyancy above the LFC is referred to as "CAPE" (convective available potential energy). One key assumption made in this theory is that the parcel does not dilute due to mixing of environmental air with this parcel (Holton, 2004, p.295). This potential energy is then transformed into the kinetic energy of the parcel (assuming the CAPE is positive). Once an ascending parcel reaches the LFC, its internal temperature decreases at a rate lower than the surrounding environment, due to the continued latent heat release due to condensation. This assumes that the parcel remains saturated with respect to the environment above this level. Oftentimes, the latent heat of fusion (i.e., from freezing) is ignored when calculating CAPE. CAPE can be defined as:

$$CAPE = \int_{p_{el}}^{p_{lfc}} (b^{'}(z))dp, \tag{1.6}$$

where p_{lfc} is the pressure of the level at which convection will occur freely, and p_{el} is the pressure of the equilibrium level, or level of neutral buoyancy where the parcel reaches zero buoyancy. CAPE is a key parameter for the parameterization of moist convection in a climate or weather model as it is often used for the mass flux closure.

However, this formulation of CAPE neglects the fact that water vapour acts to decrease the air density and thus is sometimes corrected for in calculating CAPE. In place of the specific volume, a quantity referred to as the "virtual temperature" (T_v) is introduced, which is the temperature that a parcel of dry air would have to have in order to have the same density as the parcel of air that has water vapour (at the same pressure). T_v is defined as (from AMS, 2012):

$$T_v = T\frac{(1+\frac{q}{\epsilon})}{(1+q)}, \tag{1.7}$$

where q is the water vapour mixing ratio and ϵ is the ratio of the gas constant for dry air, R_d (287 K^{-1} kg^{-1}), to the gas constant for water vapour R_v (461 J K^{-1} kg^{-1}) which is $\approx$ 0.623. Using the virtual temperature, the equation for CAPE then becomes (Doswell & Rasmussen, 1994):

$$CAPE = g\int_{z_{el}}^{z_{lfc}} \Big(\frac{(T_v)_p - (T_v)_e}{(T_v)_e}\Big)dz. \tag{1.8}$$

Note that we have switched the integration to be over geometric height coordinates here from pressure coordinates. Even this formulation of CAPE, however, is not perfect as it

still neglects dilution of buoyant parcels due to "entrainment" of drier environmental air and condensate loading (i.e., cloud water and ice that weigh down the parcel) which both act to decrease parcels' buoyancy. Entrainment refers to the dilution of air withing a parcel with air from the environment, and detrainment the opposite, where air from the parcel is mixed into the environmental air.

1.1.4 Quasi-equilibrium theory and radiative-convective equilibrium

In the tropics (30°S-30°N is often used as a definition of the tropics), CAPE is often positive, especially over oceans. The amount of water vapour the atmosphere can hold increases approximately exponentially with increasing temperature by the Clausius-Clapeyron relation ($\approx 7\%\text{K}^{-1}$). So regions with warmer sea surface temperatures (SSTs) will tend to have more atmospheric water vapour available for rising parcels, and thus more latent heat is available to be released to achieve positive buoyancy. Folkins & Braun (2003) found that there is a sharp increase in convective rainfall where (SSTs) exceed 26°C which is typically true in much of the tropics. Because the tropics typically have positive CAPE and small CIN (convective inhibition - negative CAPE), i.e., the tropics are convectively unstable. Rainfall from moist convection is the predominant source of rainfall in these regions, with "stratiform" (non-convective) precipitation, typically associated with organized weather systems, much less frequent than in the mid-latitudes.

A model of convection that has been used in convective parameterization schemes in climate and weather models is the model of quasi-equilibrium (Arakawa & Schubert, 1974) (see Emanuel (2007) for more on this theory). Moist convection, through the latent heat of condensation, acts to warm the environmental atmosphere. In a region where moist convection is frequent in the tropics, the atmospheric lapse rate tends towards "moist adiabatic" ($\approx 6.5\text{K/km}$) which is the lapse rate that a saturated lifted parcel would experience. This is because any temperature gradients that do develop in the tropics (which will show in the next section) are quickly removed so that temperatures become very horizontally uniform in the tropics. Thus, since convection can adjust the temperature in the free troposphere in the tropics very far removed from where the convection is occurring. The moist adiabatic lapse rate (Γ_s) is typically defined as followed (from Holton (2004), p.292):

$$-\left(\frac{dT}{dz}\right)_{moist} \approx \Gamma_s \approx \frac{g}{c_p} \cdot \frac{(1+\frac{L_c q_s}{RT})}{1+\frac{0.622*L_c^2 q_s}{c_p R T^2}}, \tag{1.9}$$

where c_p is the specific heat of dry air, and the rest of the variables have the same definitions as defined earlier. This lapse rate is also known as the pseudoadiabtic lapse rate (Holton (2004), p.292) and is thermodynamically irreversible. This lapse rate is a function of the local saturation mixing ratio, and decreases with higher temperature as the saturation mixing ratio increases. Note that this lapse rate assumes that all the condensate is removed from the parcel once it is created. Also, this expression assumes that all the condensate produced is liquid, but if ice is produced, you can replace L_c with the latent heat of fusion.

Once the environmental lapse rate becomes moist adiabatic (and CAPE is ≈ 0 Merlis (2012)), moist convection will no longer occur until the CAPE builds up to become positive again. This occurs relatively rapidly via heating of the mid-upper troposphere from condenstional heating which acts to stabilize the atmosphere and reduce CAPE ($\approx$ 12 hours or less) and then CAPE builds up again by radiative cooling of the free atmosphere on a much longer timescale ($\approx$ 20 days) (Merlis, 2012) as the cooling rates. The balance between convective heating and radiative cooling is referred to as "radiative-convective equilibrium" (Manabe & Wetherald, 1967).

The cycle of CAPE build-up and release is always repeating itself and the assumption is that the time mean CAPE over long time periods does not change (Emanuel, 2007). This tendency for the tropical temperature profile to relax towards a moist adiabatic profile has been incorporated into the convection schemes of many climate models, however, based on observations, this only appears to hold in regions of heavy convection. In reality, convection in the tropics does not always extend to the tropopause (cumulus congestus) and there is a deviation from the moist adiabat at the melting level (Folkins, 2013).

1.2 The Tropical Circulation

1.2.1 Background

In tropical dynamics, we can start by writing down the governing equations for hydrostatic atmospheric motion, temperature and mass continuity (in isobaric coordinates) in the

Eulerian framework (from the perspective of a fixed location in space):

$$\left(\frac{\partial}{\partial t} + \mathbf{V} \cdot \nabla_p + \omega \frac{\partial}{\partial z}\right)\mathbf{V} + f\mathbf{k} \times \mathbf{V} = -\nabla_p \Phi, \tag{1.10}$$

$$\left(\frac{\partial}{\partial t} + \mathbf{V} \cdot \nabla_p\right)T - \sigma\omega = Q_{tot}, \tag{1.11}$$

$$\frac{\partial u}{\partial x} + \frac{\partial v}{\partial y} + \frac{\partial \omega}{\partial p} = 0, \tag{1.12}$$

where $\mathbf{V}$ is the total vector wind, Φ is the geopotential, ∇_p is the horizontal del operator on constant pressure surfaces, T is the temperature, σ is the static stability ($\sigma = \frac{RT}{c_p p} - \frac{\partial T}{\partial p}$) and Q_{tot} is the total diabatic heating rate. ω is the Lagrangian (from the perspective of a parcel following the fluid flow) pressure vertical velocity, $\frac{dp}{dt}$ (the total or material derivative, $\frac{d}{dt}$ is used to make it clear that is is a Lagrangian quantity). f is the Coriolis parameter $f = 2\Omega \sin\phi$ (where Ω is the angular rotation rate of the Earth and ϕ is the latitude. Additionally, hydrostatic balance is assumed:

$$-\rho g = \frac{dp}{dz}, \tag{1.13}$$

from which we can then derive a relation between the vertical gradient of geopotential in pressure coordinates, and the temperature, by using the ideal gas law:

$$\frac{d\Phi}{dp} = -\frac{RT}{p} \tag{1.14}$$

To understand tropical dynamics, it is important to note that geostrophic balance is not a valid approximation for the large scale flow. This can be seen by examining the Rossby number (the ratio of the advection and Coriolis terms in 1.10:

$$R_o = \frac{(\mathbf{V} \cdot \nabla_p)\mathbf{V}}{f\mathbf{k} \times \mathbf{V}} \approx \frac{U}{fL}, \tag{1.15}$$

using characteristic length (L) and velocity (U) scales of 10^6 m and 10 m s^{-1}, and assuming a Coriolis parameter of $\approx 10^{-5}$ s^{-1}, therefore, $R_o \gtrapprox 1$ in the tropics (Holton, 2004, p.388) and gets larger the closer to the equator one is. As a consequence, the advection and Coriolis terms are nearly equal in magnitude and in steady-state in the tropics, the tropical dynamics can not be approximated as a balance between the Coriolis and geopotential gradient terms (Holton, 2004, p.388). If assumed $f\mathbf{k} \times \mathbf{V} = -\nabla_p \Phi$, then wind speeds would tend ∞ toward the equator (because the Coriolis parameter goes to zero there),

which is nonphysical. Therefore, in equatorial regions, geopotential height gradients, and by extension temperature gradients (see eq. 1.14), are negligible. Thus, one can drop the horizontal advection term in 1.11 and if one assumes steady state, 1.11 can be simplified and written as:

$$-\sigma\omega = Q_{tot}. \tag{1.16}$$

This is known as the "weak temperature gradient" (WTG) approximation (Charney, 1963; Sobel et al., 2001). Note, we can introduce the potential temperature, θ, in place of T in the parameter σ:

$$\sigma = \frac{T}{\theta}\frac{\partial\theta}{\partial p}. \tag{1.17}$$

This temperature, which has similarities, to density, is defined as the temperature that a parcel of air would have if moved adiabatically to a reference pressure (typically near the surface), p_o:

$$\theta = T\left(\frac{p_o}{p}\right)^{\left(\frac{R_d}{c_p}\right)}, \tag{1.18}$$

where p_o is the reference pressure, and p is the pressure of the parcel.

Eq. 1.16 implies that the total diabatic heating at any point in the tropics is balanced by vertical temperature advection (which is upward motion, ω, multiplied by the static stability, σ). This vertical temperature advection term is also referred to as the adiabatic cooling term. Any temperature gradients that do develop in the tropics are generally removed quickly by gravity waves generated by convection (Sobel et al., 2001). This simple relation is vital to understanding tropical dynamics and the tropical circulations which will be discussed in the next sections.

One type of common traveling wave solution that can be found from eq. 1.10 and eq. 1.12 in the tropics is the equatorially trapped Kelvin wave. These waves travel eastward in the deep tropics, and are "trapped" near the equator by the Coriolis force. To find this solution we first approximate the Coriolis parameter, f, as varying linearly with y (Cartesian distance) instead of the sine of the latitude; an equatorial β-plane approximation. We center this approximation about the equator and can define f as follows (Holton, 2004, p.395):

$$f = \beta y, \tag{1.19}$$

where $\beta = 2\Omega/a$, Ω is the rotation rate of the Earth, and a is the radius of the Earth. We also make the approximation of removing the non-linear terms from the x-y momentum equations and assume there is no meridional velocity, v. We are also interested in deviations of geopotential to describe the wave, so we assume a constant geopotential height field with mean geopotential $\Phi_m = Z_m/g$ and perturbations about the mean state, Φ'. Assuming a mean state with no time mean u or v velocity, with small deviations ($'$,v') about the mean locally to get (Holton, 2004, p.395):

$$\frac{\partial u'}{\partial t} = -\frac{\partial \Phi}{\partial x}, \tag{1.20}$$

$$\beta y u' = -\frac{\partial \Phi}{\partial y}, \tag{1.21}$$

$$\frac{\partial \Phi'}{\partial t} + \Phi_m(\frac{\partial u'}{\partial x}) = 0. \tag{1.22}$$

We examine zonal traveling wave solutions of the form:

$$u' = \hat{u}(y)e^{i(kx-\omega t)}, \tag{1.23}$$

$$\Phi' = \hat{\Phi}(y)e^{i(kx-\omega t)}, \tag{1.24}$$

where $\hat{u}$ and $\hat{\Phi}$ only vary in the y direction, ω is the frequency and k is the zonal wavenumber. Substituting these into eqs. 1.20-1.22, one obtains:

$$-i\omega\hat{u} = -ik\hat{\Phi}, \tag{1.25}$$

$$\beta y\hat{u} = -\frac{\partial \hat{\Phi}}{\partial y}, \tag{1.26}$$

$$-i\omega\hat{\Phi} + \Phi_m(ik\hat{u}) = 0. \tag{1.27}$$

Elimination of $\hat{\Phi}$ by solving for $\hat{\Phi}$ in eq. 1.26 and substituting into eq. 1.27 gives the following:

$$\beta y\hat{u} = \frac{\omega}{k}\frac{\partial \hat{u}}{\partial y}, \tag{1.28}$$

which can be solved easily to obtain a solution for the zonal wind structure associated with the Kelvin wave:

$$\hat{u} = u_o e^{-\beta y^2 k/2\omega}, \tag{1.29}$$

which describes a wave in the zonal wind field that has a Gaussian structure in the y-direction, and no variation in the zonal direction, with a maximum in zonal wind, u_o, at the equator. It can also be shown that the dispersion relation for an equatorially trapped Kelvin wave is:

$$c \equiv \sqrt{\frac{\omega}{k}} = \sqrt{\Phi}_m, \tag{1.30}$$

where c is the phase speed of the Kelvin wave.

1.2.2 Walker circulation

The Walker circulation is named after Sir Gilbert Walker who while working in India noticed that occasionally the summer monsoon rains would not materialize. He discovered that this seemed to be related to sea level pressure (SLP) gradient changes between the western and eastern equatorial Pacific. The oscillation of this pressure gradient is referred to as the "southern oscillation" and is typically calculated as a difference in SLP between Darwin, Australia and Tahiti, in the central Pacific (Holton, 2004, p.382-383). Typically, the SLP over the Maritime Continent and far western tropical Pacific is lower than the SLP in the central/eastern Pacific, but this pressure difference can shrink or even reverse during El Nino events. This pressure gradient causes winds to blow from east to west in the tropical Pacific (trade winds), with rising motion and low-level convergence over the Maritime Continent (Indonesia and environs) and sinking motion and low-level divergence over the eastern Pacific (Bjerknes, 1969). The rising motion and upper-level divergence over the Maritime Continent is caused by the relatively warmer waters (sometimes referred to as the western Pacific warm pool) in that region which creates an environment of positive CAPE, and thus convection is favoured there. This region of zonally enhanced time mean convection generates significant diabatic heating in the mid and upper troposphere which acts to increase geopotential heights and create a horizontal pressure gradient out of the region and thus creates a region of upper-level divergent winds flowing outward horizontally from the region. By mass continuity, air from below moves upward and a compensating region of descending air and upper-level convergence forms in the eastern Pacific where convection is much less frequent (see figure 1.2 for a plot of the time mean vertical motion associated with the Walker circulation from reanalysis). Some describe the Walker Circulation as a standing Kelvin wave of wavenumber-1 being forced by diabatic heating (Stechmann & Ogrosky, 2014).

One way to measure the strength of the Walker circulation is to measure upper-tropospheric horizontal divergence (which gives information about the vertical motion by

continuity). This field is obtained using the fundamental theorem of vector calculus (also known as a Helmholtz decomposition) which states that a vector field can be decomposed into divergenceless (rotational) and irrotational (divergent) components. Stated mathematically, the horizontal vector wind, $\mathbf{V}$, can be written as (Holton, 2004, p.389):

$$\mathbf{V} = \mathbf{V_{rot}} + \mathbf{V_{irr}}, \tag{1.31}$$

$$\nabla \times \mathbf{V_{irr}} = 0, \tag{1.32}$$

$$\nabla \cdot \mathbf{V_{rot}} = 0. \tag{1.33}$$

From these two components, a stream function and a velocity potential can be constructed. A velocity potential, χ can be constructed from the divergent (irrotational) component of the wind so that:

$$\nabla\chi = \mathbf{V_{irr}}, \tag{1.34}$$

which satisfies eq. 1.32 since the curl of the gradient of a scalar field is 0.

This scalar field is typically evaluated in the upper troposphere, such as at the 200 hPa level, and is often used for measuring the strength of the upper-level divergence associated with the ascending region of the Walker circulation (Tanaka et al., 2004). Since the Walker circulation is a zonally asymmetric circulation, the zonal mean needs to be removed to ascertain the contribution Walker circulation contribution to the divergence. This will be referred to as χ^* in this thesis, where the star indicates a deviation from the zonal mean, and this notation will be consistent throughout this thesis. Also, we will use the notation χ_{200} to indicate the velocity potential calculated at the 200 hPa level.

The zonal asymmetry in diabatic heating in the tropics causes the zonal asymmetry in divergence, and hence the zonal (Walker) circulation. This asymmetry is due to the fact that SSTs are warmer in the western Pacific than in the eastern Pacific. The primary balance for the Walker circulation is between diabatic heating and adiabatic cooling in the ascending region (eq. 1.16) and between radiational cooling and adiabatic heating in the descending region (also, eq. 1.16). Thus, any changes to the rate of diabatic heating, Q_{tot}, or the static stability, σ, can affect the strength of the circulation, ω.

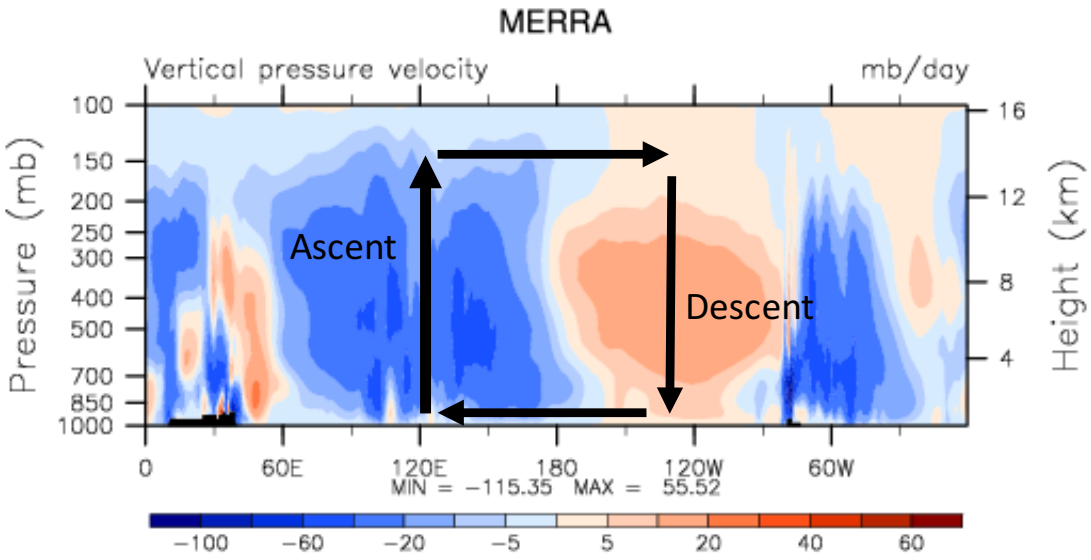

Figure 1.2: Schematic of the wavenumber-1 Walker circulation with ascent over the Maritime Continent ($\approx$ 120E) and compensating descent over the eastern Pacific ($\approx$ 120W). The shading is the meridional (north-south) mean annual mean ω (units of hPa day^{-1}) from the MERRA reanalysis (1979-2013) (Rienecker et al., 2011). Note that there are other weaker regions of ascent/descent over Africa and South America associated with the wavenumber-2 components of the Walker circulation. In this thesis we will focus on the dominant Walker circulation.

1.2.3 Response to climate change

While the amount of water vapour in the Earth's atmosphere increases with increasing surface temperature close to the C-C relation (see section 1.1.2), rainfall in climate models does not. This is because global mean evaporation is energetically constrained to increase at a lower rate, and global precipitation must balance evaporation. The evaporation rate is constrained by the amount of downward shortwave (solar) and longwave (infrared) radiation at the surface (which then goes into heating the oceans). In a warming climate, downward infrared flux at the surface increases as the atmosphere gets warmer and emits more infrared radiation upward and downwards which acts to increase the evaporation rate (Boer, 1993). The increase in evaporation/precipitation rate with climate change is estimated at 1-3% K^{-1} (Schneider et al., 2010; He & Soden, 2015; Boer, 1993), much less than the $\approx$ 7% K^{-1} increase for water vapor. The uncertainty in rate of increase of evaporation/precipitation with climate change is likely due to uncertainty in the change in incoming solar radiation due to changes in clouds (Allen & Ingram, 2002).

Another way to constrain the precipitation response to global warming is to examine the tropospheric energy budget. The tropical mean net latent heating from precipitation (net of precipitation produced and evporation of falling precipitation) must balance the radiative cooling of the free troposphere to maintain energy balance (Mitchell et al., 1987; Takahashi, 2009; O'Gorman et al., 2012; Su et al., 2017). This can be expressed in this simple relation (from O'Gorman et al., 2012):

$$\langle L\delta\overline{P}\rangle \approx \langle \delta\overline{Q}_{rad,TOA}\rangle - \langle \delta\overline{Q}_{rad,CB}\rangle, \tag{1.35}$$

which implies there is a balance between the tropical mean, time mean net latent heating of condensation in the free troposphere, and the difference in time mean radiative cooling at the top of atmosphere (TOA) and cloud base (CB). This difference in radiative cooling between the TOA and cloud base represents the total radiative cooling in the free troposphere. Note that locally, the heating from condensation does not exactly balance the radiative cooling and Q_{tot} is non-zero, this balance only holds in the tropical mean. As the planet warms, the difference in radiative cooling between the TOA and surface will increase, allowing for increased precipitation.

Since global mean precipitation is expected to increase with climate change, one might expect the tropical circulations to increase in strength as well due to the increased condensational heating. However, this has not been found to be the case with global climate models. The first study to examine the mechanisms behind the weakening of the tropical circulation with climate change was Knutson & Manabe (1995) who showed that the increased tropospheric stratification (static stability) more than offsets the increased diabatic heating means the ascending regions (regions with negative ω) of the tropical circulations must weaken (eq. 1.16). The tropical mean static stability increases due to the maximum of warming in the tropical upper troposphere because of the shift in the moist adiabatic lapse rate (the temperature profile in the tropics is nearly moist adiabatic).

More recent studies have examined other physical mechanisms for the weakening of the tropical circulation due to global warming. One popular mechanism is the weakening of upward convective mass flux due to hydrological cycle constraints (Held & Soden, 2006; Vecchi & Soden, 2007; Chadwick et al., 2012), with the weakening found to mainly be in the Walker circulation component of the tropical circulation. Held & Soden (2006); Vecchi & Soden (2007); He & Soden (2015) found that the main driver is the mean increase in SST in the CMIP5 models (Taylor et al., 2011). The mechanism is as follows: while the boundary layer specific humidity must increase at a rate dictated by the Clausius-Clapeyron relation ($\approx 7\%\mathrm{K}^{-1}$), the global mean evaporation rate is constrained to increase at a much slower rate (see section 1.1.2). Assuming that most of the moisture in convective plumes is precipitated out (i.e., parcels from the boundary layer reach all the way to the level of

neutral buoyancy with the only loss of water content from precipitation), this implies the upward convective mass flux must slow down. In other words, the updrafts are not as fast, but carry more water mass and thus the precipitation rate can be the same as in a cooler climate with faster updrafts. Using this simple model, a relation can be developed to estimate the tropical mean convective mass flux, $\langle M_c \rangle$ (Held & Soden, 2006):

$$\left\langle \frac{\delta M'}{M'} \right\rangle = \left\langle \frac{\delta P}{P} \right\rangle - \left\langle \frac{\delta q_{bl}}{q_{bl}} \right\rangle, \tag{1.36}$$

where M' is the inferred convective mass flux, P is the precipitation rate and q_{bl} is the boundary layer mixing ratio (see figure 1.3 for a schematic). Here, angle brackets represent the tropical mean. The term on the right, representing the change in the amount of moisture the atmosphere can hold, is directly related to the C-C relation and can be estimated as 0.07 per K or warming, while the precipitation term has a bit more uncertainty of $\approx$ 0.01-0.03 per K of warming. This implies that $\langle \frac{\delta M'}{M'} \rangle$ will be negative in a warmer world; in other words, the convective mass flux in the tropics will decrease.

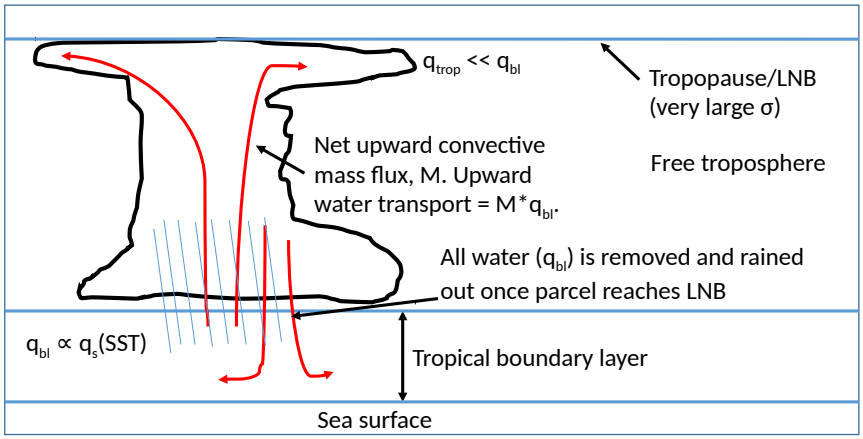

Figure 1.3: Schematic of the Held & Soden (2006) model of the hydrological cycle in the tropics.

However, this assumes that a majority of the convective mass flux in the tropics are contained in so-called "hot-towers" (Riehl and Malkus, 1958) which transport parcels rapidly from the boundary layer to the tropopause with no change in moist static energy. However, recent modeling studies using cloud-resolving models show that there are unlikely to be many parcels that make it to the tropopause undiluted (Romps & Kuang, 2010), because a significant amount of detrainment occurs above the boundary layer (Romps, 2010).

The situation is further complicated by the fact that shallow convection and stratiform rainfall accounts for a non-negligible fraction of total rainfall in the tropics (mainly in regions of cooler SST) (Schumacher & Houze, 2003). In fact, shallow convection has been shown to have its own closed circulation in the tropics (Folkins, 2008) which could open a pathway for water vapour to be recharged into the boundary layer instead of all being rained out by deep convection. If the efficiency of rainfall generation per unit of convective mass flux changes with climate change, it could, if the change is large enough, result in an increase of convective mass flux with climate change. A more general potential flaw in this line of reasoning to explain the weakening of the Hadley and Walker circulations is that while the overall upward motion may decrease in the tropical mean, it does not necessarily mean that the local circulations will necessarily weaken, because local precipitation changes can influence the circulation strength (Merlis & Schneider, 2011). Local precipitation can increase slower or faster with climate change than the tropical or global mean constraint, which arises from the constraint on the global mean evaporation response to climate change.

Often, the pressure vertical velocity, ω, is used as a proxy for the convective mass flux (such as in Vecchi & Soden (2007); Schneider et al. (2010)). However, it is not clear physically why upward ω, which is part of the large scale circulation, should be thought of as representative of the sub-grid scale convective mass flux, which is a parameterized quantity. In order to maintain hydrostatic balance in the grid box average, the mass in each grid box is conserved so any upward removal of mass due to upward convective mass flux is balanced by a compensating downward mass flux in the same grid box (Ian Folkins, personal communication). Therefore, the direct contribution to the grid box mean vertical motion from convective mass flux in a hydrostatic model such as a GCM is zero and the effect of convective mass flux on ω is only via the heating generated by condensation from convective updrafts.

Another line of thinking used to explain the weakening of the Walker circulation in response to climate change (similar to the static stability argument) uses the concept of "gross moist stability", which is outlined in Wills et al. (2017). This theory starts with the assumption that the Walker circulation strength is simply the zonally-anomalous total energy input into the ascending region (Q^*_{tot}) divided by the gross moist stability. The gross moist stability of a column can be defined as the pressure-weighted vertical integral of the vertical advection of MSE (moist static energy, hereafter referred to as h) in pressure coordinates:

$$GMS(x,y) = \int_{p_{LCL}}^{p_{trop}} \left(\frac{\partial(h(x,y,p))}{\partial p} \omega(x,y,p) \right) dp, \tag{1.37}$$

$$h = c_p T + gz + L_v q. \tag{1.38}$$

The integral is taken from the lifting condensation level (or level of free convection), to the tropopause. Outside of these regions, vertical motions are small (Wills et al., 2017). This represents the effective stability that is felt by the convection and is a measure of the efficiency of convection to transport h vertically. z is the geometric height above mean sea level or some other reference height, and q is the water vapour mixing ratio. The authors go on to show that GMS will increase in a warmer world if one makes the approximation that the vertical derivative of h becomes simply: $\Delta h = h_{trop} - h_{LCL}$. They go on to show the increase in the term gz dominates in global warming, and thus causes Δh and thus GMS to increase with global warming and the Walker circulation becomes more "efficient" at transporting h. In other words, the increase in tropopause height and thus the depth of the convection causes the GMS to increase and thus the circulation weakens because it can transport more energy per unit of mass flux. One potential flaw, that the authors themselves acknowledge, is that this theory neglects the contributions to the zonally anomalous energy input (total diabatic heating) from processes such as cloud radiative heating, which may change in warmer climate.

While there is nearly unanimous consensus among the CMIP5 models of a weakening of convective mass flux (Chadwick et al., 2012) and the tropical circulations, with the weakening of the Walker circulation being the most robust (He & Soden, 2015), studies of historical observations are inconclusive: some show that the Walker circulation may be strengthening (L'Heureux et al., 2013; Sandeep et al., 2014; Sohn et al., 2016), while others show weakening (Vecchi et al., 2006; Power & Kociuba, 2011). Additionally, modeling studies have shown little relationship between global mean convective mass flux and the strength of the Walker circulation and suggest that the pattern of SSTs and land-sea interactions may be important (Sandeep et al., 2014; Li et al., 2015). A consistent message across these prior studies is that convective parameterization could be a key factor influencing simulated trends in Walker circulation strength. This thesis attempts to determine the sensitivity of the simulated change in Walker circulation strength to the convective scheme in a single GCM.

1.3 Objectives and research questions

This project was inspired by Sohn et al. (2016) which argues that the CMIP5 models have unrealistically large values of static stability in recent decades and thus have a weakening trend in the Walker circulation that is not observed. They also speculate that this stabilization trend is likely related to the parameterization of convection. Therefore, some research questions that could be answered using this scheme are: does the convective scheme have a

significant impact on the representation of the tropical circulation in a general circulation model in today's climate? Does the scheme also affect the response of the the tropical circulation to climate change? Does the tropical mean convective mass flux weaken as shown in other studies? Since the IF scheme is much different than the ZM/Hack schemes used in the CAM4 (as will be outlined in chapter 2), one might expect there would be differences in the simulation of the tropical circulations when this new scheme. The improved temperature/static stability profile may also lead to an improved simulation of the tropical circulations. Therefore, the null hypothesis would be that switching convective schemes has no impact on the tropical circulations, whether in modern climate, or in future ones.

To test this hypothesis, we can run simulations of the CAM4 with the default convective scheme and ones with the IF scheme. We can run both "control" simulations for the modern climate, and those for a warmer climate. Since existing literature has shown that the increase in global mean SST and thus increase in near surface water vapour is the main driver of the slowdown of the tropical circulations under climate change (Held & Soden, 2006; Ma et al., 2011; Vecchi & Soden, 2007; He & Soden, 2015), we can conduct experiments where we simply raise the global mean SSTs by a uniform amount to test the tropical circulation response to global warming.

Chapter 2

Data and methods

2.1 The NCAR CAM4 model

To perform the simulations for this thesis, the CAM4 (Community Atmosphere Model) general circulation model (GCM) from NCAR was used (Neale et al., 2013). An in-depth technical description of the model is described in Neale et al. (2010). The CAM4 is a global, hydrostatic, full atmosphere model using an Eulerian dynamical core and is typically used for climate simulations, but has no ocean model component for atmosphere-ocean coupling. The CAM4 is part of a larger model package, which includes ocean and ice sheet models, called the CESM (Community Earth System Model, Kay et al. (2014)). For this thesis we will perform atmosphere-only experiments using version 4 of the CAM (CAM4) from version 1.0.2 of the CESM (release summary here: http://www.cesm.ucar.edu/models/cesm1.0/tags/#CESM1_0_2). The IF scheme Fortran code has been uploaded by the author to github.com[1] and is only known to work with CESM 1.0.2. The CESM (and its predecessor, CCSM) is included in the CMIP3/5 suite of models used for the IPCC (Taylor et al., 2011).

All simulations used 26 vertical levels with a 1.9x2.5° resolution lat/lon grid (the f19_f19 finite volume grid). In all the simulations discussed in this thesis, the finite volume (FV) dynamical core was used in the CAM4. To perform the simulations, a system with a large amount of CPUs was necessary to ensure timely completion. For this task, the GPC cluster on the SciNet system at the University of Toronto was chosen (http://www.

[1] github repository URL (Fortran code created by Ian Folkins): https://github.com/CAM4-IF/thesis/tree/master/CAM4-IF

scinethpc.ca/gpc/). Generally, the simulations were run using 64 processors for 48 hours to complete a 30-year simulation. Higher resolution simulations ($\approx 1^{\circ}$) were performed to test the sensitivity of the results to simulation, but no significant differences were found in the solutions for the mean-state tropical climate, and were unlikely to justify the much increased computational cost.

2.1.1 Zhang-McFarlane deep convective scheme

To simulate moist convection in a global climate model with a horizontal resolution large than $\mathcal{O}(\ 10$ km), a parameterization scheme is needed as the convective cells would be smaller than the grid spacing (dx) used in most GCMs today (dx $\mathcal{O}(\ 100$ km)) (see figure 2.1). This is in contrast to large scale precipitation produced by the large scale circulation produced by clouds of large horizontal extent, where much larger grid scales are sufficient and the atmosphere can be approximated as being hydrostatic. Even today, many decades after the first convective scheme was devised by Arakawa and Schubert in 1974 (Arakawa & Schubert, 1974), they are still being used in GCMs because the resolution has not increased to a level in which convection can be explicitly resolved. This will remain the case for at least the near future, as most GCMs (for climate simulation purposes) do not have a grid mesh much finer than $dx \approx 25$ km, and most are much coarser.

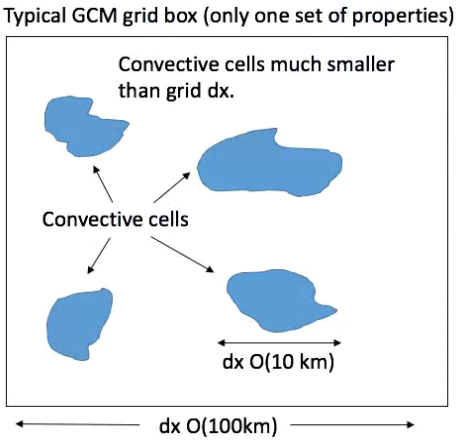

Figure 2.1: Schematic of a typical scenario in the tropics where the convective cloud cells are much smaller than the size of a GCM grid box dx.

A convective scheme uses "mass flux closure" to relate large scale environmental vari-

ables to the sub-grid scale convective plume updrafts and vice-versa. The total convective mass flux in a grid box, M_c, can be defined simply as follows (if the grid box is composed of n parcels with different convective mass fluxes):

$$M_c = \sum_{i=1}^{n} \rho_p w_p f_p, \tag{2.1}$$

where ρ_p is the density of the parcel, w_p is the vertical velocity (in Cartesian coordinates) of the parcel and f_p is the fractional area of the grid cell occupied by that particular parcel.

The large scale variables in each grid box (convective mass flux, relative humidity, temperature, etc.) take on the grid-box average of the sub-grid variables. In other words, the scheme uses mass flux closure to determine a unique grid-box averaged convective mass flux given the grid-box environmental variables. The scheme used in the CAM4 (ZM or "Zhang-Mcfarlane" scheme) (Zhang & McFarlane, 1995) uses CAPE (see eq. 1.8) as the (sole) environmental variable for mass flux closure. The CAM4 actually uses two convective schemes; the main one for deep convection and the other for shallow convection. This shallow scheme, the "Hack" scheme (Hack, 1994) handles shallower convective plumes that do not span the whole depth of the troposphere. In this section we will just focus on the ZM scheme, however.

The ZM scheme uses an ensemble "plume" approach where a spectrum of updrafts are created in each grid box with the same cloud base updraft mass flux (M_{cb}) (Neale et al., 2010, p.89). Each plume has a different total fractional entrainment rate (i.e., the rate of mixing of mass of drier environmental air into the plume), λ, and thus above the cloud base the plumes will have a variety of different updraft mass fluxes (λ appears to represent the total amount of entrainment through the entire plume). This means that this is a dilute plume parameterization, with dilution with the environment taken into account. Detrainment of the plume into the environment is limited to the very top of the convective plumes and this height is defined as z_D. The updraft mass flux, M_u, for the ensemble mean is defined as a function of z (Neale et al., 2010, p.90) and (Zhang & McFarlane, 1995):

$$M_u(z) = M_{cb}\left(\frac{e^{\lambda_D}(z_D - z) - 1}{\lambda_0(z_D - z)}\right). \tag{2.2}$$

λ_D is the specific entrainment rate of of that plume at a given height, z, which is a function of the total factional entrainment rate λ assigned to the plume, with smaller values of λ reaching higher z_d because less buoyancy is lost in the plume. λ_0 is the detrainment rate for the shallowest convective plumes and is the largest entrainment rate in the ensemble.

All that is needed is to find M_{cb} and assign a λ to each of the plumes in the ensemble. To calculate the cloud base updraft mass flux in the ZM scheme, a simple mass flux closure relation based on quasi-equilibrium theory (see 1.1.4) is used (Neale et al., 2010, p.93):

$$\frac{\partial(\text{CAPE})}{\partial t} = -M_{cb}F, \tag{2.3}$$

where,

$$M_{cb} = \frac{\text{CAPE}}{\tau F}. \tag{2.4}$$

Here, F is the rate of consumption of CAPE per unit of M_{cb} and τ is the timescale for CAPE consumption. Using these two relations we can define the CAPE consumption rate as:

$$\frac{\partial(\text{CAPE})}{\partial t} = -\frac{\text{CAPE}}{\tau}. \tag{2.5}$$

These relations provides a simple relationship between CAPE and the starting (cloud base) mass flux in the CAM4 model. In this way, the CAPE consumption rate increases as CAPE increases and the cloud base convective mass flux increases and convection is a self-limiting process. Moist convection will only occur when CAPE is positive and above a small threshold value in this scheme.

The deep convective precipitation production, P_{prod}, can be determined from the updraft mass flux as (Zhang & McFarlane, 1995):

$$P_{prod}(z) = C_0 M_u(z) l(z), \tag{2.6}$$

where $C_0 = 2 \cdot 10^{-3} m^{-1}$ is a liquid to rain conversion constant, and l is the liquid water content. Thus, the deep convective precipitation production in this scheme is linearly proportional to the updraft mass flux. An important approximation made in this scheme is that P_{prod} below the freezing level is 0, and thus the plumes must extend above this level to produce precipitation (Zhang & McFarlane, 1995).

The downdraft parameterization in this scheme is the similar to that as for updrafts to originate only where $P_{prod} > 0$, which would be above the freezing level only. The ensemble mean downdraft mass flux, M_d as a function of z is given as (Zhang & McFarlane, 1995):

$$M_d(z) = \alpha M_{cb} \left(\frac{e^{\lambda_D}(z_D - z) - 1}{\lambda_0 (z_D - z)} \right), \tag{2.7}$$

where the variables here are the same as before, with α being a proportionality constant to ensure that the net cloud base mass flux of the ensemble is positive and is defined as:

$$\alpha = 0.2\left(\frac{[P_{prod}]}{[P_{prod}] - [E]}\right), \tag{2.8}$$

where $[P_{prod}]$ is the vertically integrated precipitation production in the cloud and $[E]$ is the vertically integrated evaporation. The largest value α can have is 0.2, and the lowest is 0 if there is not precipitation. This relation ensures that the downdraft mass flux is no more than 0.65 of the updraft mass flux (Zhang & McFarlane, 1995). The convective precipitation evaporation rate locally in the CAM4 is simply a function of relative humidity and is defined as (Neale et al., 2010, p.102):

$$E = K_E(1 - RH)(P_{flux})^{0.5}. \tag{2.9}$$

K_E is a constant (taken to be $0.2 \cdot 10^{-5}$ (kg m^{-2} s^{-1})$^{-0.5}$s^{-1}), RH is the relative humidity, and P_{flux} is the local convective rainfall flux which is a total of rainfall received from levels above. As the rainfall rate increases, the evaporation rate will go up as the square root of the rainfall rate, and the evaporation rate will also increase as relative humidity decreases. Thus, downdrafts are stronger for regions which have higher rainfall rates, for the same relative humidity. Note that the convective scheme parameters τ, K_E, α and C_0 are somewhat "tunable" and some studies (such as Yang et al., 2013) have looked at tweaking these parameters to create an improvement in the simulated climate in the tropics.

2.2 IF convective scheme

An alternate convective scheme being developed by Ian Folkins at Dalhousie University ("IF scheme") will be used in the simulations to test the sensitivity of tropical dynamics in the CAM4. This scheme was originally designed to improve the diurnal cycle of rainfall over land (Folkins et al., 2014), and is now being developed to improve the simulation of the tropical temperature profile and the simulation of the MJO. One reason to desire a better tropical temperature profile is so that models can better simulate CAPE in the tropics and thus give better confidence to the simulation of tropical updrafts and downdrafts. Also, an improved static stability profile should lead to a better representation of the Hadley and Walker circulations, assuming the distribution of diabatic heating is not degraded (Sohn et al., 2016; Mitas & Clement, 2006). Since this model is still under development, there is

much room to tweak and play with different parameters in the model which makes it ideal for sensitivity studies. The description of the scheme in this section is based on personal communication with Ian Folkins, Folkins et al. (2014) and a paper that Ian Folkins is currently writing.

There are major differences between the IF scheme and the ZM scheme. The most fundamental would be that the IF scheme handles both shallow and deep modes of convection together, with the same mass flux closure. Also, in the IF scheme, no longer is the convective mass flux simply a function of CAPE, but also is a function of the rainfall rate of the previous timestep and the convective mass flux type is partitioned into shallow and deep (Ian Folkins, personal communication) and this removes the need for having a separate shallow convective scheme. Additionally, parcels are lifted from the 4 lowest model levels with positive CAPE, not just the lowest model level (Folkins et al., 2014). Another important note about this scheme is that the default cloud microphysics scheme is replaced in regions where this scheme is activated. This scheme will be described briefly in this section as well. This cloud scheme has been set-up to run from 38°S-38°N *and* regions where CAPE calculated from the surface is > 0.

2.2.1 Updrafts

The starting mass fluxes for a spectrum of parcels is calculated at each of the 4 lowest levels (i) and the mass per unit area, M_i, is defined as (Folkins et al., 2014):

$$M_i = \begin{cases} f_s(P)A(P)\left(\frac{\Delta t}{\tau}\right)\left(\frac{\text{CAPE}_i}{\text{CAPE}_{scale}}\right)\left(\frac{dp}{g}\right) & \text{Shallow modes} \\ (1-f_s(P))A(P)\left(\frac{\Delta t}{\tau}\right)\left(\frac{\text{CAPE}_i}{\text{CAPE}_{scale}}\right)\left(\frac{dp}{g}\right) & \text{Deep modes,} \end{cases} \tag{2.10}$$

where $f_s(P)$ is a sigmoidal function (varying from 0 to 1) of the precipitation rate of the previous time step that is used to determine the fraction of mass flux for the shallow modes with the remaining fraction the amount of mass in the deep modes. $A(P)$ is a so-called "amplification factor", which is again a sigmoidal function that is dependent on the precipitation rate of the previous time step. Δt is the time step and τ is the timescale for CAPE consumption (same as in the ZM scheme) which is set to 30 hours in this scheme. CAPE_i is the CAPE of the specific parcel, and CAPE_{scale} is set to 500 J kg^{-1}. dp is simply the pressure thickness of the grid box.

The sigmoidal functions, $f_s(P)$ and $A(P)$ are defined in the following way:

$$A(P) = A_{min} + \frac{A_{add}}{1 + e^{-P_{norm}}}, \tag{2.11}$$

$$f_s(P) = \left(A_{min_s} + \frac{A_{add_s}}{1 + e^{-P_{norm_s}}}\right), \tag{2.12}$$

with A_{min} and A_{add} are prescribed parameters, with P_{norm} defined as:

$$P_{norm} = \frac{P - P_{half}}{P_{scale}}, \tag{2.13}$$

where P_{half} is the value of P for which $A(P) = A_{min} + \frac{A_{add}}{2}$ and P_{scale} is a prescribed scaling factor. The parameters take on different values in the two formulations, with A_{add_s} usually set to -1. This sigmoidal amplification factor approaches 1 (0 for $f_s(P)$) at higher rain rates, and thus $f_s(P)$ (the fraction of the shallow modes), approaches 0 at high rain rates, and all of the mass flux is in the deep modes (from eq. 2.10). The limit of the amplification factor is $A_{min} + A_{add}$. This method of mass flux closure method causes mass flux and rain rates to have a certain "memory" and causes regions of strong convection to cluster and this is thought to be physically realistic (see Mapes, 1993). This self-organization may not occur in the ZM scheme from the mass flux closure. Some examples of $A(P)$ functions for various values of the parameters are shown figure 2.2:

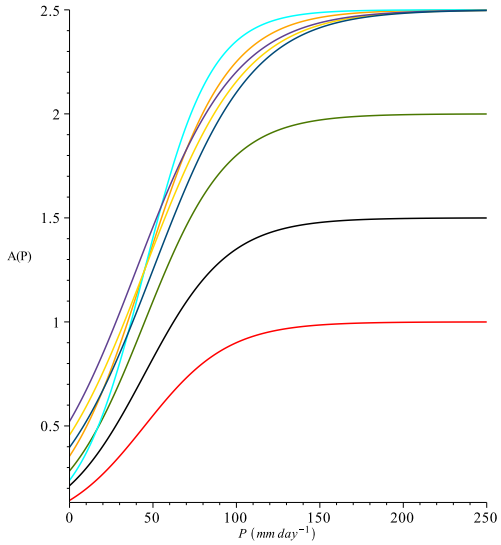

Figure 2.2: Example of various $A(P)$ functions with different (typical) values for the parameters. In all cases, A_{min} is set to 0, and A_{add} sets the top vertical asymptote. P_{half} varies from 45 to 50 and P_{scale} is either 25 or 30 and this sets the width of the region between the minimum of $A(P)$ and A_{add}. The values of A_{add}, P_{half} and P_{scale} are, 2.5, 45 mm day^{-1} and 25 mm day^{-1}, respectively, for both versions of the CAM4-IF (orange line).

After the starting updraft parcel mass spectra (shallow and deep) are defined eq. 2.11 the parcel will entrain environmental air from the outside environment which reduces buoyancy until a certain target buoyancy is reached and the parcel will then completely detrain once the buoyancy is < 0. If there is enough condensate in the parcel, it will begin to precipitate at any level (whereas in the ZM scheme convective precipitation is confined to above the freezing level). As the parcel rises, the parcel condensate detrains into the background atmosphere as a function of relative humidity:

$$E_{det} = f_{det}(RH_{det} - RH)dz, \tag{2.14}$$

where f_{det} is a prescribed parameter and if the environmental RH is above RH_{det} (RH_{det}=0.82), the E=0. For the parameterization of precipitation, first, there is a certain fraction of the updraft condensate that is removed at each level (0.24 for the deep modes and 0.30 for the shallow modes). What happens with this removed condensate then depends on the environmental relative humidity. If it is above 0.65, all of this condensate becomes precipitation, and if it is below 0.40, it is all evaporated and for values between, a linear interpolation to determine the fraction of evaporation to precipitation is used. If the environmental temperature at the level which detrainment occurs is below 0, and the background RH is

above 0.40, then some fraction of this condensate becomes so called "anvil snow" and this fraction f_{an} is determined, again, by a sigmoidal function which depends on P. This falling anvil snow can then produce downdrafts when it falls through the melting level.

2.2.2 Downdrafts

Downdrafts can be produced in two ways in the CAM-IF. The first way to generate a downdraft is in the region below the melting level. To generate a downdraft here, from either evaporating precipitation or detrained condensate, the relative humidity needs to be below a threshold level of 0.88. Similar to the ZM scheme, the local evaporation rate (kg m^{-2}) is in fact a function of the local precipitation rate (see eq. 4.2.2) (Ian Folkins, personal communication). However, in this case the relationship is linear, and there is a also a linear dependence on the saturation mixing ratio. The evaporation parameterization in the IF scheme is as follows (Ian Folkins, personal communication):

$$E = kq_s A_{RH} m_{layer} P \Delta t, \tag{2.15}$$

Where k is a constant which is 0.05 for rain generated from updrafts and 0.10 for downdrafts generated from anvils, q_s is the saturation mixing ratio inside the downdraft parcel, A_{RH} is another sigmoidal parameter, m_{layer} is the mass of the grid cell per unit area. The other variables have the same definitions that have been defined previously. The amplification factor, A_{RH} is defined as (0 for parcel RH below 0.9):

$$A_{RH} = 0.1 \cdot log\left(1 + \frac{0.9 - RH_{parcel}}{0.1}\right). \tag{2.16}$$

This factor effectively sets the dependence of the downdraft evaporation rate to relative humidity. The downdraft parcel then descends so long as its effective buoyancy, b_{test}, is negative. b_{test} is defined in the CAM4-IF as:

$$b_{test} = 0.5(b_i + b_{i+1}) + b_r. \tag{2.17}$$

b_r is a fudge factor that is meant to represent the extra negative buoyancy due to the mass of the precipitation in the parcel and is set to -0.02 m s^{-2}, b_i is the parcel buoyancy at level i after taking into account the evaporation at that level and b_{i+1} is the buoyancy once the parcel is moved to the level below.

Another source of downdrafts originates from the melting level, and are assumed to form from melting snow precipitating down from the anvils above. These downdrafts are

parameterized in exactly the same method as described above for the downdrafts below the melting level, except they can only descend a maximum of two levels and have an extra "boost" from the latent heat (cooling) of melting. These downdrafts are only initiated in the first level below the melting level (taken to be 273K). All the snow from above is assumed to melt and then the rain in the parcel can evaporate in the same manner as described above.

2.2.3 Cloud scheme

As mentioned previously, the cloud scheme in the CAM4 is also replaced with the IF scheme in regions equator-ward of 38°N/S. The largest radiative effect is seen from the cloud ice aspect of the scheme (Ian Folkins, personal communication) and I will briefly discuss this here. There are two contributions to ice clouds in the new scheme; detraining ice condensate from the convective scheme, and in-situ cloud that forms in regions where the relative humidity with respect to ice is high enough (above 0.80). The vertical profile of detraining ice condensate has a Gaussian shape and the mass mixing ratios of cloud ice from detrainment and in-situ formation are defined as follows:

$$q_{ice,det}(z) = q_{ice,tot} e^{\left(-\left(\frac{z-12}{\Delta z}\right)^2\right)}, \tag{2.18}$$

for the ice mass mixing ratio from detrainment, and:

$$q_{ice,in}(z) = q_{scale}(RH_{ice} - 0.80) log\left(1 + \frac{q_{s,ice}}{q_{scale}}\right), \tag{2.19}$$

for the ice mass mixing ratio for in-situ ice cloud. Here, the height, z, is in units of km, for simplicity. For heights above 12km, Δz=2.25km and Δz=4.0 km for levels below this height. $q_{ice,tot}$ is the total detrained ice mass mixing ratio which is then distributed vertically in the Guassian profile. RH_{ice} is the relative humidity *with respect to ice* at the level, z, and for RH_{ice}-0.80 < 0, $q_{ice,in}$ is set to 0. $q_{s,ice}$ is the environmental saturation mixing ratio with respect to ice (which is lower than q_s) at that level and $q_{scale} = 2.0 \cdot 10^{-5}$.

Finally, this new ice scheme replaces the default Kristjansson scheme which relates the particle effective radius of ice particles (Kristjnsson et al., 2000) in the CAM4 (see pg. 123-124 and figure 4.2 of Neale et al. (2010)) to temperature with a different relation described in Garrett et al. (2003). This parameterization of the effective radius assumes smaller particles which absorb more solar radiation and this has an impact on the cloud radiative heating rate in the upper troposphere (as we will show in future sections).

2.2.4 Model tuning

Since this scheme is still under development, the scheme has gone through a number of iterations. Most of these iterations were simply adjustment of parameters, mainly to improve the tropical temperature profile, or to improve tropical precipitation. Other iterations, however, involved significant code changes. Some of the parameters that were changed from previous versions were A_{add} (see eq. 2.11) which affects the amplitude factor in the mass flux closure and q_{scale} (see eq. 2.18) which controls the amount of ice detrained into the upper troposphere and thus affects shortwave and longwave heating there. Also, the parameter b_r (see eq. 2.17) which controls the strength of downdrafts below the melting level, is another parameter that was changed in previous versions of the model. The Garrett ice crystal parameterization of the effective radius mentioned in the previous section can be turned on or off if needed gives a larger amount of shortwave heating in the upper troposphere. Together, these parameters can help tune the modeled tropical temperature profile and precipitation.

The version that we will refer to as "CAM4-IF-t" in this thesis is the version with the most realistic tropical temperature profile, and uses the "default" version of the scheme where all parameter values are the same as described in the previous three subsections. We also constructed an alternative version of the CAM4-IF model, which features a tropical time mean rainfall pattern somewhat closer to observations (see figure 3.3), but a slightly degraded tropical temperature profile (see figure 3.2). The purpose of this is to test the sensitivity of the circulation response to the representation of the time mean tropical rainfall in the control simulation. In the "CAM4-IF-r" version, downdrafts below the melting level are turned off by turning up b_r to 6 m s^{-2} which effectively prevents any downdrafts that form from penetrating down to the lower levels, i.e., negative buoyancy is artificially cut off below the melting level in this version. This version produces a somewhat better tropical rainfall pattern, but a slightly degraded tropical mean temperature profile. Most of the differences between previous versions are quite incremental and may not have many statistically significant differences in the simulation of aspects of the tropical climate.

2.3 Reference datasets

2.3.1 Observation-based products

The main goal of recent iterations of CAM-IF is to create a realistic tropical temperature profile. To do this, one needs to have a good observational dataset in the deep tropics.

Since reanalysis likely has errors in the representation of the structure of tropical temperature (Mitas & Clement, 2006), high-resolution radiosonde data is preferred for model validation. So, here we use data from the SPARC US high-resolution radiosonde archive (Love, 2013) from a number of islands in the tropics (mainly in the tropical western Pacific) for comparison to profiles of model vertical profiles of temperature. Below is a table and map of the sites for which data is available for:

Table 2.1: SPARC high-resolution US tropical radionsonde sites used in this thesis

Radiosonde site	Lat	Lon
GUA - Guam	13.55°N	144.80°E
HIL - Hilo, Hawaii	19.72°N	204.93°E
JUA - San Juan, Puerto Rico	18.43°N	294.00°E
KOR - Koror, Palau	7.33°N	134.48°E
LIH - Lihue, Hawaii	21.98°N	200.65°E
MAJ - Majuro, Marshall Islands	7.08°N	171.38°E
PAG - Pago Pago, American Samoa	14.33°S	189.28°E
PON - Pohnpei, Micronesia	6.97°N	158.22°E
TRU - Truk Lagoon, Micronesia	7.47°N	151.85°E

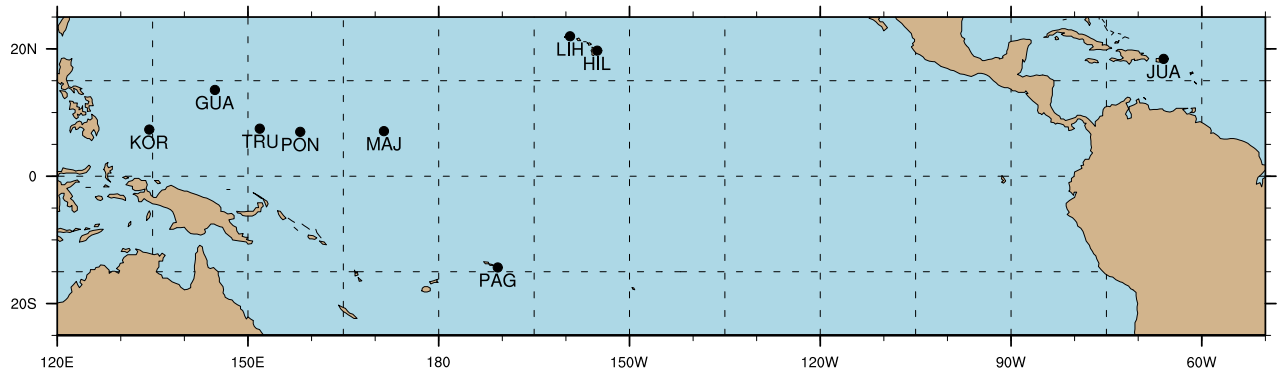

Figure 2.3: Map of tropical radiosonde sites from the SPARC US high-resolution radiosonde archive that are indicated in table 3.1.

However, the radiosonde dataset is quite limited spatially, and although temperature variations in the tropics are small (see section 1.2.1), to gauge tropical mean quantities, a more continuous dataset is needed. So we will use reanalysis data for comparison of

simulations to modern climate as well. There are a variety of reanalysis datasets available, however, the MERRA (from NASA) and ERA-Interim (from ECMWF) reanalyses are thought to have the most accurate representation of the climate since 1979. Also, we have climate model simulations from the CMIP5 AMIP (Atmospheric Model Intercomparison Project) model suite (Taylor et al., 2011) that we can use to compare with our climate simulations of the modern climate (AMIP models are atmosphere-only runs like the ones we have performed here). Combined, the radiosonde data, reanalysis data and other GCM model data can help gauge if the IF scheme is improving on, or degrading the modern tropical climate in the CAM4 model compared to observations and other models.

Historical precipitation data is available in a variety of forms, rain gauges, satellite data (since 1979) and reanalysis data. All datasets will have random and systematic errors/biases (e.g., errors in measurements from observations, biases in the model used for reanalysis, biases in the data assimilation used for the reanalysis model, interpolation errors, and attenuation errors in satellite retrievals, to name a few). Also, it has been suggested that rainfall in the GPCP precipitation product is likely biased too low when the global mean energy budget is considered (Trenberth et al., 2009; Trenberth & Fasullo, 2013). This likely is also the case in TRMM and other satellite datasets as they also have similar tropical mean values to GPCP. So here we take a blend of 6 precipitation datasets to use to compare our simulations with in the modern climate. Information on these datasets is detailed in the table below:

Table 2.2: Datasets used to create a blend of observational datasets for mean tropical precipitation. All datasets were given equal weight in this blend and the land only data, PREC/L, was included for land gridpoints only. The MERRA/ERAI datasets are also used for other atmospheric variables in this thesis.

Dataset name	Time period	Citation	Type
CMAP	1979-1998	(Xie & Arkin, 1997)	Satellite and rain gauge
GPCP	1979-2009	(Adler et al., 2003)	Satellite and rain gauge
TRMM	1998-2009	(Liu et al., 2012)	Satellite
MERRA	1979-2013	(Rienecker et al., 2011)	Reanalysis
ERA-Interim	1989-2005	(Dee et al., 2011)	Reanalysis
PREC/L	1948-2001	(Chen et al., 2002)	Rain gauge

2.3.2 CMIP5 AMIP simulations

In addition to observational datasets, other climate model simulations are also used for comparison. The CMIP5/CFMIP AMIP (Atmospheric Model Intercomparison Project and Cloud Forcing Model Intercomparison Project) (Bony et al., 2011) models were used as they are performed in a similar manner to our simulations with a time series of monthly observed SSTs with no ocean model. Also, the AMIP4K (AMIP SSTs, but with a 4K uniform SST warming) simulations were used for some variables as well, to compare with the +4K SST simulations. The AMIP models that were used in this thesis are outlined in the table below, along with what variables were available:

Table 2.3: AMIP model list. Asterisks indicate variable was available, and dashes indicate it was not.

		Variables available		
Model name	Institution	u/v wind	temperature	precipitation
ACCESS1-0	CSIRO	-	*	-
bcc-csm1-1	BCC	-	*	*
CanAM4	CCCma	*	*	*
CCSM4	NCAR	*	*	*
CESM1-CAM5	NCAR	*	*	*
CNRM-CM5	CNRM-CERFACS	*	*	*
CSIRO-Mk3-6-0	CSIRO	-	*	-
FGOALS-g2	LASG-CESS	-	*	*
GFDL-CM3	NOAA GFDL	-	*	-
GISS-E2-R	NASA GISS	-	*	-
inmcm4	INM	-	*	-
IPSL-CM5A-LR	IPSL	*	*	*
IPSL-CM5A-MR	IPSL	-	*	*
IPSL-CM5B-LR	IPSL	*	*	-
MIROC5	MIROC	*	*	*
MIROC-ESM	MIROC	-	*	-
MPI-ESM-LR	MPI-M	-	*	*
MPI-ESM-MR	MPI-M	-	*	*
MRI-CGCM3	MRI	*	*	*
NorESM1-M	NCC	-	*	-

2.4 Experimental design

We conduct experiments with the CAM4 default, and CAM4-IF versions, where repeating climatological monthly mean SSTs (an average over the years 1981-2001 from HadISST (Rayner et al., 2003) are imposed as the lower boundary condition (i.e. the ocean surface temperatures are a function of the month, not the year). To perform the +4K SST simulations (to test the sensitivity of the tropical circulations in the model to climate change using a different convective scheme), a 4K offset was simply added to this control SST boundary condition file. A uniform 4K SST warming experiment is used in the "AMIP4K" experiments in the CFMIP project of CMIP5 (Bony et al., 2011). These type of atmosphere-only simulations allow us to isolate the affects of the convective scheme on the tropical circulation, with no coupling with the ocean to complicate things. Many other earlier iterations of the CAM4-IF model have been run, and these are included in some sections in the thesis. The particular component set (compset) used was the F_2000 compset. This component set uses repeating prescribed monthly mean sea surface temperatures and sea ice with no year-to-year variations. Also atmospheric CO_2 and other greenhouse gasses are fixed (CO_2 concentrations are fixed at 367 ppm, CH_4 at 1760 ppb).

Additionally, AMIP-type experiments (Taylor et al., 2011) were performed using a time-series of monthly SSTs (again, from HadISST) for 1998-2005. These type of simulations were used for comparison to radiosonde observations as the time period of these observations is only from 1998-2011, so using a monthly average for years 1981-2001 would not be adequate. The AMIP-type experiments used the F_AMIP compset, where CO_2 is not fixed, and real monthly mean atmospheric CO_2, and other greenhouse gas, concentrations are used. These runs were used to compare against radiosonde observations. Model output was in monthly mean NetCDF files and post-processing was performed using NetCDF Operators (NCO - http://nco.sourceforge.net/) and Climate Data Operators (CDO - https://code.zmaw.de/projects/cdo).

Chapter 3

Influence of convective scheme: present climate

Before examining the differences in the uniform 4K SST warming response of the CAM4-IF compared to the CAM4, we first examine how the CAM4-IF compares to the CAM4 default in the present climate. If there are larger biases in CAM4-IF than CAM4 default, it could call into question any conclusions made about this new models' response to climate change. Even if these were the case, however, it could still prove to be a helpful idealized model in understanding tropical dynamics. The purpose of this chapter is to study the CAM4-IF in the modern climate to see if it has a significantly worse mean-state when compared to observations than the CAM4 default.

In this section we will show that some biases in CAM4-IF are larger than those in CAM4 default, but not large enough to completely call into question the IF scheme's representation of convection and the tropical variables we are most interested in (temperature, precipitation and winds), are comparable to or in fact better simulated compared to observations than the CAM4 default. Since most of the dynamics in the tropics are driven by convection as baroclinic instability is almost entire absent due to small temperature gradients, any change in the scheme could be expected to produce differences in the simulation of tropical phenomenon (but perhaps may not change tropical mean quantities, though). The biggest issue with the IF scheme appears to be an overactive South Asian Summer Monsoon (SASM, Fan et al. (2012)). In this section, we will compare the modern simulations from the default CAM4 to the two versions of the CAM4-IF (CAM4-IF-t and CAM4-IF-r) outlined in the previous section.

3.1 Tropical temperature profile

Generally, biases in time mean temperature ($\overline{T}$) in the tropical troposphere are small (usually less than 1-2K) in the tropics in the three CAM4 control simulations. However, it is the vertical derivative of temperature (the lapse rate), that is more important to the large circulations (as this is proportional to the static stability). Although it is often assumed the tropical mean temperature profile is essentially pseudoadiabtic (Emanuel, 2007), there are some small deviations, such as around the melting level ($\approx$ 500 hPa or 18000 feet above sea level in the tropics, though there is some variation) and in the lower troposphere (Folkins, 2013) (see figure 3.1 for an example of real deep tropical lapse rates compared to a moist adiabat). We see that the tropical mean lapse rate profiles (figure 3.2**c**) of the three models are all qualitatively similar and close to reanalysis, and have the same deviations from the pseudoadiabat seen in figure 3.1. However, the $\overline{T}$ profile in the CAM4-IF-t version is improved over the CAM4 in the deep tropical convecting regions, with the CAM4-IF having a lower pressure-weighted RMSE at most SPARC deep tropics radiosonde sites than all the AMIP model members (see figure 3.2 and table 3.1). This also extends to the tropical mean lapse rate profile as well (figure 3.2**c**). This would indicate that the CAM4-IF has a better representation of the tropical mean static stability, σ.

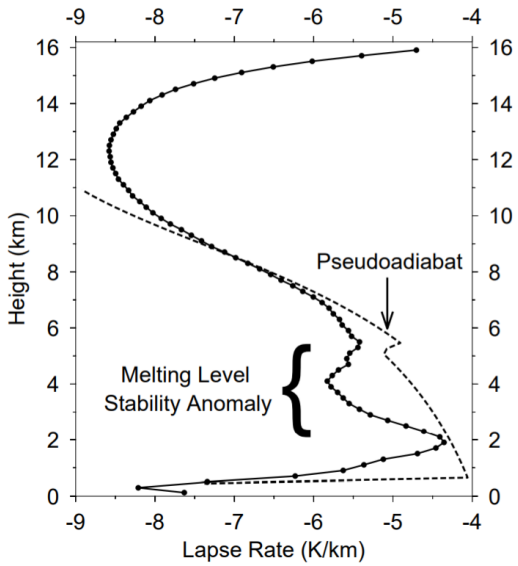

Figure 3.1: Figure 3 from Folkins (2013) (used with permission). The solid dark curve represents an average the time mean lapse rate of five radiosonde stations in the far western Pacific (same as in figure 2.3 from 1998-2009. The dashed line indicates the curve for a parcel rising pseudoadiabatically from the surface with a temperature of 299.5 K and a relative humidity of 80%.

Generally, most AMIP models have a lower tropospheric cold bias and some models have an even larger upper tropospheric cold bias (maximum around 850 hPa), while the CAM4 has a mid tropospheric warm bias (maximum around 500 hPa). This would lead to an improvement of the lapse rate ($\frac{\partial T}{\partial z}$) profile as well and is seen in figure 3.2**b** and **c** at Koror and in the tropical mean. See table 3.1 for root-mean-squared error values for eight other SPARC radiosonde sites in the deep tropics. Note that in the deep tropics, due to the WTG approximation (see chapter 1), horizontal temperature variations in the free troposphere are small over large distances, and using one radiosonde site to represent an entire grid box of $\approx$ 200x200 km should be a reasonable approximation and this is what was done here.

I discussed in section 1.2.1 about how the tropical mean static stability is important for the strength of the tropical circulations, especially the Walker circulation. Since the time mean static stability (integrated through the troposphere) is determined by $\frac{\partial \overline{T}}{\partial z}$, ensuring the vertical profile of $\overline{T}$ is as close to observations as possible in a climate model should help in the correct representation of the strength of the tropical circulations in a climate model (all else being equal) (Sohn et al., 2016; Mitas & Clement, 2006). Also, an improved tropical temperature profile would lead to an improved geopotential height field, and thus an improved representation of the circulation in the tropics. It would appear that the CAM4-IF is fairly successful at improving the $\overline{T}$ profile over the default CAM4, and is better than all the AMIP members at many radiosonde sites in the deep tropics.

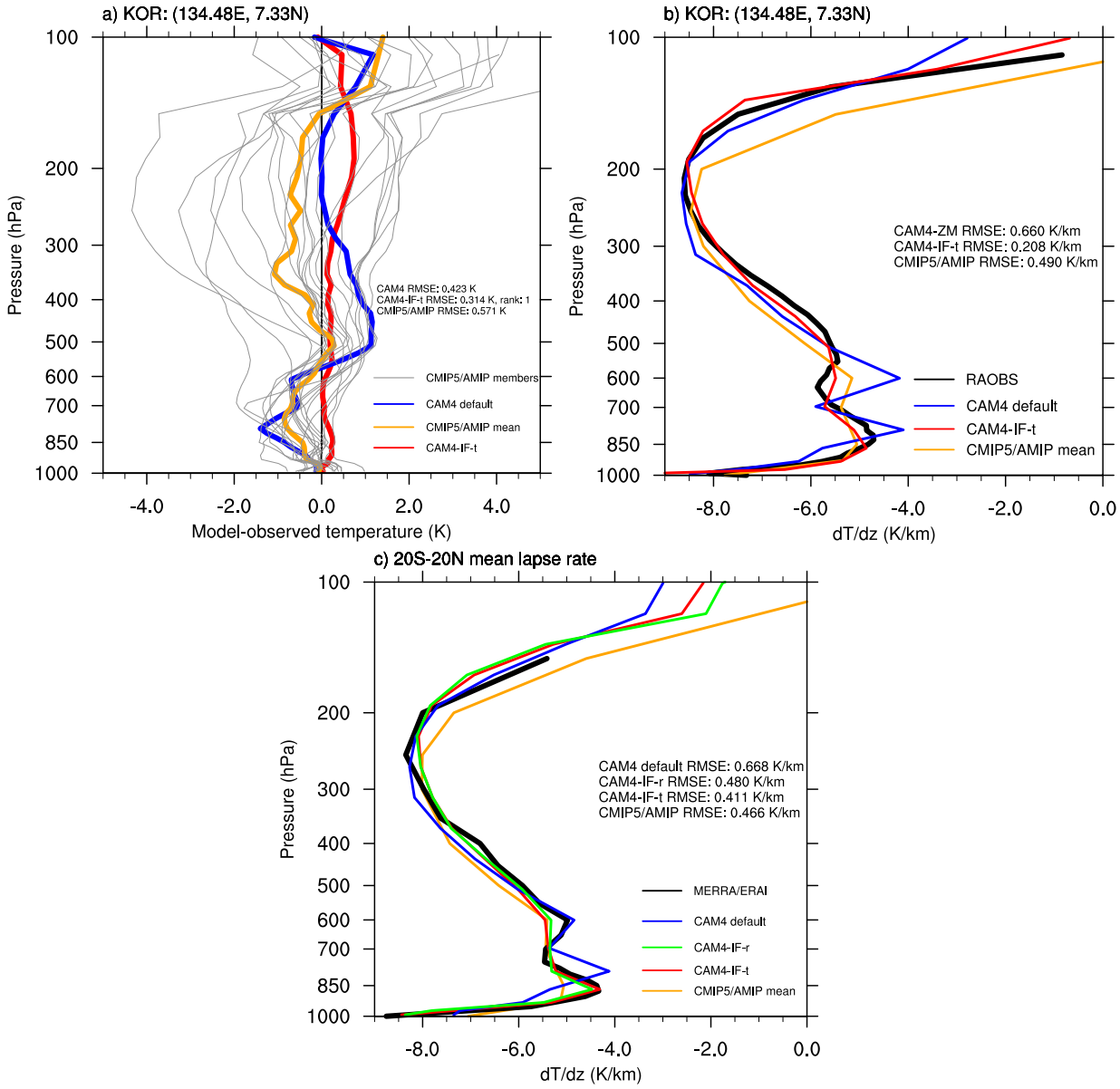

Figure 3.2: **a**: Time mean (1998-2005) model minus observed temperature profile for Koror (see table 2.1. **b**: Time mean Koror lapse rate profile ($\frac{\partial \overline{T}}{\partial z}$) for the CAM4 default, CAM4-IF-t and the CMIP5 AMIP multi-model mean compared to radiosonde data (RAOBS). **c**: Time mean, 20°S-20°N mean lapse rate for the three CAM4 models, and the CMIP5 AMIP multi-model mean compared to a MERRA/ERA-interim reanalysis blend. Overall, the CAM4-IF-t improves upon the CAM4 and is better than the AMIP mean in terms of the lapse rate profile throughout the deep tropics, particularly with the low-level stability maximum near 850 hPa. Note the y-axis scale is logarithmic in all three panels. All runs here were conducted using the AMIP protocol.

Table 3.1: Pressure-weighted RMSEs for various SPARC high-resolution radiosonde sites for the CAM4, CAM4-IF-t and the AMIP mean for 1998-2005 (all AMIP-style simulations). The rank of the CAM4-IF compared to the CAM4, and the 20 AMIP members is indicated in the right column, with a rank of "1" indicating that the CAM4-IF-t has the lowest pressure-weighted RMSE of all models. The CAM4-IF-t has the lowest pressure-weighted RMSE at most locations in this dataset. Note, the radiosonde dataset is from 1998-2011, but there is only data up to 2005 available for all AMIP models and the CAM4 only has complete boundary conditions to run until the end of 2005.

Temperature RMSE					
Site	CAM4	CAM4-IF-t	CAM4-IF-r	AMIP mean	CAM4-IF-t rank
GUA	0.454	0.419	0.349	0.559	1
HIL	0.513	0.500	0.486	0.515	2
JUA	0.411	0.373	0.290	0.445	1
KOR	0.423	0.314	0.423	0.571	1
LIH	0.574	0.415	0.415	0.632	4
MAJ	0.257	0.227	0.255	0.534	1
PAG	0.648	0.609	0.520	0.674	1
PON	0.452	0.393	0.446	0.604	1
TRU	0.450	0.376	0.408	0.618	1

3.2 Hydrological cycle

In this section we examine the time mean tropical precipitation ($\overline{P}$) of the CAM4/CAM4-IF control simulations compared to tropical precipitation estimates from observational-based and model-based datasets (figure 3.3 and tables 3.2 and 3.1). Here we will focus on the CAM4-IF-r version as this is the version that has improved tropical rainfall, but the CAM4-IF-t (with the default IF scheme) has been included in the figures and tables for reference. The observational rainfall blend (figure 3.3**d**) indicates that the region of maximum $\overline{P}$ is situated in the far western Pacific, over Papua New Guinea and just east of Papua New Guinea. Dry zones are situated over the eastern and southeastern tropical Pacific, across northern Africa, and in the southern tropical Atlantic. This is indeed what is seen in both CAM4 models, but both have larger local maxima of $\overline{P}$. We see also that the CAM4-IF-r and the CAM4 have similar tropical mean rainfall RMSEs, with the CAM4-IF-r also having a slightly higher pattern correlation (here, and for the rest of this thesis, r_{pat} indicates the spatial correlation coefficient) with the observational dataset. The CAM4-IF-r model has a zonal mean pattern of rainfall (see zonal mean graph to right of each panel) that is closer to observations than the CAM4 default. Overall, the CAM4-IF-r has a slightly better representation of tropical $\overline{P}$ than the CAM4 default,

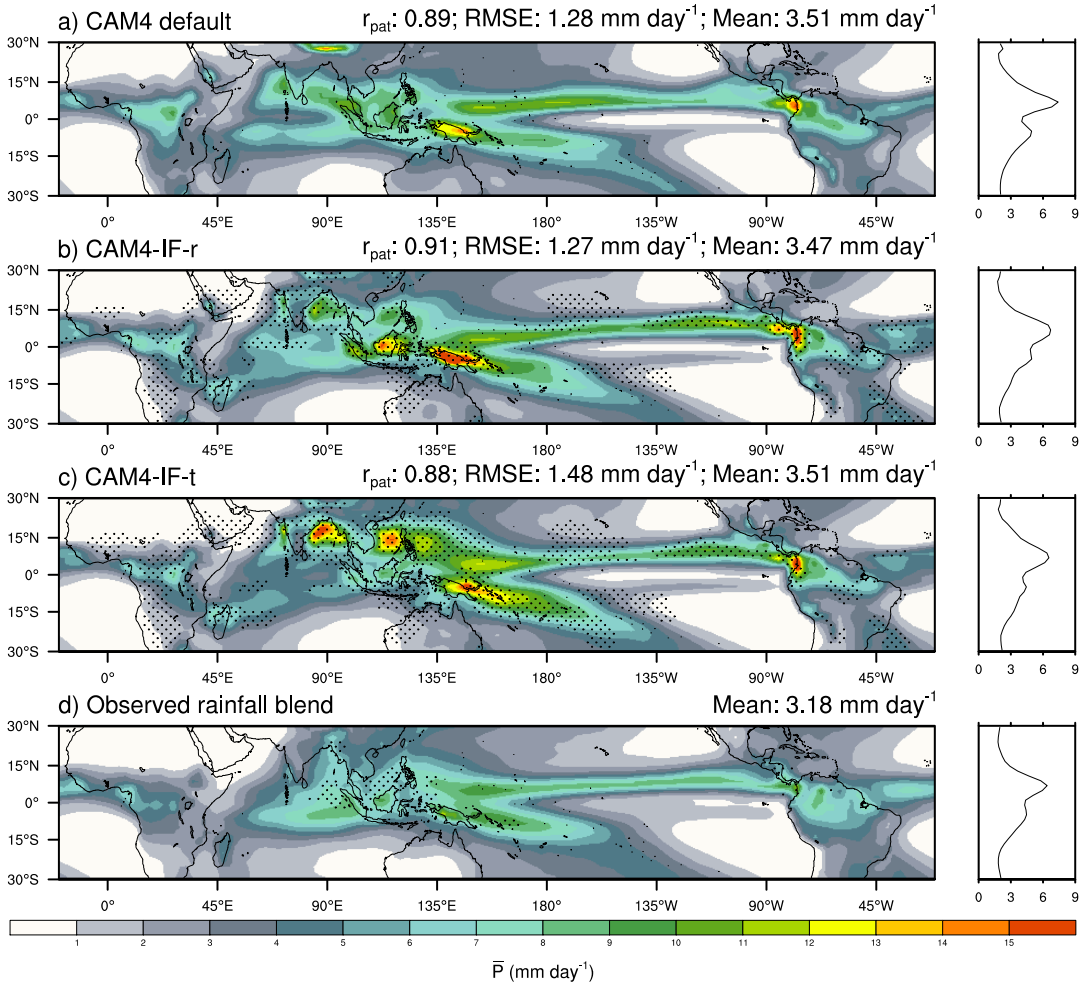

Figure 3.3: Time mean precipitation rate (30°S-30°N region, which will refer to as the tropical mean in this thesis), $\overline{P}$, for **a**: the default CAM4, **b**: the CAM4 with the IF scheme that produces a tropical mean, time mean rainfall distribution with the lowest RMSE (root mean squared error for the tropics) when compared to reanalysis, **c**: the CAM4 with the IF scheme that produces tropical temperature profiles closest to those observed from radiosondes. In **b and c**, stippling indicates regions where the difference between the CAM4-IF and CAM4 default rainfall is greater than 1 mm day^{-1} above the standard deviation of the observational blend. **d**: Observational rainfall blend mean (see table 2.2), with stippling indicating regions where the standard deviation of the dataset blend is $>$ 1 mm day^{-1}. r_{pat} represents the spatial correlation for the tropics, and the mean is the tropical mean $\overline{P}$. For this figure, and all other 2-d spatial plots in this thesis, raster smoothing has been used for aesthetic purposes.

A seasonal and regional breakdown of the differences between observed and simulated $\overline{P}$ is shown in table 3.2. For the tropical region, the CAM4-IF-r has a lower RMSE of rainfall

over ocean regions in the DJF, JJA and the annual mean (ANN) than the CAM4 default, with a higher RMSE over tropical ocean regions for these same time periods, except for JJA. The biggest degradation in the CAM4-IF-r is seen in DJF, with an improvement seen in JJA, indicating a better representation of the SASM circulation. Both model versions have lower RMSEs in the time mean (ANN) than in DJF and JJA, indicating that the seasonal cycle of the rainfall in the tropics is more poorly represented than the time mean rainfall.

Table 3.2: Seasonal and regional table for $\overline{P}$. All RMSEs are a comparison with the observational blend described in section 2.3.

ANN Rainfall RMSE (mm/day)			
Model	Region	30°S-30°N	15°S-15°N
Default CAM4	Land	1.66	1.78
	Ocean	1.05	1.29
CAM4-IF-r	Land	1.73	2.19
	Ocean	0.99	1.21
CAM4-IF-t	Land	1.56	1.77
	Ocean	1.43	1.60
DJF Rainfall RMSE (mm/day)			
Model	Region	30°S-30°N	15°S-15°N
Default CAM4	Land	2.29	2.67
	Ocean	1.74	2.30
CAM4-IF-r	Land	2.44	3.14
	Ocean	1.90	2.31
CAM4-IF-t	Land	2.06	2.58
	Ocean	2.00	2.26
JJA Rainfall RMSE (mm/day)			
Model	Region	30°S-30°N	15°S-15°N
Default CAM4	Land	2.94	2.38
	Ocean	2.10	2.49
CAM4-IF-r	Land	2.67	2.95
	Ocean	1.90	2.34
CAM4-IF-t	Land	2.79	2.70
	Ocean	2.62	2.74

Both models have a higher tropical mean rainfall rate than the blended observations (see figure 3.3 and table 3.1), although the mean values are close to those seen in reanalysis data (the satellite data included in this "blend" bring down the tropical mean). Also, in figure 3.4 we see that $\langle \overline{P} \rangle$ ranges from 3.27 mm day^{-1} to 3.93 mm day^{-1} for the AMIP control run simulations, providing support that the satellite rainfall estimates may be too low in the tropical mean. The tropical mean precipitation in the CAM4/CAM4-IF models is near the median of the AMIP members of 3.54 mm day^{-1}. When the RMSEs of the CAM4 default and CAM4-IF-r are compared to the 12 AMIP control model RMSEs, we find that both models lie well within the range of RMSEs from these models and are generally within the inter-quartile range, with some variation depending on which observational dataset is used for comparison.

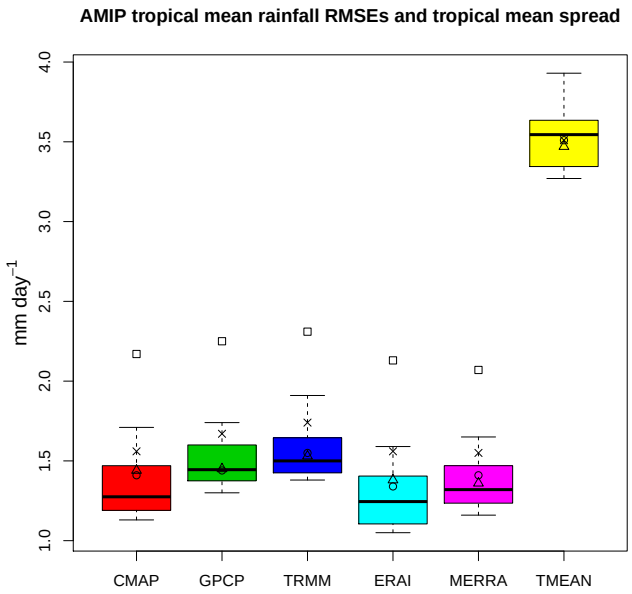

Figure 3.4: Box plots of the spread of RMSEs of $\langle \overline{P} \rangle$ for the CMIP5 AMIP control simulations compared to different observation and reanalysis data sets (leftmost five boxes), and the spread in the tropical mean rainfall (TMEAN). Outliers are indicated in boxes, and in all cases this is the FGOALS-g2 model. The CAM4 models is indicated as a circle, the CAM4-IF-r as a triangle, and the CAM4-IF-t as an x.

3.3 The tropical circulation

We examine the regions of ascent and descent associated with the tropical circulation by examining the spatial pattern of mid-tropospheric (500 hPa), time mean ω in figure 3.5 and the tropical mean in figure 3.6. This is a commonly used metric, as this is typically around the level at which vertical motions in the troposphere reach their maximum (Vecchi & Soden, 2007). We will refer to the time mean ω at 500 hPa as $\bar{\omega}_{500}$. Observational data of $\bar{\omega}_{500}$ (figure 3.5**d**), in this case a MERRA/ERA-interim reanalysis blend, indicate that most ascent ($\bar{\omega}_{500} < 0$) in the tropics occurs over the Maritime Continent and adjacent waters, with descent ($\bar{\omega}_{500} > 0$) occurring in much of the eastern tropical Pacific. The CAM4 and CAM4-IF-r have this general pattern of $\bar{\omega}_{500}$, but with a larger magnitude of the ascent and descent. Also, both models tend not to have enough ascent in the eastern Indian Ocean. The RMSE is slightly lower and the pattern correlation slightly higher in the CAM4-IF-r compared to the CAM4 default, indicating there is a slight improvement in the representation of the tropical circulation in the CAM4-IF-r when compared to this reanalysis blend.

Figure 3.7 shows $\bar{\chi}^*_{200}$ for the three different CAM4 versions with reanalysis data overlayed. This is time mean 200 hPa χ (see eq. 1.34) with the zonal mean removed, as was done in Tanaka et al. (2004). This field is used to gauge the strength and spatial pattern of the Walker circulation via the large scale upper-level divergence and is much less noisy than the divergence field itself and is computed using spherical harmonics in NCL. The reanalysis data indicates that the maximum of upper-level divergence (negative $\bar{\chi}^*_{200}$) should be just north of Papua New Guinea, and just east of the southern Philippines (around 0°N, 135°E). However, we see that the CAM4 default has a maximum in the far eastern Indian Ocean, much farther west (by about 30°-40° of longitude). The CAM4-IF-t model, however, has the maximum in ascent almost exactly where reanalysis suggests it should be, although, the magnitude is larger. This would tend to indicate that the CAM4-IF has a more accurate representation of where the maximum tropospheric heating is occurring. The CAM4 shows a positive bias in divergence over central Africa compared to reanalysis, with the CAM4-IF-t having upper-level convergence in that region. The tropical mean RMSE is a bit higher in the CAM4-IF-t simulation, however, the pattern correlation is improved. Overall, the CAM4-IF-t may have a better representation of the ascending region of the Walker circulation than the CAM4 default, but may be too strong.

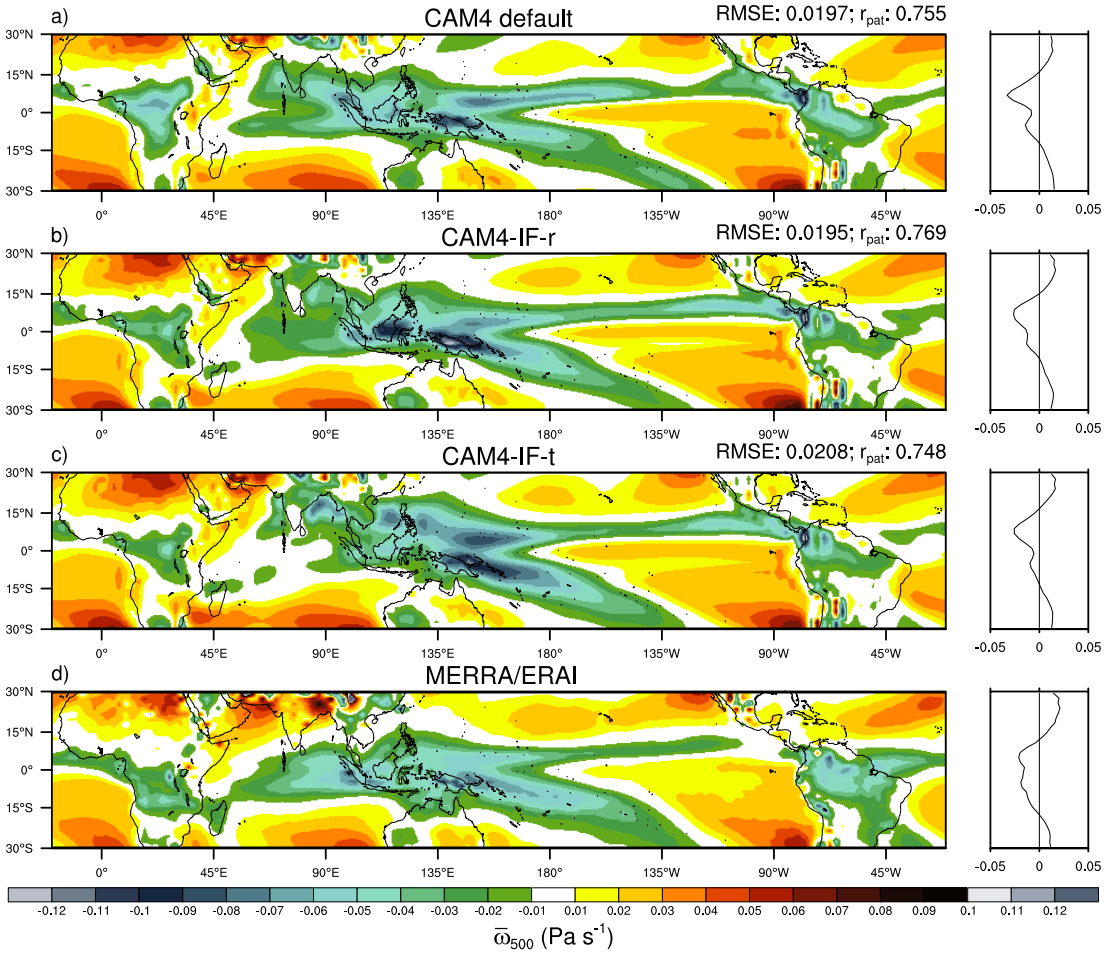

Figure 3.5: **a-c**: Control run $\bar{\omega}$ at 500 hPa. d): Same as **a-c**, but for a MERRA/ERAI reanalysis blend

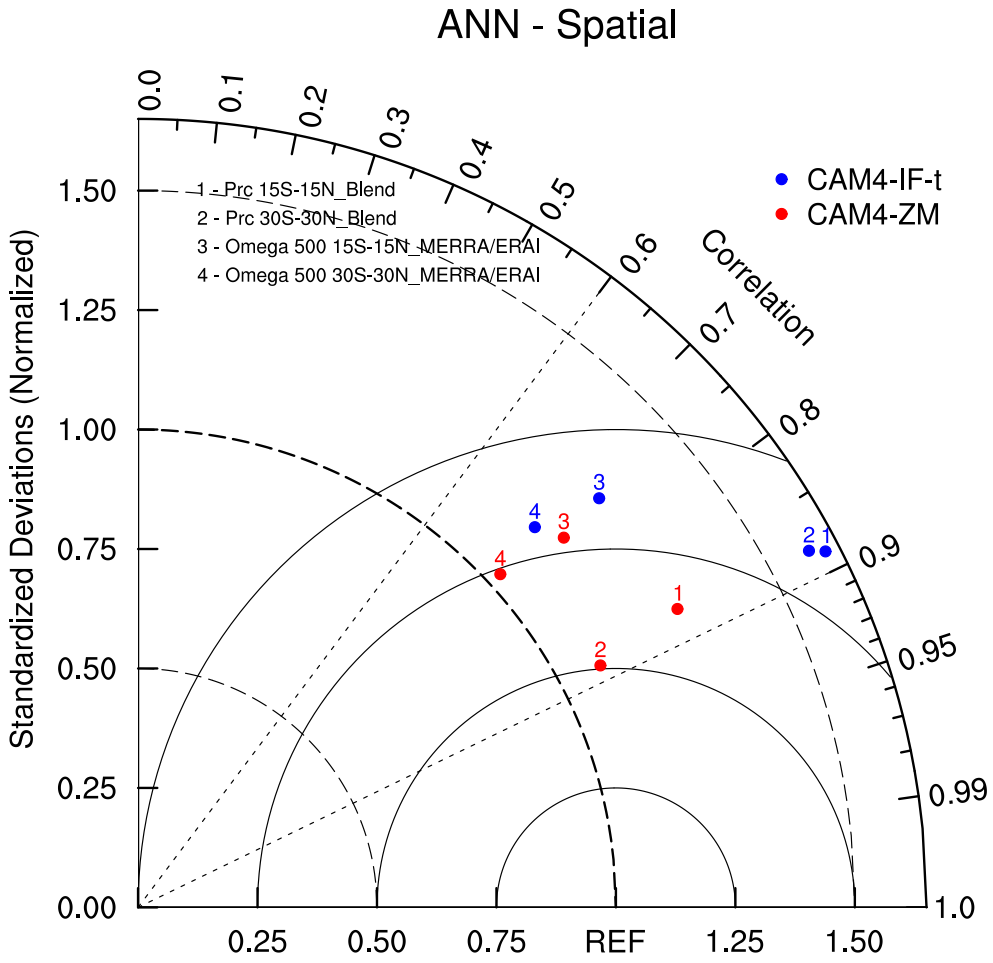

Figure 3.6: Taylor diagram (Taylor, 2001) showing the 15°S-15°N and 30°S-30°N $\overline{P}$ and $\overline{\omega}_{500}$ variance and spatial correlation compared to a MERRA/ERA-Interim reanalysis blend for the CAM4-IF-t and CAM4. The closer a point is to "REF", the lower the RMSE.

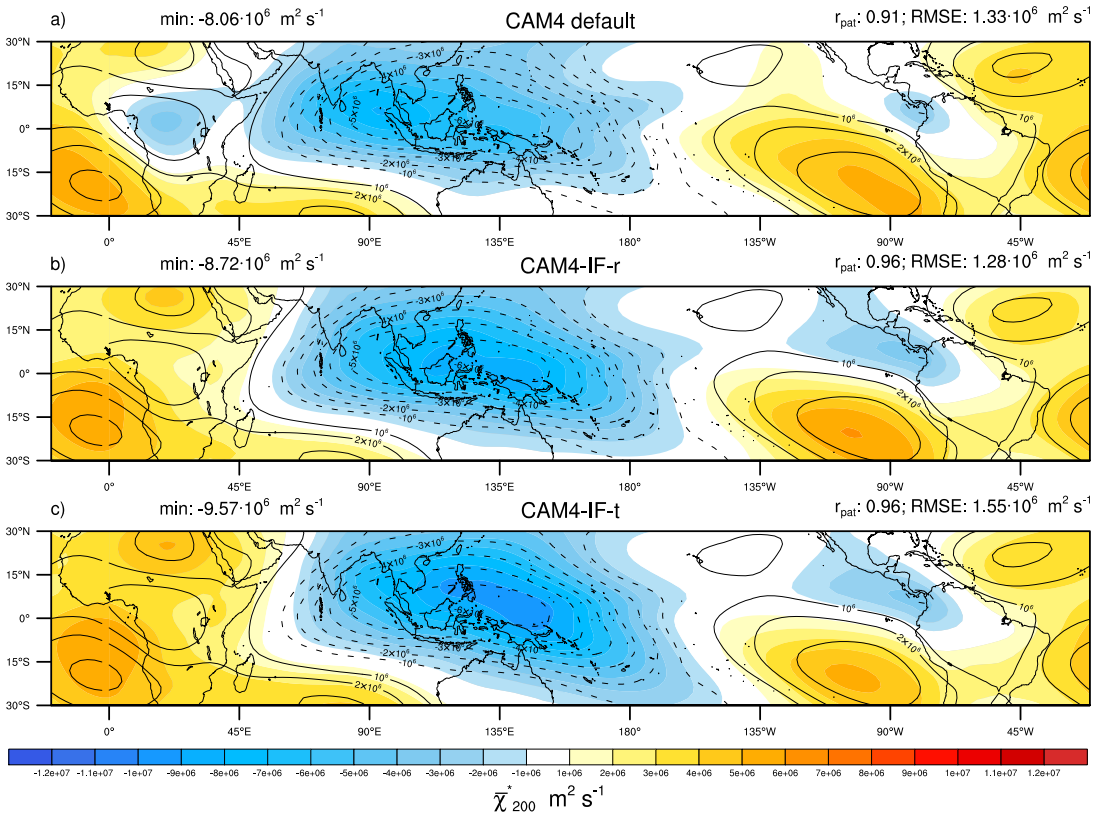

Figure 3.7: **a)-c)**: Control run 200 hPa $\overline{\chi}^{*}_{200}$ (shaded) with an ERAI/MERRA reanalysis blend overlaid as contours. Spacing is 10^6 m^2 s^{-1} for both contours and shading.

In the tropics, the strength of the convective mass flux controls the variations in diabatic heating rate through condensational heating and this diabatic heating controls ω (for a constant static stability). Thus, there should be a strong relation between the two variables. We see immediately from figure 3.8 that the CAM4 time mean, column integrated convective mass flux (hereafter, $\overline{M}_{int}$) which is defined as the vertical integral of $\overline{M}_c$ from 100-1000 hPa, normalized by the thickness of the layer (similar to what was done in Chadwick et al. (2012)):

$$\overline{M}_{int} = \int_{100}^{1000} \frac{\overline{M}_c}{900} dp, \tag{3.1}$$

is larger than in the CAM4-IF versions throughout the tropics. An observational dataset to compare the simulations to was not available as this variable can not be directly observed as it occurs on such a small scale. Even if this variable was available in reanalysis, it

would simply be derived from the convective parameterization of the model used for the reanalysis and would not be strongly constrained by observations. Note that this variable is the mean sub-grid scale convective mass flux directly from the convective scheme in each grid box and is the sum of the convective mass flux from the deep and shallow convective mass flux. While the CAM4 default and CAM4-IF versions have comparable tropical mean levels of precipitation, the CAM4 has significantly more upward convective mass flux and thus a smaller amount of precipitation produced per unit of mass flux, especially in regions of low $\overline{P}$. The spatial correlation of $\overline{M}_{int}$ with the vertically integrated $\overline{\omega}_{int}$ is quite high and thus these two quantities and $\overline{P}$ (which itself is highly correlated with negative $\overline{\omega}$), are spatially closely related, as expected.

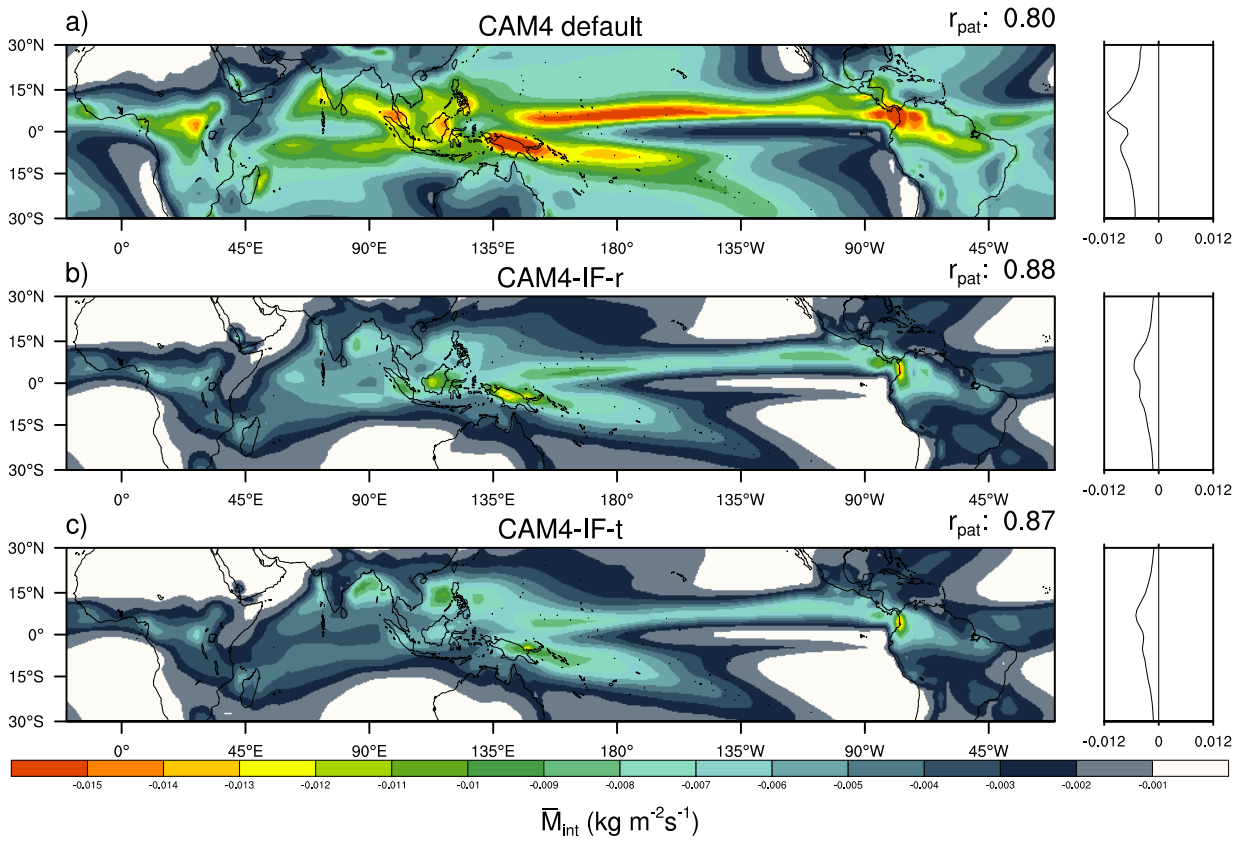

Figure 3.8: **a)-c)**: $\overline{M}_{int}$ - pressure-thickness weighted vertically integrated mass flux from 1000-100 hPa with the pattern correlation between $\overline{M}_{int}$ and the pressure-thickness weighted vertically integrated integrated omega for the same interval indicated. Here the sign convention for upward mass flux is taken to be negative similar to that of ω.

3.4 Summary

Overall, it appears that the CAM4-IF version of the CAM4 improves on some features of the tropical climate; the tropical temperature and lapse rate profile and the tropical circulation. Also, the tropical precipitation is slightly improved in the CAM4-IF-r model. There is a deterioration in the precipitation representation in the versions of the CAM4-IF-t, mainly in the SASM region and the Indian Ocean. These variables are influenced by the convective scheme, either from the the parameterization of convective mass flux, or more indirectly via diabatic heating. We also see that the overall tropical convective mass flux is quite different in the CAM4-IF models, indicating that switching convective schemes has a major impact on the convective mass flux and thus the distribution of diabatic heating.

Chapter 4

Influence of convective scheme: future climate

4.1 Hydrological cycle and the tropical circulation

Here we will examine the response of the CAM4 default and CAM4-IF models to a 4K SST warming. We will mainly focus on an examination of time mean quantities such as annual means. We find that the while the tropical circulations do weaken in the CAM4-IF, the tropical mean convective mass flux does not weaken as theory would suggest. This suggests that the hydrological cycle argument to the weakening of tropical mean convective mass flux may be sensitive to the type of convective scheme used.

In response to a uniform 4K SST increase, the atmosphere warms and thus the radiative cooling in the free troposphere increases, while the global mean surface temperature increases fairly uniformly by around 4.3-4.4K (plot not shown). This larger global mean surface temperature increase than the 4K increase in SST could be explained by some transport of some the air in the tropical troposphere where the temperature increase is larger than 4K to the surface over land regions, and/or decreased cloud cover over land regions. The ocean warming causes the atmosphere to precipitate more due to the increased tropospheric radiative cooling (by an amount that balances the increased latent heat flux from the ocean) in these experiments as the SSTs are fixed and do not respond to changes in radiative forcing. The global mean tropospheric temperature increases more than 4K (by as much as 9K in the deep tropics) because of the increased condensational heating due to the very large increase in water vapour capacity of the atmosphere due to the C-C relation. This means the tropical mean tropospheric lapse rate decreases in the

warmer climate (static stability increases). The tropical (and global) mean precipitation response among the CAM4 and CAM4-IF models has some variation and is in the range of $\approx$ 16-19% which implies an increase of $\approx$ 3.5-4.5% K^{-1} (see table 4.1).

We will now examine figure 4.1, the spatial distribution of the tropical $\overline{P}$ response in the three models, with a comparison to the CMIP5 AMIP4K multi-model mean. The CAM4 default has a general increase in precipitation in wet regions, with some expansion poleward also seen. The areas where precipitation decreases are quite small, mainly confined to parts of Africa, the Maritime Continent and South America. This general pattern is also seen in both CAM4-IF versions (which are quite similar qualitatively), and a decrease in $\overline{P}$ is seen in northern India, that is not seen in the CAM4 default. The overall spatial pattern of the $\overline{P}$ response of the three models is also similar to that of the CMIP5 AMIP multi-model mean (panel **d**), but is larger in magnitude. In fact, the three CAM4 models have large regions over the tropical oceans where the response is above the maximum response seen in the 12 AMIP models (as indicated by stippling). The general response of tropical rainfall to this uniform 4K increase could be described a poleward intensification of the climatologically wet regions, with some regions near the equator seeing a decrease. There are also reductions in $\overline{P}$ seen in various regions of Africa in the three CAM models and a robust regions of decrease (indicated by hatching) seen in the AMIP mean. The overall response seen in figure 4.1 is fairly consistent with the "rich-get-richer" pattern of tropical $\overline{P}$ change (Held & Soden, 2006; Chou et al., 2009), with most of the increases in $\overline{P}$ occurring over the ocean. It appears that overall, a more "double-ITCZ" pattern is developing in the three CAM models, and to a lesser extent in the AMIP4K multi-model mean. This precipitation response should not be confused with the "double-ITCZ" issue seen in climate models which is mainly due to excessive precipitation in the Southern Hemisphere side of the tropics (most of the precipitation increases seen here is in both hemispheres). The overall pattern seen in all four panels may simply be due to the fact that the ascending regions of the Hadley cells are moving further away from the equator and expanding north. Also, all three CAM4 models have a larger tropical mean increase in precipitation than the CMIP5 AMIP4K multi-model mean.

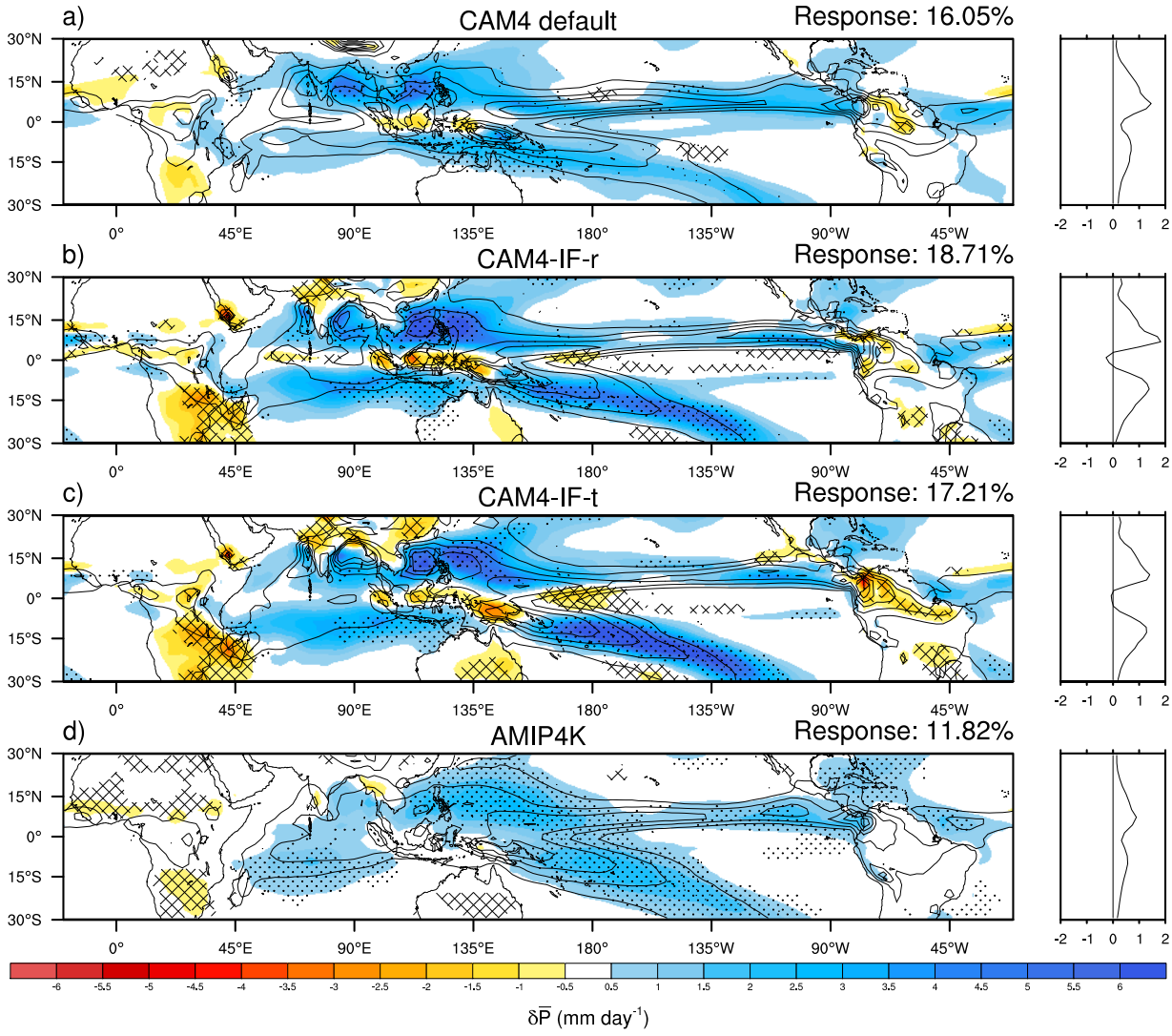

Figure 4.1: **a-d**: $\overline{P}$ response from a 4K SST warming (shaded) with control run climatology (2 mm day^{-1} contours, starting at 4 mm day^{-1}) for the three CAM4 models and the CMIP5 AMIP4K multi-model mean. In **a-c**: stippling and hatching is used to indicate regions where the $\overline{P}$ response is above the maximum AMIP4K members' response (stippling) or vice versa (hatching). The stippling (for positive responses) and hatching (for negative responses) in **d** indicates regions where 10 or more of 12 models agree on the sign of the response. The zonal mean profiles of the response are on the right of each panel. The tropical mean percentage responses are indicated. The range of tropical mean increases in $\overline{P}$ in the AMIP4K models is $\approx$ 10-16%, so the CAM4 model responses here exceed the upper range of tropical mean $\overline{P}$ responses seen in the CMIP5 AMIP models.

In figure 4.2 and table 4.1 we examine the predicted tropical overturning circulation response to this uniform 4K SST increase. We find that the relationship between the inferred mass flux response and the actual overturning circulation response for the 10 models in the table (CAM4 default and CAM4-IF model versions) is moderate (r=0.57). We measured the overturning circulation strength by $\langle \overline{\omega}^{\uparrow}_{500} \rangle$, as was done in (Vecchi et al., 2006), where $\overline{\omega}^{\uparrow}_{500}=\overline{\omega}_{500}H(-\overline{\omega}_{500})$. This uses notation from Schneider et al. (2010) and Merlis & Schneider (2011) and represents the tropical mean, time mean 500 hPa upward vertical motion and is used as a proxy for the convective mass flux in (Vecchi et al., 2006). We find that the actual overturning reduction is generally less, and in some case half of the inferred convective mass flux decrease based on the hydrological cycle. This would seem to indicate that the response of $\langle \overline{\omega}^{\uparrow}_{500} \rangle$ does not give a perfect estimation of the convective mass flux response. This is also seen in figure 4b in (Vecchi & Soden, 2007) for the coupled CMIP5 models.

Table 4.1: Column 2: Response of tropical mean $\overline{P}$. Column 3: response of tropical mean $\bar{q}_{bl}$ (average water vapour mixing ratio of three lowest model levels to provide an estimate of boundary layer specific humidity). Column 4: response of the inferred tropical mean convective mass flux using the actual response of tropical mean $\bar{q}_{bl}$. Column 5: response of the inferred tropical mean convective mass flux using an estimate of 7% K^{-1} as an estimate for the response of tropical mean $\bar{q}_{bl}$. Column 6: response of tropical mean $\overline{\omega}^{\uparrow}_{500}$. All responses here are fractional responses to the uniform 4K SST warming. Note, the other CAM4-IF models shown in this table are the previous iterations of the CAM4-IF models.

+4K SST response					
Model	$\delta\overline{P}/\overline{P}$	$\delta(\bar{q}_{bl})/\bar{q}_{bl}$	$\frac{\delta\overline{P}}{\overline{P}} - \frac{\delta(\bar{q}_{bl})}{\bar{q}_{bl}}$	$\frac{\delta\overline{P}}{\overline{P}} - 0.07(\Delta\overline{T})$	$(\delta\overline{\omega}^{\uparrow}_{500})/\overline{\omega}^{\uparrow}_{500}$
1) Default CAM4	0.161	0.302	-0.142	-0.130	-0.054
2) CAM4-IF-r	0.192	0.281	-0.089	-0.093	-0.041
3) CAM4-IF-t	0.185	0.285	-0.099	-0.103	-0.068
4) CAM4-IF 1	0.190	0.289	-0.097	-0.112	-0.068
5) CAM4-IF 2	0.177	0.274	-0.095	-0.099	-0.061
6) CAM4-IF 3	0.190	0.285	-0.116	-0.119	-0.041
7) CAM4-IF 4	0.177	0.293	-0.112	-0.120	-0.091
8) CAM4-IF 5	0.176	0.288	-0.092	-0.096	-0.096
9) CAM4-IF 6	0.192	0.285	-0.135	-0.138	-0.033
10) CAM4-IF 7	0.159	0.294	-0.101	-0.108	-0.104

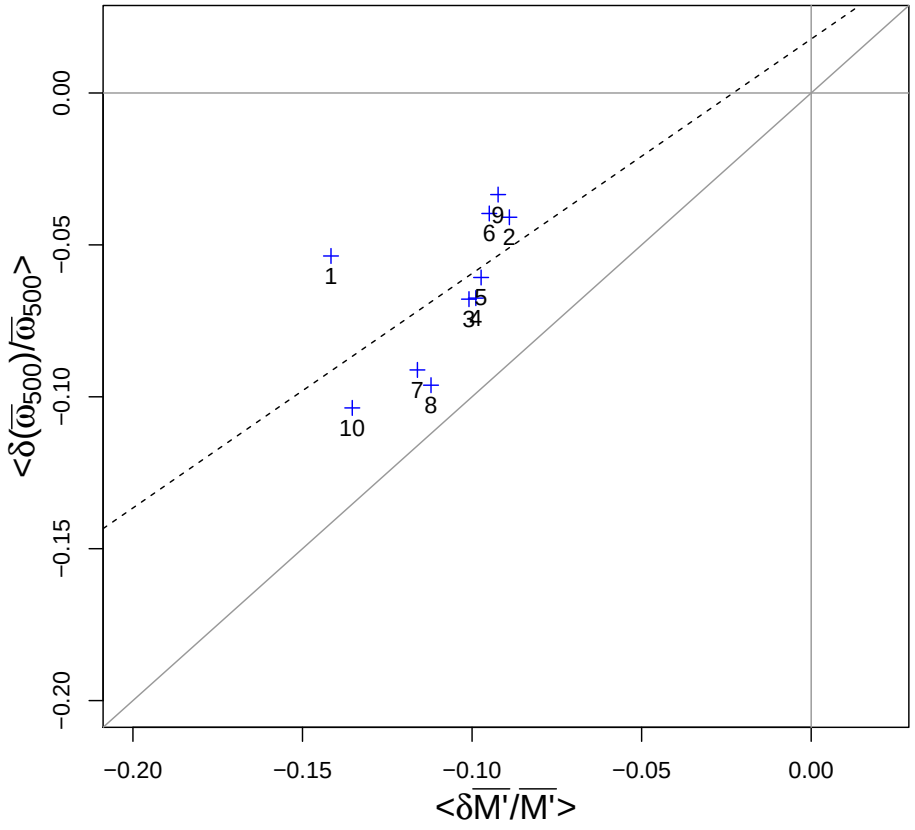

Figure 4.2: Fractional response of $\langle \bar{\omega}^{\uparrow}_{500} \rangle$ compared to the inferred mass flux fractional response, $\delta \overline{M}^{\uparrow} / \overline{M}^{\uparrow} \equiv \langle \delta \overline{P} / \overline{P} \rangle - \langle \delta \bar{q}_{bl} / \bar{q}_{bl} \rangle$, in various versions of the CAM4-IF. Model "1" is the default CAM4 (the numbered model versions in table 4.1 correspond to the numbers in this plot). The dashed line is the linear least-squares fit, with the solid line indicating what the relationship would be if there was a one-to-one relationship between inferred mass flux and $\bar{\omega}^{\uparrow}_{500}$.

4.2 Physical explanation

4.2.1 Convective mass flux

Previously, in table 4.1 we find that the inferred mass flux decreases in all versions of the CAM4-IF and the CAM4 default under a 4K SST warming. This does not mean that the actual tropical mean convective mass flux (computed from the convective scheme) decreases as theory predicts, however. Here, we use the response of $\overline{M}_{int}$ (introduced in chapter 3) to compare to the response of $\overline{M}'$ (as defined in eq. 1.36), the inferred mass flux ($\overline{M}' = \overline{P}/\overline{q_{bl}}$), as was done in Chadwick et al. (2012). Note that we add the shallow and deep convective mass fluxes together to get a total mass flux, $\overline{M}_c$. This is likely to be a better measure then just using the mass flux at an individual level as the integrated mass flux is proportional to the precipitation, and indeed as we will show, the responses of $\overline{M}_c$ (convective mass flux at a given level) can be quite different at different vertical levels (Chadwick et al., 2012). Even with an increased vertical resolution, one would still want to avoid using the response at one level as there should be some vertical structure to the convective mass flux, although the profile would presumably be smoother. We will show that the tropical mean $\overline{M}_{int}$ actually increases in the CAM4-IF versions, but decreases as expected in the CAM4 default simulation. This is direct contradiction to what was expected by theory (Held & Soden, 2006; Vecchi & Soden, 2007) and to what is seen in the CMIP5 models (for the same metric) (Chadwick et al., 2012).

The tropical mean response of $\overline{M}_{int}$ (figure 4.3) shows some very interesting and surprising features. We find that the mass flux does indeed weaken in the CAM4 (figure 4.3**a**), as expected, although by much less than the $\approx 14\%$ predicted from table 4.1. However, $\overline{M}_{int}$ does not weaken in the CAM4-IF models, and in fact increases by $\approx 16\%$ in the CAM4-IF-r. There is also very interesting vertical structure in the response, with an opposite-signed response in mass flux below 600 hPa between the default CAM4 and the CAM4-IF models. The CAM4 default sees a strong increase around 500 hPa, likely due to the minimum seen in the climatology (likely associated with the melting level downdrafts) moving upwards in the warming climate. This highlights why picking a single level to calculate the $\overline{M}_c$ response at is not an accurate reflection of the vertically integrated response. Where all three models do agree (on the sign at least), is the upward expansion of the convective mass flux as the convection depth increases over Africa (which corresponds well with the $\overline{P}$ response shown in figure 4.1.

The second column of 4.3 shows that the structure of the $\bar{\omega}$ response is quite different from that of $\overline{M}_c$, which clearly demonstrates that $\bar{\omega}$ and $\overline{M}_c$ can have different responses

and are only loosely related. This is the case for all three models, with the exception being over the land areas of Africa and South America.

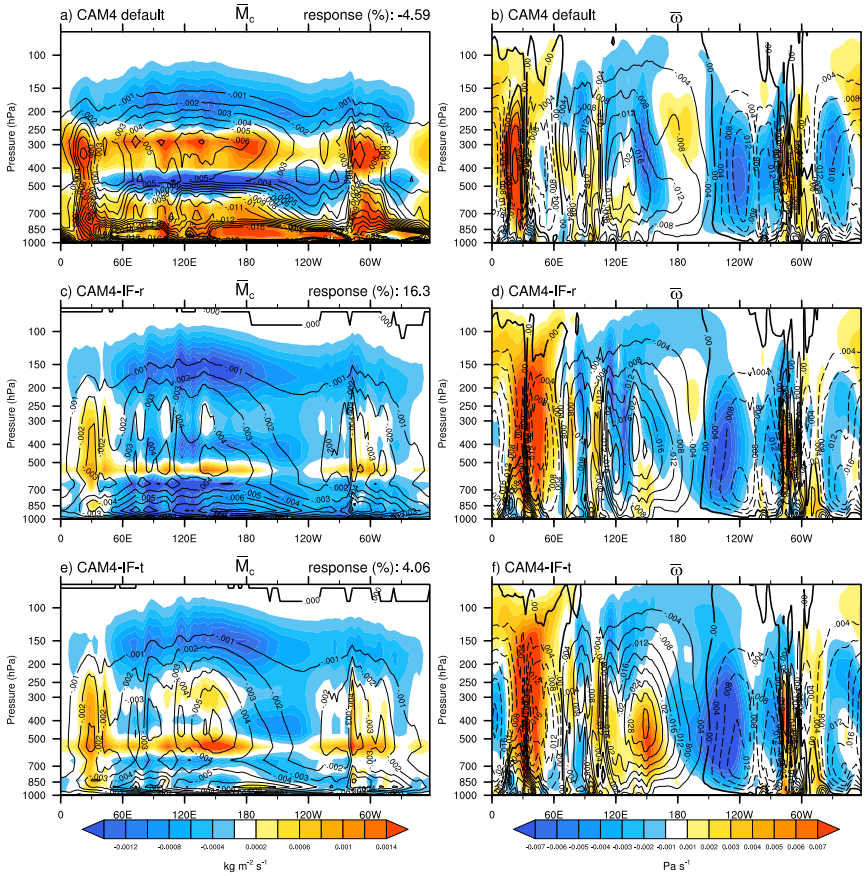

Figure 4.3: **a, c, e**: response of the annual mean 30°S-30°N mean convective mass flux for the two CAM4-IF models and the default CAM4 with the same plots but for omega in the second column (**b, d, f**). A negative sign convention is used here for the convective mass flux to indicate upward motion, similar to $\bar{\omega}$. Negative contours are solid and positive contours are dashed. Note the positive response in tropical mean vertically integrated $\overline{M}_c$ ($\overline{M}_{int}$) seen in the CAM4-IF models compared to the negative response predicted in column 4 & 5 of 4.1 and the negative response in tropical mean ascent seen in column 6 of the same table.

Figure 4.4 shows the spatial response of $\overline{M}_{int}$ and vertically integrated $\bar{\omega}$ ($\bar{\omega}_{int}$): there is a strong spatial relationship in the response of these two variables, with the correlation ranging from 0.75 to 0.87 among the three models. The CAM4-IF models have a much larger spatial extent of regions where $\overline{M}_{int}$ is increasing compared to the CAM4 default,

especially in the CAM4-IF-r. All three models agree on a decrease (please note, that a positive response indicates a *weakening* of $\overline{M}_{int}$ because upward mass flux is negative) in $\overline{M}_{int}$ and $\overline{\omega}_{int}$ over the Maritime Continent near the equator. Also, all three models have a minimum in $\delta\overline{M}_{int}$ near the equator, and the CAM4-IF models have relative minima (a strengthening of convective mass flux) just off the equator around 15°S-15°N (see zonal mean plots to the right of each panel). Unfortunately, the convective mass flux data from the AMIP4K experiment is unavailable, so a comparison of how well ω and M_c correlate in the AMIP4K suite is not possible.

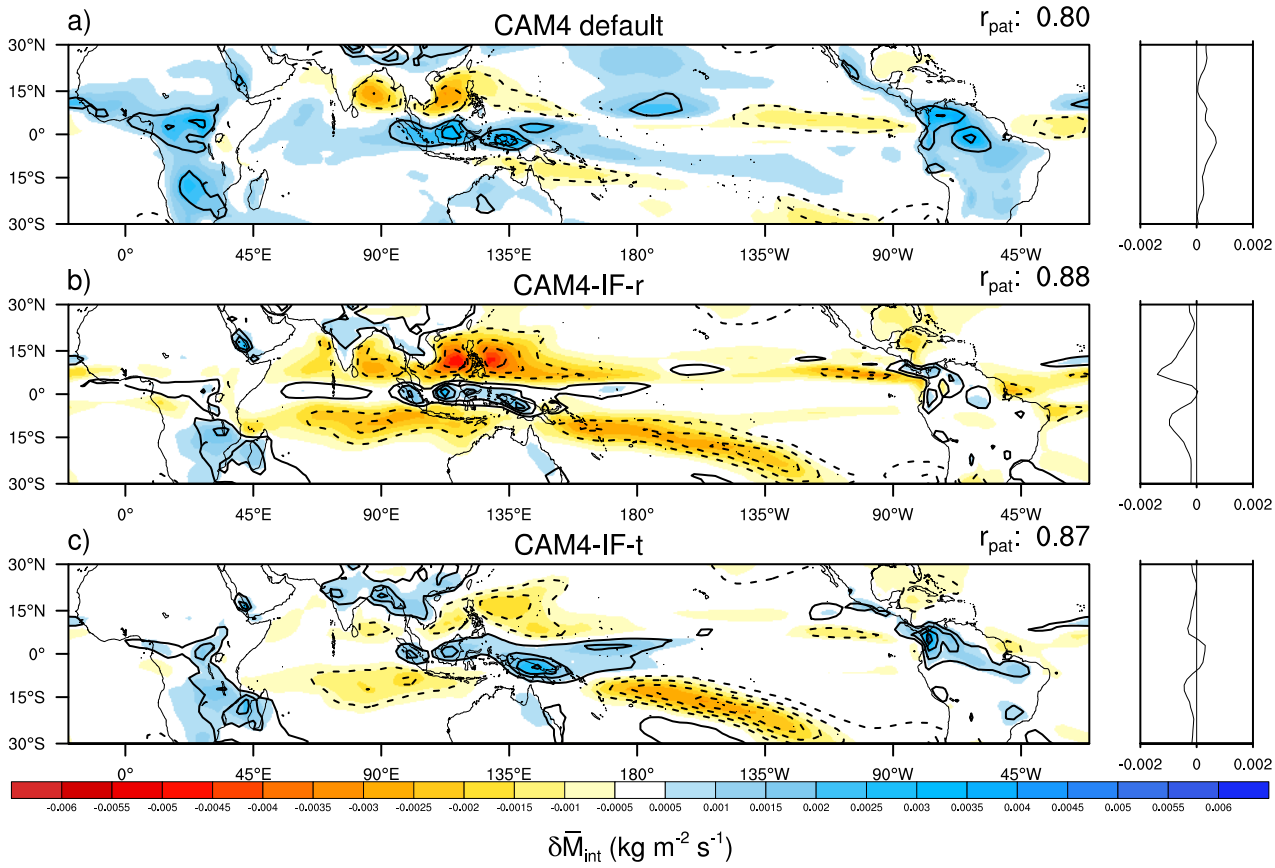

Figure 4.4: **a-c**: As in figure 3.8, but for the response, and with $\overline{\omega}_{int}$ indicated in contours, with negative indicating a negative (increased upward motion) response, and solid a positive one.

The vertical structure of $\overline{M}_c$ in the control runs and in the response is different between the CAM4-IF and the CAM4 default (figure 4.5). The CAM4 default has a more "bottom-heavy" profile with a maximum of mass flux in the lower troposphere, with the maximum

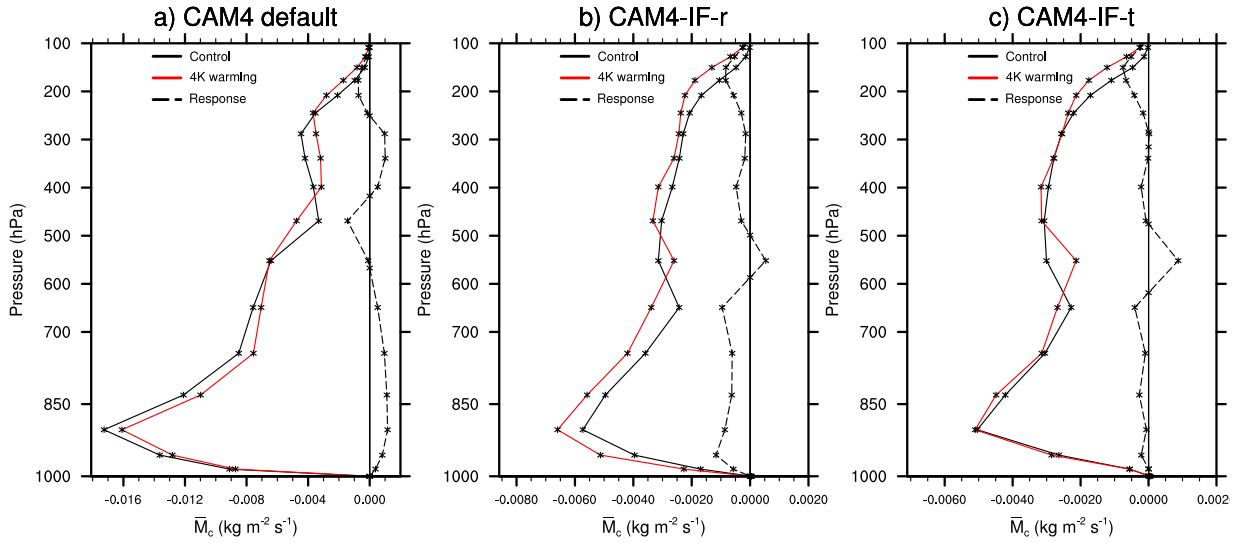

Figure 4.5: **a-c**: vertical profiles of the annual mean tropical mean *total* convective mass flux response and control/4K run climatologies. Note the vertical scale is not logarithmic as in previous figures to emphasise the lower troposphere.

in the lower troposphere in the CAM4 approximately a factor of three larger than that of the CAM4-IF models and tropical mean $\overline{M}_{int}$ approximately a factor of two greater than that of the CAM4-IF models. Comparing these three profiles to the profiles in the CMIP5 models (figure 2 in Chadwick et al. (2012)), the CAM4-IF models are most qualitatively similar to the HadGEM2-ES model. It is very clear that the net convective mass flux increases in both CAM4-IF versions in the 4K SST warming runs, except for a decrease between 500 and 600 hPa associated with an upward shift in the melting level minimum (there is a minimumin $\overline{M}_c$ near the melting level because there is a local maximum of downdraft generation here).

Examining the updraft and downdraft components of tropical mean $\overline{M}_c$, $\overline{M}_u$ and $\overline{M}_d$ in the CAM4-IF models (figure 4.6) shows that both versions actually have a qualitatively similar vertical profile of updraft mass flux response of 0-10^{-3} kg m^{-2} s^{-1} (**c-d**). However, the difference in downdraft mass flux in the control and response between the two CAM4-IF models is quite revealing. The CAM4-IF-r has penetrative downdrafts turned off (see 2.2.2 for more information on the downdraft parameterization in the IF scheme), so downdrafts originating from below the melting layer do not exist. So while the CAM4-IF-t control version has a maximum of $\overline{M}_d$ below 850 hPa, the CAM4-IF-r version has a maximum between 600-700 hPa. The freezing level maximum in both models shifts upward in response to the uniform 4K SST warming with no significant changes in the

magnitude of this maximum. On the other hand, $\overline{M}_d$ increases below the melting level in the CAM4-IF-t, with the maximum staying at the same level. This asymmetry in $\overline{M}_d$ explains why the $\overline{M}_c$ response in the lower troposphere is weaker in the CAM4-IF-t than in the CAM4-IF-r even though the CAM4-IF-t has a larger increase in $\overline{M}_u$ in the lower troposphere. Also, the fact that the integrated updraft mass flux increases more than the increase in integrated downdraft mass flux in the CAM4-IF-t explains how the total integrated convective mass flux still increases in the CAM4-IF-t. This highlights that the downdraft mass flux response appears to be important to the total mass flux response as both models have a fairly similar updraft mass flux response, but the model with lower tropospheric downdrafts (CAM4-IF-t) has a smaller increase.

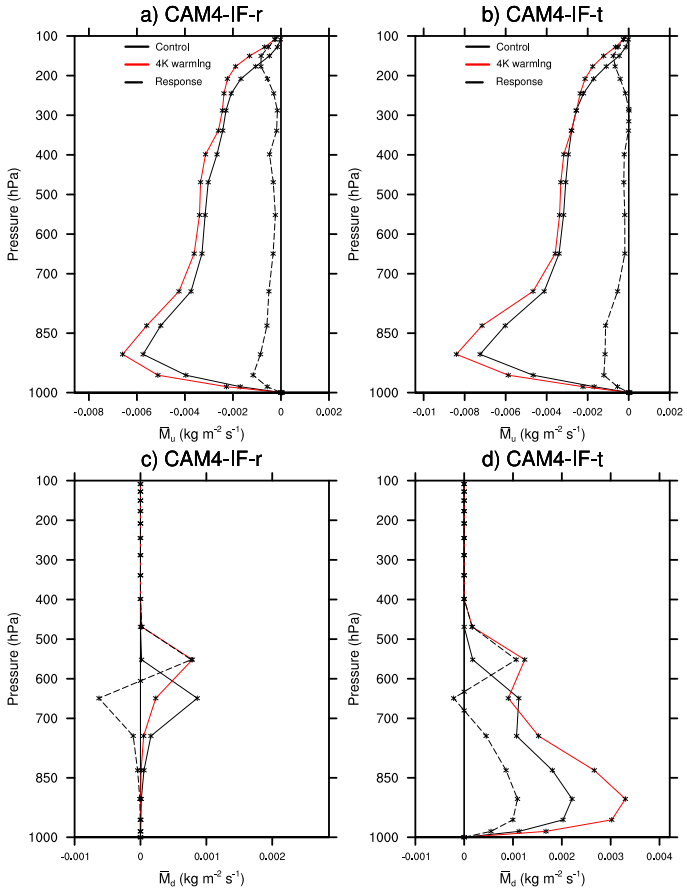

Figure 4.6: **a and b**: Vertical profiles of the annual mean tropical mean updraft mass flux, $\overline{M}_u$, for the CAM4-IF models. **c and d**: Downdraft mass flux, $\overline{M}_d$, for the CAM4-IF models.

Figure 4.7 **a-c** shows the relationship between $\overline{M}'$ and $\overline{M}_{int}$ at each gridpoint (where $\overline{P} > 4$ mm day^{-1}) in the control and +4K climate. As we have shown previously in figure 4.4, the response of $\bar{\omega}_{int}$ and $\overline{M}_{int}$ are strongly spatially correlated, so a different signed response in the tropical mean $\bar{\omega}$ and mass flux responses in the CAM4-IF models would imply that the relationship between these two variables is changing under climate change, even though they remain very closely related in their spatial patterns. They are closely related because the tropospheric heating rate, which is largely controlled by the convective mass flux in the tropics, controls ω (from eq. 1.16). We see that the there is a fairly strong correlation between $\overline{M}_{int}$ and $\overline{M}'$ on a gridpoint-by-gridpoint basis in all three models in both the control and warmer climate, however the slope is much steeper than one for the CAM4 default, indicating the efficiency of $\overline{M}_{int}$ to produce precipitation is lower than what would be predicted by theory. There are also a number of points with high $\overline{M}_{int}$, but low $\overline{M}'$ and these may be associated with orographic forced precipitation (Chadwick et al., 2012). Note that in the CAM4-IF models the red points appear to shift up the y-axis, indicating that for that gridpoints with the same estimated mass flux ($\overline{M}'$) have a higher $\overline{M}_{int}$ in the warmer climate. In other words, the relationship between $\overline{M}'$ and $\overline{M}_{int}$ is changing in the warmer climate (this is most obvious in the CAM4-IF-r version). Another way to measure the relationship between $\overline{M}'$ and $\overline{M}_{int}$ is looking at the y-intercepts, which actually decrease in the CAM4 default, but increase in the CAM4-IF models in response to climate change. The interpretation of this would be that the mass flux is becoming more efficient at producing precipitation in the warmer climate in the CAM4 default, and becoming less efficient in the CAM4-IF models.

Figure 4.7 **g-i** examines the relationship between the $\overline{M}_{int}$ fractional response and $\bar{\omega}_{int}$ fractional response at each gridpoint, while **g-i** examines the relationship between $\overline{M}_{int}$ and $\bar{\omega}_{int}$ in the control and warmer climates. We see that the fractional responses of the two variables are fairly well correlated in the three models, but the most interesting feature is the y-intercepts. In all three models, these are non-zero, indicating that the relationship between the two variables at each gridpoint is offset. That is to say, in the CAM4-IF models for example, there is still an increase in integrated convective mass flux at some gridpoints where $\bar{\omega}_{int}$ is decreasing. The opposite is true for the CAM4 default. This indicates that the relationship between ω and $\bar{\omega}_{int}$ is changing in the warmer climate as well, with the convective mass flux likely not as efficient at producing heating (which creates the upward motion) in the CAM4-IF models, with the opposite seen in the CAM4 default. This is why the convective mass flux response is not a perfect measure of the overturning strength response and vice-versa - they can have opposite-signed tropical mean responses.

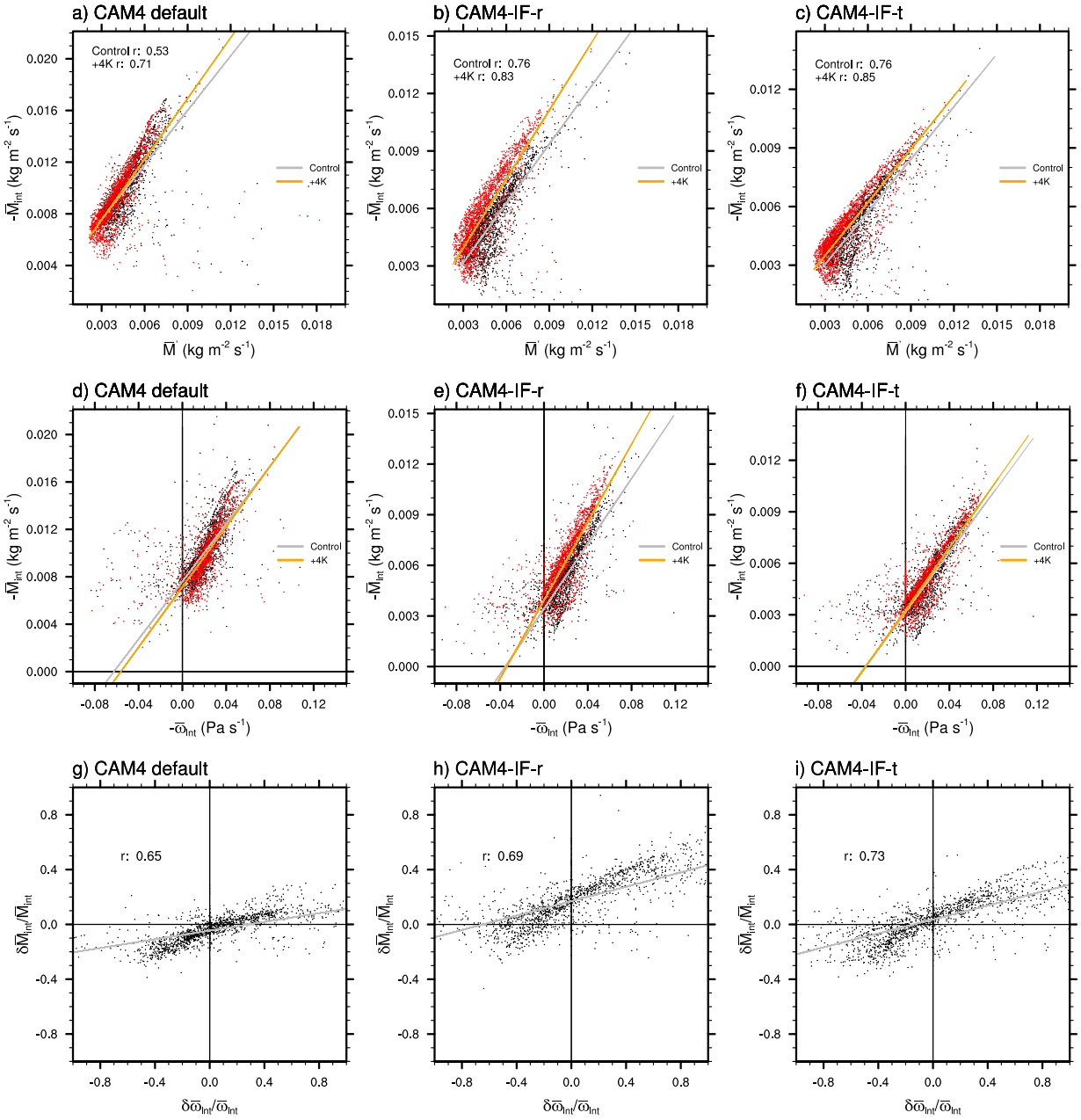

Figure 4.7: **a-c**: $-\overline{M}'$ vs. $-\overline{M}_{int}$ for each model control (black points) and +4K SST run (red points) for the region 30°S-30°N, only for grid points where the precipitation rate is > 4 mm day^{-1}. **d-f**: $-\overline{\omega}_{int}$ vs. $-\overline{M}_{int}$ for the same grid points as **a-c** with linear least-squares best fit lines for regions where $-\overline{\omega}_{int} > 0$. **g-i**: $\frac{\delta\overline{M}_{int}}{\overline{M}_{int}}$ vs. $\frac{\delta\overline{\omega}_{int}}{\overline{\omega}_{int}}$ for the same grid points as in **a-f** with the linear least-squares fit line and correlation coefficient indicated. Note the scales vary between plots except for **g-i**.

In summary the convective mass flux response in the CAM4-IF models does not seem to be consistent with the hydrological cycle argument for mass flux weakening of (Held & Soden, 2006). While the inferred convective mass flux weakens in the CAM4-IF models, the actual mass flux does not. This could mean that there is a large change in precipitation efficiency in the CAM4-IF model with the 4K SST warming. In the very least, it does seem that the convective scheme does affect the convective mass flux response as this does not occur in the CAM4 with the ZM/Hack schemes. Also, these are +4K SST AMIP experiments, not fully coupled climate change simulations, so it may not be valid to compare directly to the coupled CMIP5 models, as was done in other studies such as (Chadwick et al., 2012).

4.2.2 Precipitation efficiency mechanism

A more detailed explanation is still needed for how tropical mean convective mass flux can increase in a warmer world, and this mechanism is presented here. The hydrological cycle argument which uses relation eq. 1.36 is really only an approximation and neglects those mass fluxes which do not produce preciptiation (presumably from shallow cumulus Held & Soden (2006)) and that all the moisture from the boundary layer eventually reaches the surface as "P". Some of the rainfall or cloud condensate that is evaporated could presumably be recycled into the boundary layer, and therefore we can define a precipitation efficiency, $\epsilon_p = P_{prod}/P_{surf}$ where P_{prod} is the precipitation "production" in the atmosphere and P_{surf} is the rate of precipitation which reaches the surface. Note that this definition of precipitation efficiency is similar to the "cloud microphysics precipitation efficiency" (CMPE) used in some studies (Schoenberg Ferrier et al., 1996; Sui et al., 2007). Since there is surely at least some evaporation of precipitation before it reaches the surface in the tropics, this efficiency should always be less than 1 and likely to be significantly less than 1 in drier regions. Also, P_{prod} is only produced by convective updrafts, so if instead we focus just on the response of the tropical mean convective updraft mass flux response, one can then make a modification of eq. 1.36 to become:

$$\left\langle \frac{\delta M_u'}{M_u'} \right\rangle = \left\langle \frac{\delta P_{prod}}{P_{prod}} \right\rangle - \left\langle \frac{\delta q_{bl}}{q_{bl}} \right\rangle. \tag{4.1}$$

If ϵ_p decreases in a warmer climate, the response in P_{prod} would be larger than P_{surf} and would lead to a smaller implied mass flux decrease, or even an increase, than if one assumed $P_{prod} \equiv P_{surf}$ everywhere.

Unfortunately, an estimate of precipitation production is not possible from the CAM4 model output. However, with the IF scheme, it is possible to obtain an estimate of the

tropical mean precipitation efficiency using diagnostic output fields from the model by first obtaining an estimate of evaporation of generated condensate in the atmosphere (Ian Folkins, personal communication):

$$\text{evap}=(\text{up\_wat - up\_wat\_surf})+(\text{an\_snow - an\_snow\_surf})+\text{evap\_det}=\text{P}_{prod}\text{-P}_{surf},$$

up_wat represents the amount of rain that is generated by updrafts, up_wat_surf the amount of that updraft rain that reaches the surface. There is also precipitation that falls from convective anvils that starts as snow and eventually a portion reaches the surface as rain in the tropics and this is represented by an_snow and an_snow_surf, respectively. There is also a portion of cloud condensate that does not "fall" as rain, but is simply detrained and evaporated, represented by evap_det. With these terms, eq. 4.2.2 allows us to estimate the total loss of condensed water that did not reach the surface as rainfall. This term, plus the surface precipitation rate, should represent P_{prod} that the mass flux creates.

Using eq. 4.2.2, the tropical mean, time mean, vertically integrated, evaporation rate in the control CAM4-IF-r is $1.60{\cdot}10^{-5}$ kg m^{-2} s^{-1} while it increases to $2.84{\cdot}10^{-5}$ kg m^{-2} s^{-1} in the +4K SST warming run. Adding the tropical mean $\overline{P}_{surf}$ to these two numbers gives $\overline{P}_{prod}$=$5.68{\cdot}10^{-5}$ kg m^{-2} s^{-1}, and $7.68{\cdot}10^{-5}$ kg m^{-2} s^{-1}, respectively. This represents a 35.2% increase, and is much larger than the response of $\overline{P}_{surf}$, of $\approx$ 19% (see 4.1). This gives an implied *increase* in $\overline{M}^{'}$ of 7.1%. This is not as high as the 16.2% increase seen in $\overline{M}_{int}$ (see figure 4.3), but is a much closer estimate than using P_{surf} (and has the same sign) to calculate $\overline{M}^{'}$. This means that the tropical mean ϵ_p decreased from 0.72 in the control run, to 0.63 in the +4K simulation in the CAM4-IF-r. For the CAM4-IF-t, tropical mean $\overline{P}_{prod}$ increases by 34.7%, very close to the response seen in the CAM4-IF-r version. This implies a 6.2% increase in tropical mean $M^{'}$ in this version, which is close to the tropical mean M_{int} calculated in figure 4.3 of 4.1% and the tropical mean ϵ_p decreases from 0.66 to 0.57. Thus, there is a decrease in precipitation efficiency seen in both CAM4-IF models in the warmer climate.

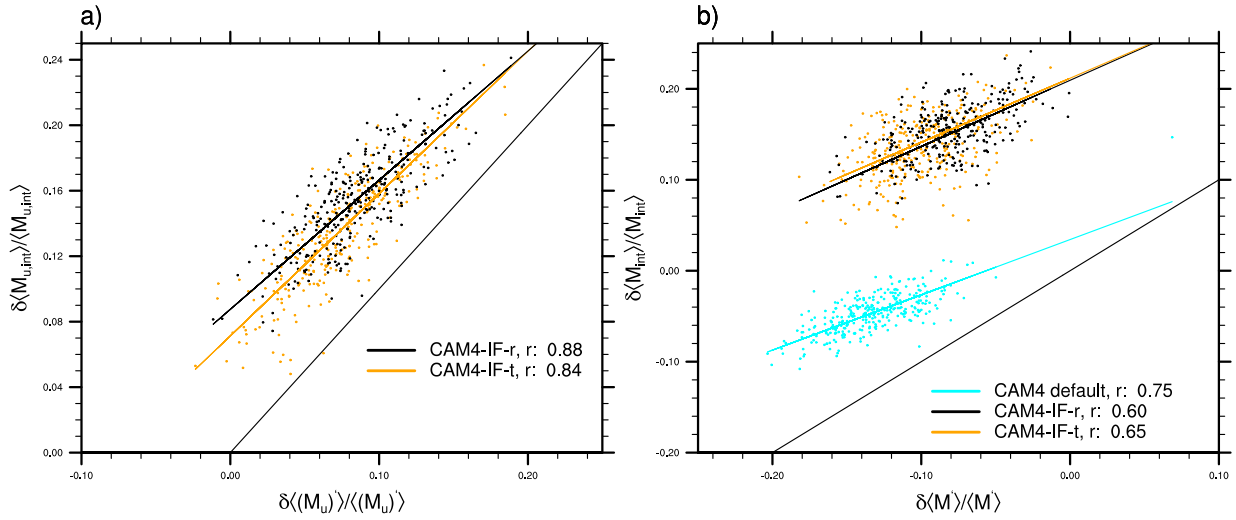

Figure 4.8: **a**: scatter plot of monthly mean tropical mean $\delta\langle M_{u,int}\rangle/\langle M_{u,int}\rangle$ and $\delta\langle M_u^{'}\rangle/\langle M_u^{'}\rangle$ for 300 months of the model runs. Correlation coefficients are indicated in the legend. **b**: same as **a**, except the x-axis is $\delta\langle M^{'}\rangle/\langle M^{'}\rangle$ and the y-axis is $\delta\langle M_{int}\rangle/\langle M_{int}\rangle$.

Figure 4.8**a** demonstrates that using eq. 4.1 gives a much better estimation of the integrated updraft mass flux in the two CAM4-IF models than from using the old relation, eq. 1.36 which estimates integrated total mass flux. This helps demonstrate that it is the precipitation efficiency change that is the reason for why eq. 1.36 is not a good estimate of M_{int} in the CAM4-IF models as eq. 4.1 is not affected by evaporation. Even for the CAM4 default, the estimated mass flux response (4.8**b**) is overestimating the reduction in M_{int}.

The net increase in tropospheric diabatic heating is not affected by the precipitation efficiency, only by the total precipitation reaching the surface. This is because diabatic cooling is created from this evaporation, and is directly proportional to the mass evaporated, multiplied by L_v, the latent heat of vaporization (there is surely some melting and sublimation as well, but the logic for this is the same). Since the converse is also true, $P_{surf} = P_{prod} - E_{trop} \propto \int_{p_{sfc}}^{p_{top}} Q_{cond} dp$ and thus only the change in net precipitation reaching the surface can change the total tropospheric diabatic heating rate due to condensation and thus ω in the tropics (all else being equal; however, the vertical structure can change depending on where the evaporation is occurring in the troposphere). Therefore, the net precipitation rate response will be more important for the local change in tropical circulation than the change in convective mass flux, if the precipitation efficiency can change. The net precipitation will always be directly proportional to the total integrated tropospheric

diabatic heating rate, while the convective mass flux may not. As long as the downdraft mass flux does not simply scale with the evaporation rate, the total convective mass flux response will not be indicative of the total tropospheric diabatic heating response. In the CAM4-IF, not all evaporation goes into generating downdrafts, so this is not the case in the CAM4-IF (Ian Folkins, personal communication).

We also examine the response of the vertical profile of tropical mean tropospheric evaporation of precipitation directly in the three models as precipitation evaporation data is available from the CAM4 default. We see in figure 4.9 that the control run vertical profiles of $\langle \overline{E} \rangle$ in the CAM4 has a peak around 700 hPa. In the CAM4-IF models, the maximum of evaporation rate is lower in the troposphere, around 850 hPa. Also, the evaporation response is much larger in the CAM4-IF models, especially in the lower troposphere, where no change is seen in the CAM4 default below $\approx$ 800 hPa. Note, this figure does not include evaporation of condensate that does fall as precipitation as this data is not available from the CAM4 default.

It could be possible that in the warmer climate that the time mean relative humidity, $\overline{H}$ is reduced in the CAM4-IF models and this would explain the very large increase in evporation that is seen, but this is not what we see in figure 4.10. There is an interesting response of relative humidity in the three CAM4 models, with a drying of the upper troposphere and a moistening below 400 hPa. This mainly appears to represent an upward shift of the control run $\overline{H}$ profile which has a minimum near 400 hPa. The overall column-integrated tropical mean change in $\overline{H}$ is very small ($< 1\%$) for all three models, so it wouldn't appear that the $\overline{H}$ response is responsible for the precipitation efficiency/evaporation response seen in the CAM4-IF models. However, the boundary layer ($<$ 850 hPa) $\overline{H}$ is decreasing by several percent in the CAM4-IF models. This decrease in boundary layer $\overline{H}$ (sub-LCL/cloud base) is thought to be associated with a decrease in precipitation efficiency (Market et al., 2003; Sherwood et al., 2014) and increased low-level mixing (Sherwood et al., 2014).

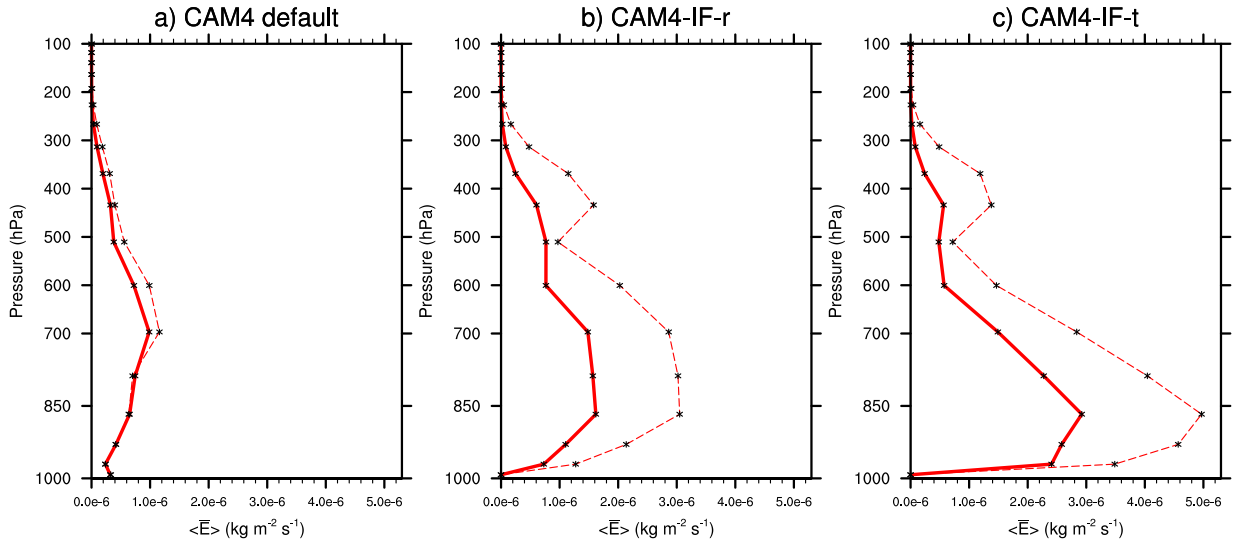

Figure 4.9: **a-c**: tropical mean, time mean, vertical profiles of total evaporation rate of rain and sublimation of snow ($\langle \overline{E} \rangle$). Solid lines indicate the control runs, and dashed lines the +4K SST runs.

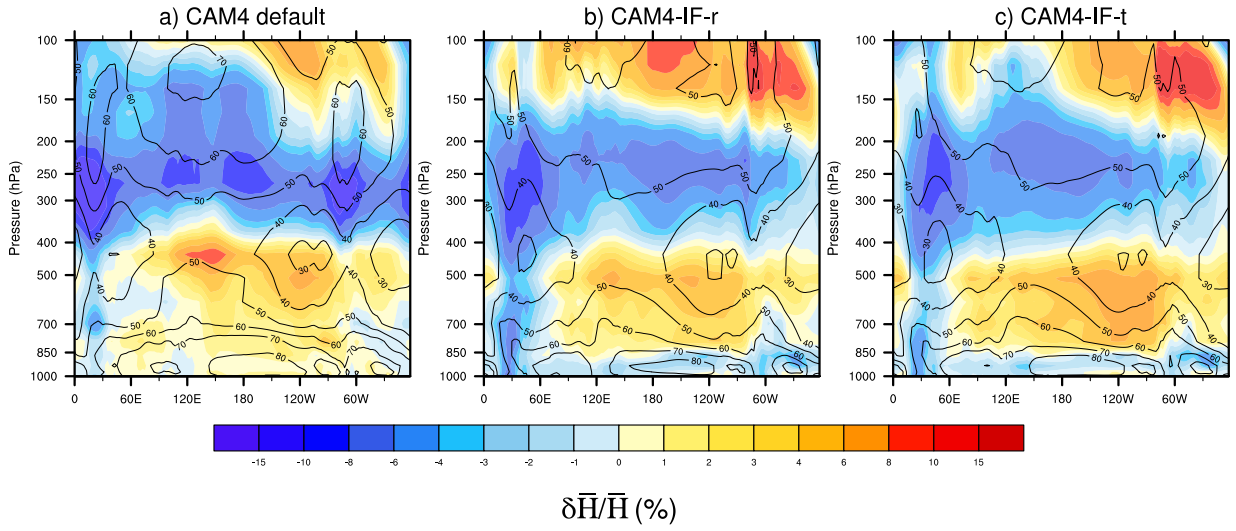

Figure 4.10: **a-c**: 30°S-30°N mean, time mean, relative humidity, $\overline{H}$ fractional response (%). The magnitude of the tropospheric integrated tropical mean change in relative humidity is $< 1\%$ in all three models.

The only other explanation for the much larger increase in evaporation in the CAM4-IF models would be the way that the evaporation of precipitation is parameterized in the scheme. From eqs. 2.9 and 2.15 we see that there is a linear dependence on the saturation mixing ratio, q_s in the IF scheme, while this is not the case in the ZM scheme. In the ZM scheme evaporation depends solely on the relative humidity of the environment and the square root of the rainfall flux. As the troposphere is much warmer in the +4K simulations, the saturation mixing ratio, which is an exponential function of temperature, will increase significantly. Thus, this would explain why the evaporation increases by a much larger amount in the CAM4-IF models.

The difference in the evaporation response in the lower troposphere between the CAM4 with ZM scheme and the CAM4 with IF scheme also helps explain the opposite-signed response in shallow convective mass flux. Since an increase in shallow convective updrafts is seen in both CAM4-IF models in figure 4.6, there would be an increase in condensational heating in the lower troposphere. Since we are looking at the tropical mean evaporation rates, this extra cooling must be balanced by extra heating somehow (see eq. 1.35), and the increase in shallow convection provide this heating. Thus, the opposite-signed response in shallow convective mass flux seen between the CAM4 default and the CAM4-IF models can be explained at least partially by the large increase in lower tropospheric evaporation seen in the CAM4-IF models, versus no significant change seen in the CAM4 default. As the evaporation rate in the ZM scheme depends on the square root of the rainfall rate (see eq. 2.9), and tropical mean precipitation is increasing, it would appear counterintuitive that evaporation would not increase in the lower troposphere, as the CAM4 default model shows. The dependence of evaporation on the saturation mixing ratio is used in the IF scheme because the lower tropospheric evaporative cooling generated beneath strong convection in other schemes is often too weak at high rain rates (Mitovski et al., 2010).

4.3 Walker circulation

As we have seen in table 4.1, there is an overall reduction in tropical mean upward motion in response to a uniform SST warming. This can then be broken down into the zonally symmetric component (Hadley circulation) and the zonally asymmetric component (Walker circulation). Here we will just focus on the Walker circulation as it is predominately influenced by tropical phenomenon, and is of great interest for seasonal-to-decadal climate variability and prediction.. However, we do find that the Hadley circulation in the CAM4 default and CAM4-IF models does weaken with the uniform 4K SST increase, with the CAM4-IF model having a stronger weakening of the boreal winter cells (not shown).

To measure the strength of the Walker circulation we will primarily use two methods; the first being the upper tropospheric velocity potential method of Tanaka et al. (2004), and the other being the average of $(\overline{\omega}^*)^{\uparrow}_{500}$ over the ascending region similar to that used in Wills et al. (2017) (the vertical motion in this region is almost always upward at every grid point, so the $(.)^{\uparrow}$ is unnecessary). We define the ascending region here as 10°S-10°N/90°E-180°E. This region corresponds approximately to the region of maximum ascent in the tropics (see figure 3.5). We also examine the responses of the local zonally anomalous precipitation and column-integrated diabatic heating for the same region which provide an estimate of the response in net heating within the ascending region. Here, the zonal means are subtracted to remove the zonally symmetric component associated with the Hadley circulation (following Wills et al. (2017)).

We see from table 4.2 that a weakening of the Walker circulation is a very robust response across all the CAM4-IF +4K simulations and the CMIP5 AMIP4K models as well. However, the variation in the magnitude of the response is quite large, ranging from a 36.3% decrease seen in the MRI-CGCM3 model to only a 3.1% in the MIROC5 (using $\frac{\delta(\overline{\chi}_{200})^*}{(\overline{\chi}_{200})}$ as a metric, see table 4.2). The $\frac{\delta(\overline{\chi}_{200})^*}{(\overline{\chi}_{200})}$ is well correlated with the metric using $(\overline{\omega}^*)^{\uparrow}_{500}$ (see table caption), so these results are not very sensitive to the metric used. Also, there is a good relationship between the local zonally anomalous $\overline{P}$ response and these two metrics, so we can also infer the response of the Walker circulation from the change in local $\overline{P^*}$ if atmospheric wind data is unavailable. The close relationship of the $\overline{Q}^*_{tot}/\overline{P}$ responses would indicate that the variability in the diabatic heating response from the local precipitation response is largely responsible for the large variability seen in the Walker circulation strength response. We will examine the response of diabatic heating and static stability in the ascending region to see if explains the differences in the response of the Walker circulation for the CAM4/CAM4-IF models.

Table 4.2: Fractional responses of various Walker circulation strength metrics for the CAM4/CAM4-IF models and for AMIP4K models which data is available. $\delta((\varpi^*)^{\uparrow}_{500})/(\varpi^*)^{\uparrow}_{500}$ is the response of the ascending region, 10S-10N/90E-180E 500 hPa, upward zonally anomalous omega. $\frac{\delta\overline{P}^*}{\overline{P}^*}$ is the repsonse of the zonally anomalous precipitation for the ascending region. $\frac{\delta(\overline{Q}_{tot})^*}{(\overline{Q}_{tot})^*}$ is the response of the zonally anomalous total diabatic heating intergrated thorough the troposphere for the ascending region. Finally, $\frac{\delta(\overline{\chi}_{200})^*}{(\chi_{200})}$ is the response of the 200 hPa zonally anomalous velocity potential for the ascending region. The CAM4-IF models generally weaken the Walker circulation more than the CMIP5 AMIP models (based on 200 hPa χ^*). The correlation between the $(\varpi^*)^{\uparrow}_{500}$ and $\overline{\chi}^*_{200}$ measures of Walker circulation strength for the CAM4-IF models is 0.86. The correlation between $\frac{\delta(\overline{Q}_{tot})^*}{(\overline{Q}_{tot})^*}$ and $\delta((\varpi^*)^{\uparrow}_{500})/(\varpi^*)^{\uparrow}_{500}$ is 0.77, while the correlation between $\frac{\delta(\overline{\chi}_{200})^*}{(\overline{\chi}_{200})}$ and $\frac{\delta(\overline{Q}_{tot})^*}{(\overline{Q}_{tot})^*}$ is 0.84. The correlation between $\frac{\delta\overline{P}^*}{\overline{P}^*}$ and $\delta((\varpi^*)^{\uparrow}_{500})/(\varpi^*)^{\uparrow}_{500}$ is 0.66 for the CAM4-IF models and 0.67 for the correlation between $\frac{\delta\overline{P}^*}{\overline{P}^*}$ and $\frac{\delta(\overline{\chi}_{200})^*}{(\overline{\chi}_{200})}$. Finally, the relationship between $\frac{\delta\overline{P}^*}{\overline{P}^*}$ and $\frac{\delta(\overline{\chi}_{200})^*}{(\overline{\chi}_{200})}$ for **all** models is 0.48.

Model	$\delta((\varpi^*)^{\uparrow}_{500})/(\varpi^*)^{\uparrow}_{500}$	$\frac{\delta\overline{P}^*}{\overline{P}^*}$	$\frac{\delta(\overline{Q}_{tot})^*}{(\overline{Q}_{tot})^*}$	$\frac{\delta(\overline{\chi}_{200})^*}{(\overline{\chi}_{200})^*}$
1) Default CAM4	-0.052	0.167	0.083	-0.133
2) CAM4-IF-r	-0.089	0.135	0.093	-0.148
3) CAM4-IF-t	-0.155	0.062	0.043	-0.250
4) CAM4-IF 1	-0.266	0.043	-0.015	-0.272
5) CAM4-IF 2	-0.237	0.098	-0.017	-0.296
6) CAM4-IF 3	-0.160	0.071	0.032	-0.225
7) CAM4-IF 4	-0.212	0.125	0.050	-0.258
8) CAM4-IF 5	-0.238	0.093	0.037	-0.290
9) CAM4-IF 6	-0.165	0.112	0.049	-0.222
10) CAM4-IF 7	-0.219	0.105	0.064	-0.194
11) AMIP - bcc-csm1-1	N/A	0.104	N/A	-0.234
12) AMIP - CanAM4	N/A	0.108	N/A	-0.074
13) AMIP - CCSM4	N/A	0.098	N/A	-0.164
14) AMIP - CNRM-CM5	N/A	0.113	N/A	-0.088
15) AMIP - IPSL-CM5A-LR	N/A	0.018	N/A	-0.065
16) AMIP - IPSL-CM5B-LR	N/A	-0.143	N/A	-0.186
17) AMIP - MIROC5	N/A	0.298	N/A	-0.031
18) AMIP - MRI-CGCM3	N/A	-0.144	N/A	-0.363

Also of interest is the overall spatial pattern of this weakening, which we examine

in figure 4.11. It is apparent qualitatively, that the CAM4-IF models have a stronger weakening of the Walker circulation as evidenced by the positive response in $\overline{\chi}^*_{200}$ over the Indian Ocean/Maritime Continent region. The region of maximum weakening of $\overline{\chi}^*_{200}$ in the ascending region is qualitatively similar in the CAM4-IF models and in the AMIP4K mean, but is focused more on the western Indian Ocean and Africa in the CAM4 default. It is apparent that the spatial pattern of the response of $\overline{\chi}^*_{200}$ is different between the CAM4 default and the CAM4-IF, highlighting the fact the spatial pattern of the response in upper-tropospheric divergence is sensitive to the convective scheme used.

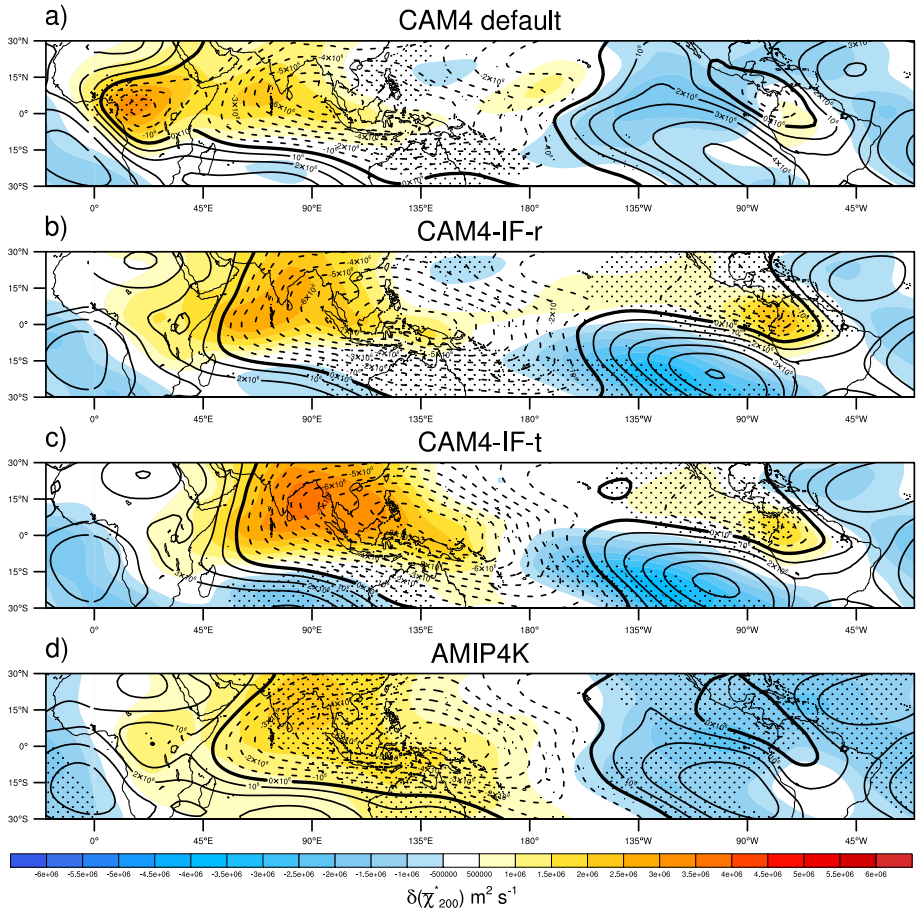

Figure 4.11: **a)-c)**: 200 hPa annual mean $\overline{\chi}^*_{200}$ response (shaded) with the control run annual mean climatology in contours. Stippling indicates regions where the response is larger in size than the largest (same-signed) response of the CMIP5 AMIP models.**d)**: The AMIP4K ensemble mean response of $\overline{\chi}^*_{200}$. Note the closer fit of the control and response of the AMIP mean to the CAM4-IF. Stippling indicates regions where 10 or more of 12 models agree on the sign of the response.

To determine the relative importance of the static stability response compared to the diabatic heating response in determining the circulation response, we can decompose the $\bar{\omega}$ in the ascending region into two components by using eq. 1.16 (Yanai et al., 1973; Li et al., 2015):

$$\delta\bar{\omega} = -\frac{\delta\overline{Q_{tot}}}{\bar{\sigma}} + \frac{\overline{Q_{tot}}}{\bar{\sigma}^2}\delta\bar{\sigma} \tag{4.2}$$

This effectively breaks the $\bar{\omega}$ response down into diabatic heating (term 1) and static stability (term 2) response terms. Thus, the total $\bar{\omega}$ response is a residual of these two terms, which are opposite in sign. Here, $\overline{Q}_{tot}$ is the sum of all the diabatic heating terms in the model; radiative heating (longwave and shortwave), moist processes (net of evaporation/condensation, sublimation and melting/freezing) and a small contribution from turbulent diffusion of heat from the land/ocean surface in the model boundary layer.

Figure 4.12 shows the response of these two terms for the three models, with the CAM4 having a weaker column-integrated (1000-50 hPa) $\bar{\omega}$ weakening of 0.0023 Pa s^{-1} with column-integrated value for term 1 in 4.2 of -0.0044 Pa s^{-1} and 0.0067 Pa s^{-1} for term 2. The same values for the CAM4-IF-r and CAM4-IF-t are 0.0032 Pa s^{-1}, -0.0024 Pa s^{-1}, 0.0076 Pa s^{-1} and 0.0047 Pa s^{-1}, -0.00039 Pa s^{-1}, 0.0069 Pa s^{-1}, respectively. Thus, it appears that the column-integrated effect of the static stability response component of the $\bar{\omega}$ response is quite similar between the CAM4 default and CAM4-IF models, with a much larger range in the diabatic heating response terms. The diabatic heating response is weaker in both CAM4-IF models than in the CAM4 default and this can be explained at least partially by the response in local precipitation (see table 4.2) in the ascending region being smaller, and thus the diabatic heating response from condensation would be smaller there.

In summary, although the tropical mean convective mass flux strengthens in the CAM4-IF models (as previously discussed), the Walker circulation actually *weakens* more than in the default CAM4 when a 4K SST warming is applied. This seems to indicate that the response of the tropical mean convective mass flux is not important to the response of the Walker circulation, or at the very least, there is a physically plausible scenario in which tropical mean convective mass flux may increase, but the Walker circulation slows down. This is in contradiction to Held & Soden (2006); Vecchi & Soden (2007) which connect the tropical mean convective mass flux response to the slowdown of the tropical circulations. Thus, it would seem that the static stability increase is the main reason why the Walker circulation slows down as the static stability must increase by a fairly constrained amount due to moist adiabatic adjustment from the 4K SST warming. This supports the "MASC" (mean advection of stability change) mechanism for tropical circulation weakening that is

postulated in Ma et al. (2011) and earlier in Knutson & Manabe (1995). The variability in the magnitude of the weakening of the Walker circulation appears to be mainly controlled by the magnitude of the diabatic heating response in the ascending region, which is related to the local precipitation change.

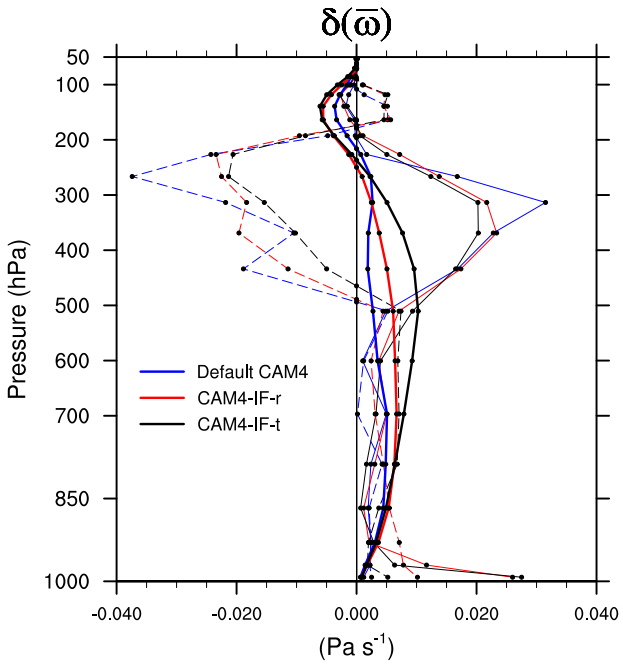

Figure 4.12: Response of $\bar{\omega}$ (thick, solid) in the ascending region (10°S-10°N/90°E-180°E) of the Walker circulation broken down into the terms in eq. 4.2. The dashed lines indicate the response of the first (diabatic heating) term in eq. 4.2, and the solid lines the second (static stability) term.

Chapter 5

Discussion and conclusion

5.1 Discussion

In summary, we have found that the convective mass flux is not as constrained as previously thought to decrease in a warmer climate. This is because the connection between the convective mass flux and the large scale circulation is not direct, but via the net heating per unit mass flux. The amount of heating per unit mass flux can change significantly if evaporation increases sufficiently. Additionally, it appears that the tropical circulations can still have a response that is opposite in sign to the tropical mean convective mass flux response; i.e., the tropical mean convective mass flux could increase, even while the tropical circulations slow down. In fact, it would appear that the tropical mean upward motion is more constrained than the convective mass flux to weaken due to climate change, due to the large increase in tropical mean static stability. This increase in static stability is independent of the convective scheme used, while the convective mass flux response is not.

The variability in the response of the Walker circulation appears to be mainly driven by differences in the diabatic heating response in the ascending region for simulations with a uniform SST warming. Since the static stability response is very similar among models with a uniform SST warming, because the tropical mean lapse rate essentially adjusts to the new warmer moist adiabat. If the hydrological cycle argument of Held & Soden (2006) were the main reason why the Walker circulation would weaken, one would not expect much spread beyond in the response to a uniform SST forcing beyond that of the variation in tropical mean precipitation response. Changes in the zonally anomalous diabatic heating in the ascending region due to changes in local precipitation (or perhaps

cloud heating), which are not as constrained as the tropical mean precipitation is, seem to be responsible to explain at least part of the variability in the Walker circulation response. Indeed, in Schneider et al. (2010) they note that applying this global mean hydrological cycle argument to the local circulations in the tropics is probably naive.

The consequences of the convective mass flux response may seem at first to likely be unimportant to important climate change metrics like climate sensitivity, however, as some recent studies have shown (Sherwood et al., 2014; Brient et al., 2016), low-level convective mixing is thought to be key to the magnitude of the low cloud feedback which is responsible for a large portion of the spread in climate sensitivity projections. It is likely that a model with a poor convective scheme could do a reasonable job with the large scale pattern of tropical precipitation, but have a poor representation of low-level mixing and thus an unrealistic climate sensitivity. Since direct measurements of low-level mixing are hard to come by in the tropics, but radiosonde data is not as scarce, a good starting point would be to use the observed temperature and moisture distributions as these are a result of this low-level mixing. This is the advantage to using the IF scheme in the CAM4 presented here - it has a superior representation of the low-level stratification of temperature than any AMIP model is consistent with the view that it has a better representation of low-level mixing.

In our simulations, we find that the climate sensitivity does not appear to be sensitive to the convective scheme, even though there are some small differences in the cloud radiative forcing response. This is similar to the results of Webb et al. (2015) which found that turning the convective scheme off in the AMIP4K simulations (which use a variety of convective schemes) had little impact on the climate sensitivity. Using the methodology of Cess et al. (1990), we find that the climate sensitivity parameter, λ, for both the CAM4 default and the CAM4-IF-t is ≈ 0.47 K W^{-1} m^{-2}. We also find that the change in CRF (cloud radiative forcing) between the control simulation, and the +4K simulations is $\approx$ -2.0 W^{-1} m^{-2} for the CAM4 default, and $\approx$ -1.6 W^{-1} m^{-2} for the CAM4-IF-t. This means the CAM4-IF-t has a slightly weaker negative (cooling) cloud feedback. Breaking this down further into the shortwave (low cloud) and longwave (high cloud) components reveals that there is a slight reduction in the shortwave (cooling) cloud radiative effect in the CAM4-IF-t, but this is more than offset by a reduction in the longwave (warming) cloud effect, which leads to a net cooling effect. In the CAM4 default there is actually increase in the cooling effect of low clouds, that is only partially offset by a small increase in the warming effect of high cloud. While the two models have the same climate sensitivity, if the CAM4-IF did not have an offsetting longwave cloud feedback, this would not be the case and the CAM4-If would indeed have a larger climate sensitivity. So the reduction in shortwave cooling does seem consistent with Sherwood et al. (2014); Brient et al. (2016), but the effect is

small in this model (CAM4-IF), even though the shallow convective mixing is increasing.

It should be very clearly noted that a uniform increase in SST is not the only factor that will influence tropical precipitation due to climate change. These experiments here are using atmosphere only models only and do not take into account the effects of changing patterns of tropical SST and the radiative effects of CO2 on the temperature structure of the tropical troposphere. These experiments should not be seen as equivalent to the RCP8.5 fully coupled climate model simulations. A good outline of the relative importance of the mean SST, CO2 and SST pattern effects is done in He & Soden (2015). The mean SST effect is thought to be most important for the overall weakening of convective mass flux and the tropical circulations in the tropics, however (Held & Soden, 2006; Ma et al., 2011; Vecchi & Soden, 2007; He & Soden, 2015). Furthermore, non-linear interactions between the atmosphere and ocean are not taken into account in these atmosphere-only simulations.

5.2 Conclusions

We have shown that indeed there are impacts on the simulation of the tropical circulation in the modern climate, and in the response of the tropical circulation to climate change. The center of the ascending region of the Walker circulation in the CAM4-IF in the present day climate is shifted more eastward over the Maritime Continent, compared to the CAM4 with the default convective scheme, and is in better agreement with reanalysis data. Also, the magnitude of the response of the tropical circulation is affected by the convective scheme, although the sign of the response does not change; both versions of the models show a weakening of tropical overturning and the Walker circulation. Thus, it would acceptable to reject the null hypothesis that the convective scheme has no affect on the tropical circulation in the modern or future climate in this model. The experiment performed here is quite simplistic, however, and as He & Soden (2015); Ma & Xie (2012) and others have shown, the SSTs certainly do not warm uniformly with climate change, and this has important impacts on the tropical circulation as well.

However, the tropical mean convective mass flux response does not decrease when the IF scheme is used and this is in contradiction to accepted theory (Held & Soden, 2006; Vecchi et al., 2006) and modelling studies (Chadwick et al., 2012). This might be cause for concern about how physically realistic the model using this scheme is, but perhaps that is the wrong way of looking at this project. A better way is to think of this experiment as a thought experiment to help better understand the ways in which a convective parameterization can affect the tropical circulations; a kind of "what if" scenario. It should also be stressed that this scheme was not tuned in any way to produce the best global climate, and was primarily

focused on improving the tropical climate. This is also the first time it has been tested for a warmer climate, and has not been tuned in any way for a warmer climate. Thus, the use of this scheme in the CAM4 for global climate projections should be discouraged.

Perhaps the most interesting and impactful result is the large increase in shallow convective updraft strength seen in the CAM4-IF model simulations. This would indicate that shallow convective mixing is increasing and is the opposite response to that which is seen in the default CAM4 simulations. As was discussed in the previous section, the climate sensitivity appears to almost identical to the default CAM4 model, which is in contrast to what would be expected with increased shallow mixing (Sherwood et al., 2014). There is a more positive shortwave cloud feedback in the CAM4-IF models, but it is offset by a decrease in high cloud that leads to a more negative longwave cloud feedback than in the CAM4 default. This decrease in high cloud could explain the very large increase seen in tropical mean precipitation in the CAM4-IF simulations, when compared to the AMIP4K models, and the CAM4 default. A decrease in high cloud cover from climate change allows for more radiative cooling in the free troposphere and this allows for more latent heating from precipitation to balance it (Su et al., 2017), and thus a larger precipitation response. Thus, our work does not necessarily disprove the results of Sherwood et al. (2014) as there are two competing processes operating in the CAM4-IF climate change simulations.

5.3 Future work

In some ways this research raises more questions than it answers, and a number of them could be explored outside of using this convective scheme. It is possible that convective mass flux may actually increase in a warmer climate, although the consequences of this are unclear, and it is certainly the case that the tropical mean precipitation response is quite constrained. One simple future project would be to implement this scheme with the newer versions of the CAM models, the CAM5 and CAM6, which still use the ZM scheme. It is possible that significant code modifications may be required for this, however. The fact that the ZM scheme is still being used in the latest versions of this model underscores how slow progress is towards creating improved convective schemes. There is a new scheme being developed for the CAM, called the UNICON scheme (Park, 2014a,b) which simulates all convective processes (including dry "turbulent" convection) and does not make any assumptions about quasi-equilibrium. However, this scheme is not being used as the default scheme in the latest CAM version (CAM6) (Richard Neale (NCAR), personal communication). In some ways, it seems that modelers are forgoing much work on convective parameterization in favour of cloud resolving models, or "super-parameterizations" (Li

et al., 2012) that will become more feasible as the model resolution is allowed to increase due to increased computing power, and are already being used today. However, they will likely not be used for the new CMIP6 experiments, to the author's knowledge (in the case of the new CAM6, it will continue to use the deep ZM scheme). It is likely that simulations that use super-parameterizations are not feasible for long time integrations and experiments where there are ensemble members (such as in CMIP) with today's computing resources.

There are many other experiments that could be performed to test the same research questions with this scheme. One of the simplest would be to perform a "patterned" SST increase experiment, which is similar to the experiments performed for this thesis, but instead of a uniform SST increase, we would use the SST spatial response pattern seen in coupled climate simulations. This experiment was not performed for this thesis as the imposed SST boundary conditions could possible overwhelm any influence of the convective scheme on the tropical circulation. The uniform 4K SST warming simulations performed here are a much more "clean" type of experiment. Another type of experiment that could help further isolate how the convective scheme affects the tropical circulation would be a so-called "aquaplanet" type simulation, where all the land coverage is removed and thus any impacts of land such as monsoon circulations would be removed. This would have been the ideal type of simulation to perform here, but unfortunately, this type of simulation was not supported in the version of CESM which worked with this scheme. As these simulations were not coupled to an ocean model, another type of experiment to perform would be coupled ocean-atmosphere simulations with increased CO_2 levels ($4xCO_2$, for example). These simulations may help fix the unrealistically strong South Asian monsoon in the seen in the CAM4-IF simulations as the large latent heat fluxes in that region needed to sustain the circulation would cause the SSTs to cool. Coupled simulations were not performed because this scheme has not been tested in a coupled model system, and is much more computationally expensive.

As this scheme is still under development, a future project could be to tune the scheme (or make more drastic changes) to improve features such as the time mean tropical precipitation representation. Additionally, the inter-annual, seasonal and sub-seasonal tropical rainfall could also be improved as we know there are issues with the South Asian Summer Monsoon. As a significant improvement in the representation is seen in the CAM4-IF-r version which has low-level downdrafts turned off, so it is likely related to low-level downdrafts. Another region for improvement would be in the representation of inter-annual variability such as the Madden-Julian Oscillation (MJO) (Madden & Julian, 1971, 1972; Zhang) and equatorial Kelvin wave activity. Power spectra analysis (figure 5.1) from the control CAM4-IF simulations did indicate some improvement in the representation of this

variability when compared to TRMM satellite rainfall data, mainly for the MJO, but was too active compared to observations in the Kelvin wave portion of the spectrum, so there is still some room for improvements in this region. Finally, one fairly simple future experiment to perform to test the impact of the parameterization of convective precipitation evaporation would be to use the ZM formulation for evaporation (eq. 2.9) in the IF scheme and determine whether the response of the tropical mean convective mass flux to climate change changes.

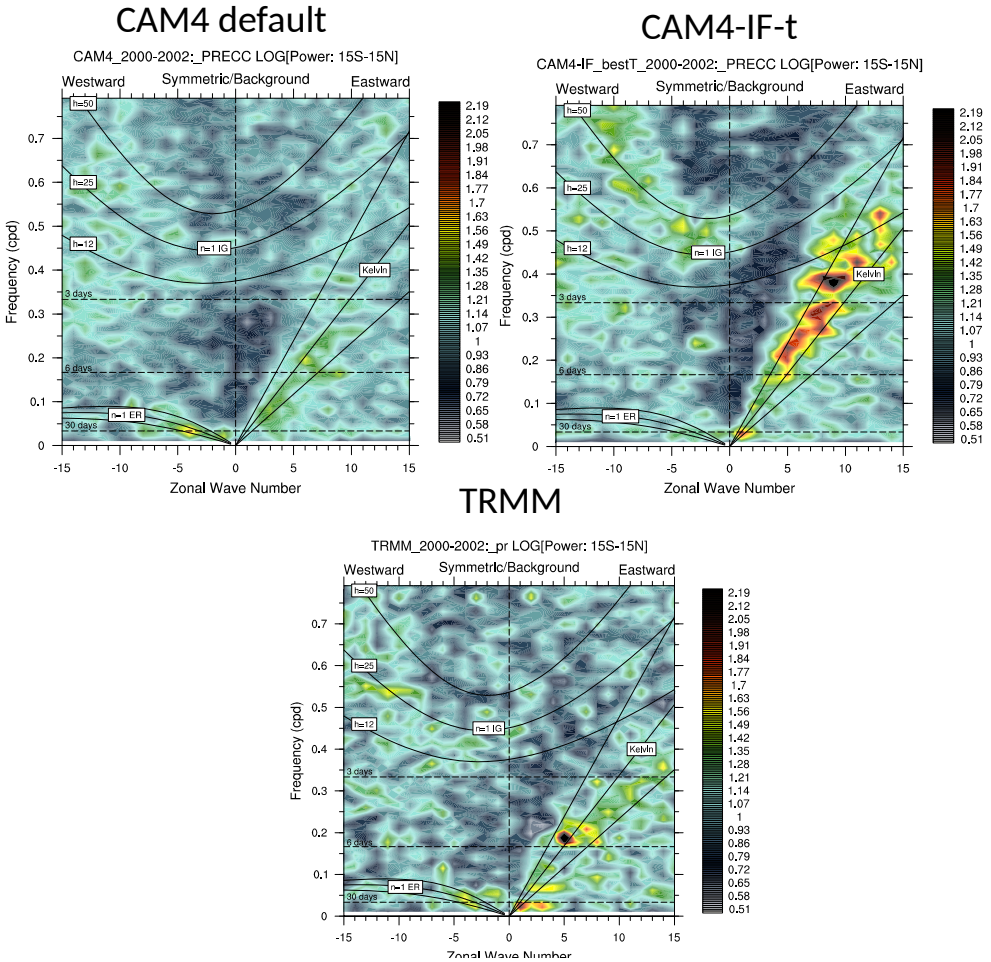

Figure 5.1: Wheeler-Kiladis diagrams (symmetric about the equator portion of spectra) for the period 2000-2002 (monthly time-series SST runs) derived from 15°S-15°N 3-hourly rainfall rates. Note that the CAM4-IF-t has more power nearer to the origin in the wavenumber 0-5 region, which is associated with the MJO, and is closer to TRMM observations. However, there is too much power in the CAM4-IF-t in the Kelvin wave portion of the spectra, especially for high zonal wavenumbers.

References

Virtual temperature - AMS Glossary, 2012. URL http://glossary.ametsoc.org/wiki/Virtual_temperature. Accessed: 2016-05-10.

Adler, R. F., Huffman, G. J., Chang, A., Ferraro, R., Xie, P.-P., Janowiak, J., Rudolf, B., Schneider, U., Curtis, S., Bolvin, D., Gruber, A., Susskind, J., Arkin, P., & Nelkin, E. The version-2 global precipitation climatology project (GPCP) monthly precipitation Analysis (1979-present). *Journal of Hydrometeorology*, volume 4(6):pp. 1147–1167, 2003. ISSN 1525-755X. doi:10.1175/1525-7541(2003)004⟨1147:TVGPCP⟩2.0.CO;2.

Allen, M. R. & Ingram, W. J. Constraints on future changes in climate and the hydrologic cycle. *Nature*, volume 419(6903):pp. 224–232, 2002. ISSN 0028-0836. doi:10.1038/nature01092.

Arakawa & Schubert. Interaction of a cumulus cloud ensemble with the large-scale environment, part I. *Journal of the Atmospheric Sciences*, volume 31(3):pp. 674–701, 1974. doi:10.1175/1520-0469(1974)031⟨0674:IOACCE⟩2.0.CO;2.

Arakawa, A. The cumulus parameterization problem: Past, present, and future. *Journal of Climate*, volume 17(13):pp. 2493–2525, 2004. ISSN 0894-8755. doi:10.1175/1520-0442(2004)017⟨2493:RATCPP⟩2.0.CO;2.

Bjerknes, J. Atmospheric teleconnections from the equatorial pacific. *Monthly Weather Review*, volume 97(3):pp. 163–172, 1969. ISSN 0027-0644. doi:10.1175/1520-0493(1969)097⟨0163:ATFTEP⟩2.3.CO;2.

Boer, G. J. Climate change and the regulation of the surface moisture and energy budgets. *Climate Dynamics*, volume 8(5):pp. 225–239, 1993. ISSN 0930-7575, 1432-0894. doi:10.1007/BF00198617.

Bony, S., Webb, M., Bretherton, C. S., Klein, S. A., Siebesma, P., Tselioudis, G., & Zhang, M. CFMIP: Towards a better evaluation and understanding of clouds and cloud

feedbacks in CMIP5 models. *Clivar Exchanges*, volume 56(2):pp. 20–22, 2011. URL http://www.euclipse.eu/downloads/CFMIP_CMIP5_Exchanges_May2011.pdf.

Brient, F., Schneider, T., Tan, Z., Bony, S., Qu, X., & Hall, A. Shallowness of tropical low clouds as a predictor of climate models response to warming. *Climate Dynamics*, volume 47(1-2):pp. 433–449, 2016. ISSN 0930-7575, 1432-0894. doi: 10.1007/s00382-015-2846-0.

Cess, R. D., Potter, G. L., Blanchet, J. P., Boer, G. J., Del Genio, A. D., Dqu, M., Dymnikov, V., Galin, V., Gates, W. L., Ghan, S. J., Kiehl, J. T., Lacis, A. A., Le Treut, H., Li, Z.-X., Liang, X.-Z., McAvaney, B. J., Meleshko, V. P., Mitchell, J. F. B., Morcrette, J.-J., Randall, D. A., Rikus, L., Roeckner, E., Royer, J. F., Schlese, U., Sheinin, D. A., Slingo, A., Sokolov, A. P., Taylor, K. E., Washington, W. M., Wetherald, R. T., Yagai, I., & Zhang, M.-H. Intercomparison and interpretation of climate feedback processes in 19 atmospheric general circulation models. *Journal of Geophysical Research: Atmospheres*, volume 95(D10):pp. 16601–16615, 1990. ISSN 2156-2202. doi:10.1029/JD095iD10p16601.

Chadwick, R., Boutle, I., & Martin, G. Spatial patterns of precipitation change in CMIP5: Why the rich do not get richer in the tropics. *Journal of Climate*, volume 26(11):pp. 3803–3822, 2012. ISSN 0894-8755. doi:10.1175/JCLI-D-12-00543.1.

Charney, J. G. A note on large-scale motions in the tropics. *Journal of the Atmospheric Sciences*, volume 20(6):pp. 607–609, 1963. ISSN 0022-4928. doi:10.1175/1520-0469(1963)020⟨0607:ANOLSM⟩2.0.CO;2.

Chen, M., Xie, P., Janowiak, J. E., & Arkin, P. A. Global land precipitation: A 50-yr monthly analysis based on gauge observations. *Journal of Hydrometeorology*, volume 3(3):pp. 249–266, 2002. ISSN 1525-755X. doi:10.1175/1525-7541(2002)003⟨0249:GLPAYM⟩2.0.CO;2.

Chou, C., Neelin, J. D., Chen, C.-A., & Tu, J.-Y. Evaluating the rich-get-richer mechanism in tropical precipitation change under global warming. *Journal of Climate*, volume 22(8):pp. 1982–2005, 2009. ISSN 0894-8755. doi:10.1175/2008JCLI2471.1.

Dee, D. P., Uppala, S. M., Simmons, A. J., Berrisford, P., Poli, P., Kobayashi, S., Andrae, U., Balmaseda, M. A., Balsamo, G., Bauer, P., Bechtold, P., Beljaars, A. C. M., van de Berg, L., Bidlot, J., Bormann, N., Delsol, C., Dragani, R., Fuentes, M., Geer, A. J., Haimberger, L., Healy, S. B., Hersbach, H., Hlm, E. V., Isaksen, L., Kllberg, P., Khler, M., Matricardi, M., McNally, A. P., Monge-Sanz, B. M., Morcrette, J.-J., Park, B.-K., Peubey, C., de Rosnay, P., Tavolato, C., Thpaut, J.-N., & Vitart, F. The ERA-Interim

reanalysis: configuration and performance of the data assimilation system. *Quarterly Journal of the Royal Meteorological Society*, volume 137(656):pp. 553–597, 2011. ISSN 1477-870X. doi:10.1002/qj.828.

Doswell, C. A. & Rasmussen, E. N. The effect of neglecting the virtual temperature correction on CAPE calculations. *Weather and Forecasting*, volume 9(4):pp. 625–629, 1994. ISSN 0882-8156. doi:10.1175/1520-0434(1994)009⟨0625:TEONTV⟩2.0.CO;2.

Emanuel, K. Quasi-equilibrium dynamics of the tropical atmosphere. *The Global Circulation of the Atmosphere*, pp. 186–218, 2007.

Evans, J.-L. & Laing, A. *Introduction to Tropical Meteorology, Ch. 5: Moisture and Precipitation*. The COMET Program (UCAR), 2 edition, 2011. URL http://www.goes-r.gov/users/comet/tropical/textbook_2nd_edition/navmenu.php_tab_6_page_2.2.1.htm.

Fan, F., Mann, M. E., Lee, S., & Evans, J. L. Future changes in the South Asian Summer Monsoon: An analysis of the CMIP3 multimodel projections. *Journal of Climate*, volume 25(11):pp. 3909–3928, 2012. ISSN 0894-8755. doi:10.1175/JCLI-D-11-00133.1.

Folkins, I. A low-level circulation in the tropics. *Journal of the Atmospheric Sciences*, volume 65(3):pp. 1019–1034, 2008. ISSN 0022-4928. doi:10.1175/2007JAS2463.1.

Folkins, I. The melting level stability anomaly in the tropics. *Atmos. Chem. Phys.*, volume 13(3):pp. 1167–1176, 2013. ISSN 1680-7324. doi:10.5194/acp-13-1167-2013.

Folkins, I. & Braun, C. Tropical rainfall and boundary layer moist entropy. *Journal of Climate*, volume 16(11):pp. 1807–1820, 2003. ISSN 0894-8755. doi:10.1175/1520-0442(2003)016⟨1807:TRABLM⟩2.0.CO;2.

Folkins, I., Mitovski, T., & Pierce, J. R. A simple way to improve the diurnal cycle in convective rainfall over land in climate models. *Journal of Geophysical Research: Atmospheres*, volume 119(5):pp. 2113–2130, 2014. ISSN 2169-8996. doi:10.1002/2013JD020149.

Garrett, T. J., Gerber, H., Baumgardner, D. G., Twohy, C. H., & Weinstock, E. M. Small, highly reflective ice crystals in low-latitude cirrus. *Geophysical Research Letters*, volume 30(21):p. 2132, 2003. ISSN 1944-8007. doi:10.1029/2003GL018153.

Hack, J. J. Parameterization of moist convection in the National Center for Atmospheric Research community climate model (CCM2). *Journal of Geophysical Research: Atmospheres*, volume 99(D3):pp. 5551–5568, 1994. ISSN 2156-2202. doi:10.1029/93JD03478.

He, J. & Soden, B. J. Anthropogenic weakening of the tropical circulation: The relative roles of direct CO2 forcing and sea surface temperature change. *Journal of Climate*, volume 28(22):pp. 8728–8742, 2015. ISSN 0894-8755. doi:10.1175/JCLI-D-15-0205.1.

Held, I. M. & Soden, B. J. Robust responses of the hydrological cycle to global warming. *Journal of Climate*, volume 19(21):pp. 5686–5699, 2006. ISSN 0894-8755. doi:10.1175/JCLI3990.1.

Hollars, S., Fu, Q., Comstock, J. M., & Ackerman, T. P. Comparisons of cloud-top height retrievals from ground-based 35 GHz MMCR and GMS-5 Satellite Observations at ARM TWP MANUS Site. *Atmospheric Research*, volume 72(1-4), 2004. doi:10.1016/j.atmosres.2004.03.015.

Holton, J. R. *An Introduction to Dynamic Meteorology*. Academic Press, 4^{th} edition, 2004. ISBN 978-0-12-354015-7. Google-Books-ID: fhW5oDv3EPsC.

Katsaros, K. Evaporation and humidity. In *Encyclopedia of Ocean Sciences*, pp. 870–877. Elsevier, 2001. ISBN 978-0-12-227430-5. DOI: 10.1006/rwos.2001.0068.

Kay, J. E., Deser, C., Phillips, A., Mai, A., Hannay, C., Strand, G., Arblaster, J. M., Bates, S. C., Danabasoglu, G., Edwards, J., Holland, M., Kushner, P., Lamarque, J.-F., Lawrence, D., Lindsay, K., Middleton, A., Munoz, E., Neale, R., Oleson, K., Polvani, L., & Vertenstein, M. The Community Earth System Model (CESM) Large Ensemble Project: A community resource for studying climate change in the presence of internal climate variability. *Bulletin of the American Meteorological Society*, volume 96(8):pp. 1333–1349, 2014. ISSN 0003-0007. doi:10.1175/BAMS-D-13-00255.1.

Knutson, T. R. & Manabe, S. Time-mean response over the tropical pacific to increased C02 in a coupled ocean-atmosphere model. *Journal of Climate*, volume 8(9):pp. 2181–2199, 1995. ISSN 0894-8755. doi:10.1175/1520-0442(1995)008⟨2181:TMROTT⟩2.0.CO;2.

Kristjnsson, J. E., Edwards, J. M., & Mitchell, D. L. Impact of a new scheme for optical properties of ice crystals on climates of two GCMs. *Journal of Geophysical Research: Atmospheres*, volume 105(D8):pp. 10063–10079, 2000. ISSN 2156-2202. doi:10.1029/2000JD900015.

L'Heureux, M. L., Lee, S., & Lyon, B. Recent multidecadal strengthening of the Walker circulation across the tropical Pacific. *Nature Climate Change*, volume 3(6):pp. 571–576, 2013. ISSN 1758-678X. doi:10.1038/nclimate1840.

Li, F., Rosa, D., Collins, W. D., & Wehner, M. F. Super-parameterization: A better way to simulate regional extreme precipitation? *Journal of Advances in Modeling Earth Systems*, volume 4(2):p. M04002, 2012. ISSN 1942-2466. doi:10.1029/2011MS000106.

Li, T., Zhang, L., & Murakami, H. Strengthening of the Walker circulation under global warming in an aqua-planet general circulation model simulation. *Advances in Atmospheric Sciences*, volume 32(11):pp. 1473–1480, 2015. ISSN 0256-1530, 1861-9533. doi:10.1007/s00376-015-5033-7.

Liu, Z., Ostrenga, D., Teng, W., & Kempler, S. Tropical rainfall measuring mission (TRMM) precipitation data and services for research and applications. *Bulletin of the American Meteorological Society*, volume 93(9):pp. 1317–1325, 2012. ISSN 0003-0007. doi:10.1175/BAMS-D-11-00152.1.

Love, P. US high vertical resolution radiosondes :: SPARC, 2013. URL http://www.sparc-climate.org/data-center/data-access/us-radiosonde/.

Ma, J. & Xie, S.-P. Regional patterns of sea surface temperature change: A source of uncertainty in future projections of precipitation and atmospheric circulation. *Journal of Climate*, volume 26(8):pp. 2482–2501, 2012. ISSN 0894-8755. doi:10.1175/JCLI-D-12-00283.1.

Ma, J., Xie, S.-P., & Kosaka, Y. Mechanisms for tropical tropospheric circulation change in response to global warming. *Journal of Climate*, volume 25(8):pp. 2979–2994, 2011. ISSN 0894-8755. doi:10.1175/JCLI-D-11-00048.1.

Madden, R. A. & Julian, P. R. Detection of a 40-50 day oscillation in the zonal wind in the tropical pacific. *Journal of the Atmospheric Sciences*, volume 28(5):pp. 702–708, 1971. ISSN 0022-4928. doi:10.1175/1520-0469(1971)028⟨0702:DOADOI⟩2.0.CO;2.

Madden, R. A. & Julian, P. R. Description of global-scale circulation cells in the tropics with a 4050 day period. *Journal of the Atmospheric Sciences*, volume 29(6):pp. 1109–1123, 1972. ISSN 0022-4928. doi:10.1175/1520-0469(1972)029⟨1109:DOGSCC⟩2.0.CO;2.

Manabe, S. & Wetherald, R. T. Thermal equilibrium of the atmosphere with a given distribution of relative humidity. *Journal of the Atmospheric Sciences*, volume 24(3):pp. 241–259, 1967. ISSN 0022-4928. doi:10.1175/1520-0469(1967)024⟨0241:TEOTAW⟩2.0.CO;2.

Mapes, B. E. Gregarious tropical convection. *Journal of the Atmospheric Sciences*, volume 50(13):pp. 2026–2037, 1993. ISSN 0022-4928. doi:10.1175/1520-0469(1993)050⟨2026:GTC⟩2.0.CO;2.

Market, P., Allen, S., Scofield, R., Kuligowski, R., & Gruber, A. Precipitation efficiency of warm-season midwestern mesoscale convective systems. *Weather and Forecasting*, volume 18(6):pp. 1273–1285, 2003. ISSN 0882-8156. doi:10.1175/1520-0434(2003)018⟨1273:PEOWMM⟩2.0.CO;2.

Merlis, T. M. *The general circulation of the tropical atmosphere and climate changes*. Ph.D. thesis, California Institute of Technology, 2012. URL http://thesis.library.caltech.edu/6533/.

Merlis, T. M. & Schneider, T. Changes in zonal surface temperature gradients and Walker circulations in a wide range of climates. *Journal of Climate*, volume 24(17):pp. 4757–4768, 2011. ISSN 0894-8755, 1520-0442. doi:10.1175/2011JCLI4042.1. ArXiv: 1009.0301.

Mitas, C. M. & Clement, A. Recent behavior of the Hadley cell and tropical thermodynamics in climate models and reanalyses. *Geophysical Research Letters*, volume 33(1):p. L01810, 2006. ISSN 1944-8007. doi:10.1029/2005GL024406.

Mitchell, J. F. B., Wilson, C. A., & Cunnington, W. M. On CO2 climate sensitivity and model dependence of results. *Quarterly Journal of the Royal Meteorological Society*, volume 113(475):pp. 293–322, 1987. ISSN 1477-870X. doi:10.1002/qj.49711347517.

Mitovski, T., Folkins, I., von Salzen, K., & Sigmond, M. Temperature, relative humidity, and divergence response to high rainfall events in the tropics: Observations and models. *Journal of Climate*, volume 23(13):pp. 3613–3625, 2010. ISSN 0894-8755. doi:10.1175/2010JCLI3436.1.

Neale, R., Richter, J., H., Conley, A., J., & Park, S. Description of the NCAR Community Atmosphere Model (CAM4.0), 2010. URL http://www.cesm.ucar.edu/models/ccsm4.0/cam/docs/description/cam4_desc.pdf.

Neale, R. B., Richter, J., Park, S., Lauritzen, P. H., Vavrus, S. J., Rasch, P. J., & Zhang, M. The mean climate of the Community Atmosphere Model (CAM4) in forced SST and fully coupled experiments. *Journal of Climate*, volume 26(14):pp. 5150–5168, 2013. ISSN 0894-8755. doi:10.1175/JCLI-D-12-00236.1.

O'Gorman, P. A., Allan, R. P., Byrne, M. P., & Previdi, M. Energetic constraints on precipitation under climate change. *Surveys in Geophysics*, volume 33(3-4):pp. 585–608, 2012. ISSN 0169-3298, 1573-0956. doi:10.1007/s10712-011-9159-6.

Park, S. A unified convection scheme (UNICON). Part I: Formulation. *Journal of the Atmospheric Sciences*, volume 71(11):pp. 3902–3930, 2014a. ISSN 0022-4928. doi:10.1175/JAS-D-13-0233.1.

Park, S. A unified convection scheme (UNICON). Part II: Simulation. *Journal of the Atmospheric Sciences*, volume 71(11):pp. 3931–3973, 2014b. ISSN 0022-4928. doi:10.1175/JAS-D-13-0234.1.

Power, S. B. & Kociuba, G. What caused the observed twentieth-century weakening of the walker circulation? *Journal of Climate*, volume 24(24):pp. 6501–6514, 2011. ISSN 0894-8755. doi:10.1175/2011JCLI4101.1.

Randall, D., Khairoutdinov, M., Arakawa, A., & Grabowski, W. Breaking the cloud parameterization deadlock. *Bulletin of the American Meteorological Society*, volume 84(11):pp. 1547–1564, 2003. ISSN 0003-0007. doi:10.1175/BAMS-84-11-1547.

Rayner, N. A., Parker, D. E., Horton, E. B., Folland, C. K., Alexander, L. V., Rowell, D. P., Kent, E. C., & Kaplan, A. Global analyses of sea surface temperature, sea ice, and night marine air temperature since the late nineteenth century. *Journal of Geophysical Research: Atmospheres*, volume 108(D14):p. 4407, 2003. ISSN 2156-2202. doi:10.1029/2002JD002670.

Riehl and Malkus, H. a. J. On the heat balance in the equatorial trough zone. *Geophysica*, volume 6:pp. 503–538, 1958.

Rienecker, M. M., Suarez, M. J., Gelaro, R., Todling, R., Bacmeister, J., Liu, E., Bosilovich, M. G., Schubert, S. D., Takacs, L., Kim, G.-K., Bloom, S., Chen, J., Collins, D., Conaty, A., da Silva, A., Gu, W., Joiner, J., Koster, R. D., Lucchesi, R., Molod, A., Owens, T., Pawson, S., Pegion, P., Redder, C. R., Reichle, R., Robertson, F. R., Ruddick, A. G., Sienkiewicz, M., & Woollen, J. MERRA: NASAs modern-era retrospective analysis for research and applications. *Journal of Climate*, volume 24(14):pp. 3624–3648, 2011. ISSN 0894-8755. doi:10.1175/JCLI-D-11-00015.1.

Romps, D. M. A direct measure of entrainment. *Journal of the Atmospheric Sciences*, volume 67(6):pp. 1908–1927, 2010. ISSN 0022-4928. doi:10.1175/2010JAS3371.1.

Romps, D. M. & Kuang, Z. Do undiluted convective plumes exist in the upper tropical troposphere? *Journal of the Atmospheric Sciences*, volume 67(2):pp. 468–484, 2010. ISSN 0022-4928. doi:10.1175/2009JAS3184.1.

Rybka, H. & Tost, H. Uncertainties in future climate predictions due to convection parameterisations. *Atmos. Chem. Phys.*, volume 14(11):pp. 5561–5576, 2014. ISSN 1680-7324. doi:10.5194/acp-14-5561-2014.

Sandeep, S., Stordal, F., Sardeshmukh, P. D., & Compo, G. P. Pacific Walker Circulation variability in coupled and uncoupled climate models. *Climate Dynamics*, volume 43(1-2):pp. 103–117, 2014. ISSN 0930-7575, 1432-0894. doi:10.1007/s00382-014-2135-3.

Schneider, T., O'Gorman, P. A., & Levine, X. J. Water vapor and the dynamics of climate changes. *Reviews of Geophysics*, volume 48(3):p. RG3001, 2010. ISSN 1944-9208. doi:10.1029/2009RG000302.

Schoenberg Ferrier, B., Simpson, J., & Tao, W.-K. Factors responsible for precipitation efficiencies in midlatitude and tropical squall simulations. *Monthly Weather Review*, volume 124(10):pp. 2100–2125, 1996. ISSN 0027-0644. doi:10.1175/1520-0493(1996)124⟨2100:FRFPEI⟩2.0.CO;2.

Schumacher, C. & Houze, R. A. Stratiform rain in the tropics as seen by the TRMM precipitation radar. *Journal of Climate*, volume 16(11):pp. 1739–1756, 2003. ISSN 0894-8755. doi:10.1175/1520-0442(2003)016⟨1739:SRITTA⟩2.0.CO;2.

Sherwood, S. C., Bony, S., & Dufresne, J.-L. Spread in model climate sensitivity traced to atmospheric convective mixing. *Nature*, volume 505(7481):pp. 37–42, 2014. ISSN 0028-0836. doi:10.1038/nature12829.

Sobel, A. H., Nilsson, J., & Polvani, L. M. The weak temperature gradient approximation and balanced tropical moisture waves. *Journal of the Atmospheric Sciences*, volume 58(23):pp. 3650–3665, 2001. ISSN 0022-4928. doi:10.1175/1520-0469(2001)058⟨3650:TWTGAA⟩2.0.CO;2.

Sohn, B.-J., Lee, S., Chung, E.-S., & Song, H.-J. The role of the dry static stability for the recent change in the pacific walker circulation. *Journal of Climate*, volume 29(8):pp. 2765–2779, 2016. ISSN 0894-8755. doi:10.1175/JCLI-D-15-0374.1.

Stechmann, S. N. & Ogrosky, H. R. The Walker circulation, diabatic heating, and outgoing longwave radiation. *Geophysical Research Letters*, volume 41(24):p. 2014GL062257, 2014. ISSN 1944-8007. doi:10.1002/2014GL062257.

Su, H., Jiang, J. H., Neelin, J. D., Shen, T. J., Zhai, C., Yue, Q., Wang, Z., Huang, L., Choi, Y.-S., Stephens, G. L., & Yung, Y. L. Tightening of tropical ascent and high clouds key to precipitation change in a warmer climate. *Nature Communications*, volume 8:p. ncomms15771, 2017. ISSN 2041-1723. doi:10.1038/ncomms15771.

Sui, C.-H., Li, X., & Yang, M.-J. On the definition of precipitation efficiency. *Journal of the Atmospheric Sciences*, volume 64(12):pp. 4506–4513, 2007. ISSN 0022-4928. doi:10.1175/2007JAS2332.1.

Takahashi, K. Radiative constraints on the hydrological cycle in an idealized radiative-convective equilibrium model. *Journal of the Atmospheric Sciences*, volume 66(1):pp. 77–91, 2009. ISSN 0022-4928. doi:10.1175/2008JAS2797.1.

Tanaka, H. L., Ishizaki, N., & Kitoh, A. Trend and interannual variability of Walker, monsoon and Hadley circulations defined by velocity potential in the upper troposphere. *Tellus A*, volume 56(3):pp. 250–269, 2004. ISSN 1600-0870. doi:10.1111/j.1600-0870.2004.00049.x.

Taylor, K. E. Summarizing multiple aspects of model performance in a single diagram. *Journal of Geophysical Research: Atmospheres*, volume 106(D7):pp. 7183–7192, 2001. ISSN 2156-2202. doi:10.1029/2000JD900719.

Taylor, K. E., Stouffer, R. J., & Meehl, G. A. An overview of CMIP5 and the experiment design. *Bulletin of the American Meteorological Society*, volume 93(4):pp. 485–498, 2011. ISSN 0003-0007. doi:10.1175/BAMS-D-11-00094.1.

Trenberth, K. E. & Fasullo, J. T. Regional energy and water cycles: Transports from ocean to land. *Journal of Climate*, volume 26(20):pp. 7837–7851, 2013. ISSN 0894-8755. doi:10.1175/JCLI-D-13-00008.1.

Trenberth, K. E., Fasullo, J. T., & Kiehl, J. Earth's global energy budget. *Bulletin of the American Meteorological Society*, volume 90(3):pp. 311–323, 2009. ISSN 0003-0007. doi:10.1175/2008BAMS2634.1.

Turner, A. G. & Annamalai, H. Climate change and the South Asian summer monsoon. *Nature Climate Change*, volume 2(8):pp. 587–595, 2012. ISSN 1758-678X. doi:10.1038/nclimate1495.

Vecchi, G. A. & Soden, B. J. Global warming and the weakening of the tropical circulation. *Journal of Climate*, volume 20(17):pp. 4316–4340, 2007. ISSN 0894-8755. doi:10.1175/JCLI4258.1.

Vecchi, G. A., Soden, B. J., Wittenberg, A. T., Held, I. M., Leetmaa, A., & Harrison, M. J. Weakening of tropical Pacific atmospheric circulation due to anthropogenic forcing. *Nature*, volume 441(7089):pp. 73–76, 2006. ISSN 0028-0836. doi:10.1038/nature04744.

Webb, M. J., Lock, A. P., Bretherton, C. S., Bony, S., Cole, J. N. S., Idelkadi, A., Kang, S. M., Koshiro, T., Kawai, H., Ogura, T., Roehrig, R., Shin, Y., Mauritsen, T., Sherwood, S. C., Vial, J., Watanabe, M., Woelfle, M. D., & Zhao, M. The impact of parametrized convection on cloud feedback. *Phil. Trans. R. Soc. A*, volume 373(2054):p. 20140414, 2015. ISSN 1364-503X, 1471-2962. doi:10.1098/rsta.2014.0414.

Wills, R. C., Levine, X. J., & Schneider, T. Local energetic constraints on Walker circulation strength. *Journal of the Atmospheric Sciences*, 2017. ISSN 0022-4928. doi: 10.1175/JAS-D-16-0219.1.

Xie, P. & Arkin, P. A. Global precipitation: A 17-year monthly analysis based on gauge observations, satellite estimates, and numerical model outputs. *Bulletin of the American Meteorological Society*, volume 78(11):pp. 2539–2558, 1997. ISSN 0003-0007. doi:10.1175/1520-0477(1997)078⟨2539:GPAYMA⟩2.0.CO;2.

Yanai, M., Esbensen, S., & Chu, J.-H. Determination of bulk properties of tropical cloud clusters from large-scale heat and moisture budgets. *Journal of the Atmospheric Sciences*, volume 30(4):pp. 611–627, 1973. ISSN 0022-4928. doi:10.1175/1520-0469(1973)030⟨0611:DOBPOT⟩2.0.CO;2.

Yang, B., Qian, Y., Lin, G., Leung, L. R., Rasch, P. J., Zhang, G. J., McFarlane, S. A., Zhao, C., Zhang, Y., Wang, H., Wang, M., & Liu, X. Uncertainty quantification and parameter tuning in the CAM5 Zhang-McFarlane convection scheme and impact of improved convection on the global circulation and climate. *Journal of Geophysical Research: Atmospheres*, volume 118(2):pp. 395–415, 2013. ISSN 2169-8996. doi: 10.1029/2012JD018213.

Zhang, C. Madden-Julian Oscillation. volume 43(2):p. RG2003, . ISSN 1944-9208. doi: 10.1029/2004RG000158.

Zhang, G. J. & McFarlane, N. A. Sensitivity of climate simulations to the parameterization of cumulus convection in the Canadian climate centre general circulation model. *Atmosphere-Ocean*, volume 33(3):pp. 407–446, 1995. ISSN 0705-5900. doi: 10.1080/07055900.1995.9649539.